Study on Energy Relaxation of Runaway Electrons in a Tokamak Plasma due to Excitation of High Frequency Waves

Toshinori MICHISHITA

January 1983

Study on Energy Relaxation of Runaway Electrons in a Tokamak Plasma due to Excitation of High Frequency Waves

Toshinori MICHISHITA

January 1983

Department of Nuclear Engineering

Faculty of Engineering

Kyoto University, Kyoto 606

Foreword

The present work examines problems relating to the interaction of the runaway electrons with the high frequency waves excited via the anomalous Doppler resonance.

The principal attention is devoted to the energy relaxation of the runaway electrons due to the wave excitation. The time development of the runaway electron energy is numerically examined based on the two dimensional quasi-linear equation. The phenomena relating to the energy relaxation of the runaway electrons are experimentally examined in a tokamak plasma.

The numerical and experimental results are avaiable for examining phenomena resulting from the interaction of the runaway electrons with the high frequency waves.

The results are also useful for examining the dynamics of the fast electrons in the magnetized plasmas, especially, in connection with the researches on the current sustain utilized by the rf-waves and on the hot electrons produced by ECH(electron cyclotron heating).

Acknowledgements

The author wishes to express appreciation to Professor Hiroshi Nishihara of Kyoto University for helpful discussions and comments during the course of this research as well as for encouragement and advices during the preparation of this manuscript.

Valuable discussions on the experiments with Dr. Masayuki Fukao of Kyoto University, who enlighted the author on plasma physics and controlled nuclear fusion research, are gratefully acknowledged.

Helpful discussions on the computer simulation with Professor Masao Okamoto of Institute of Plasma Physics in Nagoya University are also acknowledged.

The author deems it his pleasant duty to acknowledge Professors Atsuo Iiyoshi and Masahiro Wakatani of Institute of Fusion Research of Kyoto University for useful discussions and advices during the preparation of this manuscript.

The author also wishes to thank Professor Hiroshi Oshiyama of Kyoto Technical University, Drs. Yasushi Terumichi and Hidetoshi Suemitsu of Kyoto University, Messrs. Hideki Zushi of Institute of Fusion Research of Kyoto University and Sadao Masamune of Kyoto Technical University for co-operation in the experiments.

Fruitful discussions on plasma physics with Professor Hiroshi Kubo, Dr. Sadao Nakamura and Mr. Tetsumori Yuyama are deeply

acknowledged.

It is a pleasure to acknowledge Messrs. Toshio Nishigaki and Shohei Tokuhira of Data Processing Center of Kyoto University and Mr. Mitsuru Yamagiwa of Kyoto University for continuing helps during the calculation.

Computation was performed on the M-200 at Data Processing Center of Kyoto University.

Contents

Chapter 1 Introduction

Problems concerned with runaway electrons have been repeatedly investigated from the earlier stage of the research on the plasma physics and controlled thermonuclear. The reason is that the runaway electron is closely related with a fundamental kinetic dynamics in plasmas, i.e., a Coulomb collision effect.[1] The investigation on the basis of the kinetic theory has been initiated by Dreicer [2], and has been developed by Levedev, Gurevich, and Kruskal and Bernstein.[3-5] Especially, Kruskal and Bernstein have determined an analytical rigorous solution of the runaway electron production rate. This has been done by dividing the velocity space into the five regions and by expanding the distribution function in powers of the electric field. A numerical calculation using a Fokker-Planck collision model by Kulsrud et al. [6,7] has shown an consistence with the analytical results by Kruskal and Bernstein. In Fig.1, the runaway production rate S_R is given in Ref. 6 ; the value denoted by the symbol o in the figure is corresponding to that determined from the following equation with the experimental values,

tal values,

$$S_R = 0.35 \cdot n_e \nu_0 \left(\frac{E_c}{E} \right)^{\frac{3(1+Z_e)}{16}} \exp\left\{ -\frac{E_c}{E} - \left[\frac{(1+Z_e)E_c}{2E} \right]^{\frac{1}{2}} \right\} , \qquad (1.1.a)$$

$$E_c = \frac{4\pi e^3 n_e (1+Z_e) \ln\Lambda_c}{T_e} \qquad (1.1.b)$$

$$\nu_0 = \frac{4\pi e^3 n_e (1+Z_e) \ln\Lambda}{m v_e^3} \qquad (1.1.c)$$

$$\ln\Lambda_c = \ln\Lambda + \ln (v_c^2/v_e^2) \qquad (1.1.d)$$

$$v_c = \left(\frac{4\pi e^3 n_e \ln\Lambda}{mE} \right)^{\frac{1}{2}} \qquad (1.1.e)$$

where n_e, T_e, and E are the electron density, the electron temperature, and the toroidal electric field, respectively. From the equations, it is seen that the runaway phenomenon is pronounced in the cases of the low density and/or the large electric field. It is noted that the above mentioned models include only the effect of the Coulomb collisions, except for the Gurevich's work.[8)]

Another motivation for studying the runaway electrons arizes from a different viewpoint: The interaction of the runaway electrons with various kinds of the plasma collective oscillations plays a major role of the properties of the plasmas as well as the runaway electrons themselves. This is related with 1) a fundamental plasma physics associated with non-linear phenomena,[9-16)] 2) the diagnostics with utilizing microwave and hard-X-ray radiations,[17-26)] 3) the further heating and the current sustain,[27-28)] 4) the more practical

purpose such as the maintenance of the devices.

The earlier work concerned with the effect has been performed in the Model-C Stellarator.[30] The observed relaxation were interpreted as a consequence of the two stream instability. In the earlier experiments with the tokamaks, the anomalous resistance phenomenon was observed in TM-3 [31] with increse in the population of the runaway electrons. Kadomtsev and Pogutse proposed the model responsible for the phenomenon that the anomalous resistance originated from the pitch angle scattering of the runaway electrons due to the resonant wave-particle interaction via the anomalous Doppler resonance. This implies that the distribution function of the runaway electrons is governed not only by the Coulomb collisions, but also by the effect owing to the collective oscillations of the plasmas, at least, under a certain circumstance.

More distinct phenomena caused by the runaway electrons were observed in the T-6 tokamak. [22] The experiment on the T-6 revealed the feature of relaxation oscillations that were detected in the manners of the positive voltage spikes, the sudden enhancements of the diamagnetic signal, and the burst of the hard X-ray and microwave radiations. Similar effects were more quantitatively studied in the TM-3 tokamak.[23] It was also reported that the high energetic ions were produced at the instability. In the ATC and TFR, the sudden enhancements in the synchrotron radiation intensity were observed correlated with the voltage spikes.[19-21] In the NOVA-II, Michishita et al. studied the energy relaxation of the runaway electrons during

the high frequency instability and showed the drag in the time development of the electron energy.[32]

Recent theoretical works ascribe these phenomena to the interaction of the runaway electrons with the high frequency waves via the anomalous Doppler resonance.[10,11] Parail and Pogutse analytically studied in detail the instability based on the quasi-linear model. They showed that the runaway electrons form an isotropic distribution function via the anomalous Doppler resonance with the cold plasma waves and the bump in tail; sequentially, the bump decays due to the Cerenkov resonance, which produces broad spectrum in frequency.[11]

Papadopoulos et al. studied numerically the formation of the bump due to the anomalous Doppler resonance by using the one-dimensional Fokker-Planck equations.[15] Hui and Wisnor developed the investigation by using the two dimensional Fokker-Planck equation combined with the quasi-linear term.[16] They showed the excited wave spectrum in the corresponding velocity space as well as the formation of the bump in the tail. For the numerical simplicity, they restricted themselves with the special propagating angle for the associated waves. Also we have no detailed results concerned with the time evolutions of the electron-associated energies, i.e. the relaxation in energy of the electrons as well as with the wave spectrum in wavenumber space. A numerical work for the relaxation in energy was performed by Choi and Horton using the moment equations.[32] Their results reproduced the feature of the relaxation found in the experiments. Nevertheless this method also provides no direct information of the

distribution function. The energy development of the runaway electrons was studied by Michishita and Nishihara using the two dimensional quasi-linear diffusion equations combined with a Fokker-Planck collision term. They also showed the time development of the electron distribution function as well as that of the excited wave spectrum.[33]

The present work is concentrated on the energy relaxation of the runaway electrons in a tokamak plasma due to the excitation of the high frequency waves. The following two chapters are devoted to the numerical study on the dynamics in velocity space of the electrons. In Chapter 2, a quasi-linear diffusion of the electrons due to excitation of high frequency waves via anomalous Doppler resonance is examined. The quasi-linear diffusion equation is numerically solved for plasma parameters of a small tokamak NOVA-II[34] ; typically, B_t=10kG, $n_e = 5\times10^{12}$ cm^{-3}, and T_e = 100 eV. Under these conditions, a quasi-linear relaxation time is expected to be of the order of

$$t_{QL} \sim \gamma_k^{-1} \sim 10^{-8} \text{ sec} , \tag{1.2}$$

where γ_k is the maximum growth rate for the waves of interst. On the other hand, the Coulomb relaxation time for the thermal electrons is of the order of

$$t_{Coul.} \sim 10^{-6} \text{ sec} . \tag{1.3}$$

Consequently, the system will be governed by the quasi-linear process

as long as the time is much smaller than $t_{Coul.}$, or the noise levels of the excited waves are not sufficiently small. An alternating-direction implicit (ADI) method [35] is utilized to solve the finite difference equations simulating the system.

The instability of the author s interest has the relaxation period of 0.1 - 1 msec. The fact impose us to take into account also the Coulomb collisions when we study the development of the system until the Coulomb collision time scale. In Chapter 3, numerical study of the energy relaxation of runaway electrons is performed by taking into account effect of the Coulomb collisions as well as that of the excited waves.[33] This is performed by combining the quasi - linear equation with a Fokker-Planck collision term. Also a non-linear wave damping effect is taken into account. The most important result is that the electrons take place relaxation in energy with increase in the wave energy density.

The following two chapters, Chapter 4 and 5, are devoted to experimental studies on phenomena connected with the relaxation of runaway electrons in a small tokamak NOVA-II . The detail of the NOVA-II device was reported by Fukao et al.[34] The main purpose of the experiments is to investigate the energy relaxation of runaway electrons due to wave-particle interaction with excitation of high frequency when the runaway electrons develop sufficiently both in energy and in population. For this purpose, the analysis on the hard X-ray radiation signal is done together with other diagnostics. These experimental results are described in Chapter 4.[25]

In the circumstance that the relaxation repeats during the discharges, the runaway electrons are no longer freely accelerated, and their energy remain lower compared with that in the case without the instability. Dynamics of these electrons is studied from the measurement of the microwave radiations. Non-thermal radiation exhibited two distinct time behaviors at X-band. One is explained by synchrotron radiation through the pitch-angle scattering of the runaway electrons. The other is closely related with the plasma density and the runaway electron energy. These experimental results are described in Chapter 5.

In the final chapter, the author summarizes the present work and describes conclusions.

References

1) B.A.Trubnikov, 'Reviews of Plasma Physics', vol.1 ed. M.A.Leontovich

2) H.Dreicer: Phys.Rev.115(1959) 238; ibid.117(1960) 329

3) A.N.Levedev: Sov.Phys.-JETP 21 (1965) 931

4) A.V.Gurevich: Sov.Phys.-JETP 12(1961) 904

5) M.Kruskal and Ira.B.Bernstein: Princeton Plasma Physics Laboratory Report MATT-Q-20(1962)

6) R.M.Kulsrud, Y.C.Sun, N.K.Wisnor, and H.A.Fallon; Phys.Rev.Lett.31 (1973) 690

7) R.H.Coen; Phys.Fluids 19 (197) 239

8) A.V.Gurevich and Yu.N.Zhivlyuk; Sov.Phys.JETP 22 (1966) 153

9) B.B.Kadomtsev and O.P.Pogutse: Sov.Phys.JETP 26(1968) 1146

10) C.S.Liu and Y.C.Mok: Phys.Rev.Lett. 38(1978) 162

11) V.V.Parail and O.P.Pogutse: Nucl.Fusion 18(1978) 303; Sov.J.Plasma Phys. 2(1976) 228

12) V.D.Shapiro and V.I.Shevchenko ; Sov. Physics JETP 27 (1968) 635

13) I.H.Hutchison, K.Molvig and S.Y.Yuen: Phys.Rev.Lett.40(1978) 1091

14) I.Fidone, G.Ramponi and P.Brossier: Phys.Fluids 21(1978) 237

15) K.Papadopoulos, B.Hui and N.Wisnor: Nucl.Fusion 17(1977)

16) B.H.Hui and N.Wisnor ; Phys.Fluids 21 (1978) 940

17) G.Bekefi, 'Radiation Processes in Plasma' (Wiley, New York, 1966)

18) A.E.Costley, R.J.Hastie, J.W.M.Paul, and J.Chamberlain: Phys.Lev.Lett.33 (1974) 758

19) D.A.Boyd, F.J.Stauffer and A.W.Trivelpiece: Phys.Rev.Lett. 37(1976) 98

20) EQUIPE TFR: Nucl.Fusion 16(1976) 473

21) D.A.Boyd et al.; in Plasma Physics and Controlled Nuclear Fusion Research (Proc. 6th Int. Conf. Berchtesgaden 1976) 1, IAEA, Vienna (1977) 399

22) V.S.Vlasenkov, V.M.Leonov, V.G.Merezkhin and V.S.Mukhovatov; Nucl.Fusion 13(1973) 509

23) V.V.Alikaev, K.A.Razumova and Y.A.Solokov: Sov.J.Plasma Phys. 1(1975) 303; Sov.-Phys.-Tech.Phys. 20(1975)

24) P.Brossier: Nucl.Fusion 18(1978) 1069

25) T.Michishita et al.: J.Phys.Soc.Jpn. 47(1979) 1035; ibid 50 (1981) 2720

26) V.M.Morozov: Sov.J.Plasma Phys. 3 (1977) 636

27) D.K.Bhardra: Nucl.Fusion 20(1980) 619

28) T.Maekawa et al.; Physics Lett.85A (1981) 339

29) K.Ohkubo et al.; Nucl.Fusion 22 (1982) 203

30) W.Stodiek and D.J.Grove; Princeton Plasma Physics Laboratory Report MATT-Q-20(1963)

31) G.A.Bobrovskii, et al.: MATT-TRANS 92 (1969)

32) Duk-In Choi and W.Horton.Jr.; Plasma Physics 20 (1978) 903

33) T.Michishita and H.Nishihara; submitted in J.Phys.Soc.Jpn

34) M.Fukao et al.: The Memoir of Faculty of Engineering, Kyoto Univ. 39(1977) 431

35) J.Killeen and K.D.Marx, 'Methods in Computational Physics', ed.

B.Alder, S.Fernbach, and M.Rotenberg, vol.9 (1970)

36) R.H.Fowler, J.D.Callen, J.A.Rome, and J.Smith; ORNL/TM-5487,1976

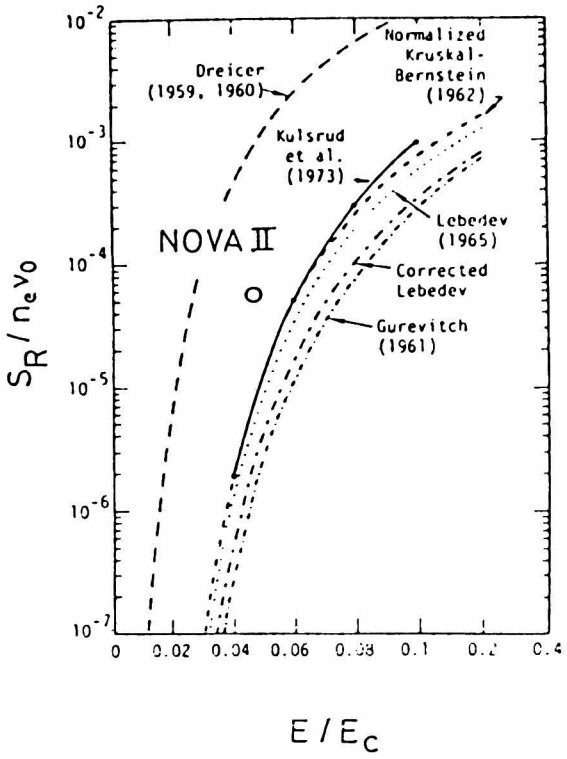

Fig. Runaway production rate S_R; the circle o is corresponding to that in the NOVA-II tokamak plasma for the case of $n_e=5\times10^{12}cm^{-3}$, $T_e=100eV$, and $Z_e=1$.

Chapter 2 Quasi-Linear Relaxation of Runaway Electrons

2.1 Introduction

It is well known that in a fully ionized plasma with a d.c. electric field, E_0, some electrons run away in velocity space from the bulk plasma electrons when their velocities exceed a certain critical value which is given by

$$v_c = \left(\frac{4 e^3 n_e \ln \Lambda}{m E_0} \right) 1/2 ,$$

where n_e is the bulk electron density, e the elementary charge, m the electron mass, and $\ln\Lambda$ the Coulomb logarithm. The electrons are continuously accelerated by the electric field almost without suffering from the Coulomb collisions. In typical present toroidal devices such as tokamaks, their energies become to be of the order of 10 MeV in the final phase of the discharges.[1,2)]

Recent experiments showed that such runaway electrons do relax in energy due to an instablity and that their energies remain appreciably lower in the low density discharges.[3-5)] Parail and Pogutse showed analytically that the relaxation is as a result of the resonant interaction of the runaway electrons with the plasma waves via the anomalous Doppler resonance.[6)] A quasi-linear process plays an essential role of such relaxation.

In the present chapter, we study numerically dynamics in velocity space of the runaway electrons under influence of plasma waves excited self-consistently via anomalous Doppler resonance.

In Section 2.2, the quasi-linear diffusion equation is described. In the published works on the problem concerned with the instability, a special propagating direction for the excited waves is employed for the analytical and numerical simplicity; the angle is corresponding to the $k_z/k=1/\sqrt{3}$. Although at this angle we have the maximum growth rate for the anomalous Doppler resonance, we have no intersection between both the effects for the propagating angle. Consequently, the quasi-linear effect due to the Cerenkov resonance never interfere with that due to the anomalous Doppler resonance in the velocity space. In the present study, no special propagating direction of the excited waves is chosen. As a result, we are able to examine the time evolution of the wave spectrum in wavenumber space. This leads us to a distinct comparison with the prediction by the analysis.

Section 2.3 gives the numerical models to be studied. An integration scheme employed is an alternating-direction implicit (ADI) method with mixed derivative terms. The method is in detail described in this section.

Section 2.4 describes the numerical results and discussion. The results involve the time development of the wave spectrum as well as that of the electron distribution function. The final section is devoted to conclusions from the present numerical

study.

2.2 Quasi-Linear Equations

For studying the time development of the electron distribution function f(v,t), we use the quasi-linear diffusion equation, which is given by

$$\frac{\partial f}{\partial t} = \frac{eE_0}{m} \cdot \frac{\partial f}{\partial v_z} + \left(\frac{\partial f}{\partial t} \right)_{QL} , \tag{2.1}$$

where E_0 is a d.c. toroidal electric field, and v electron velocity. The first term in the right hand side of eq.(2.1) represents the force term due to the electric field. At present, the electric field is assumed to be parallel to the toroidal direction. The second term represents the quasi-linear diffusion term. The term may be written by (see Appendix A)[7]

$$\left(\frac{\partial f}{\partial t} \right)_{QL} = 8\pi^2 \frac{e^2}{m^2} \Sigma \int dk \, \frac{\varepsilon_k}{k^2} \, \delta(\omega_k + n\omega_{ce} - k_z v_z)$$
$$\times \left(- \frac{n\omega_{ce}}{v_\perp} \frac{\partial}{\partial v_\perp} + k_z \frac{\partial}{\partial v_z} \right) J_n^2 \left(\frac{k_\perp v_\perp}{\omega_{ce}} \right)$$
$$\times \left(- \frac{n\omega_{ce}}{v_\perp} \frac{\partial}{\partial v_\perp} + k_z \frac{\partial}{\partial v_z} \right) f , \tag{2.2}$$

$$\varepsilon_k = \frac{|E_k|^2}{8\pi} , \tag{2.3}$$

where k is the wave numver for the waves, k_z and $k_\perp$ are its components parallel and perpendicular to the magnetic field B_t, respectively, $\omega_k/2\pi$ the wave frequency, and $\omega_{ce}/2\pi$ the cyclotron frequency. J_n are the Bessel functions. ϵ_k is the wave energy intensity with the wave number k, which is governed by the following wave equation;

$$\frac{\partial \epsilon_k}{\partial t} = 2\ \gamma_k\ \epsilon_k\ , \tag{2.4}$$

where γ_k is the linear growth rate for the waves, which is given by

$$\gamma_k = \pi \frac{\omega_k}{n_e} \frac{\omega_{pe}^2}{k^2 |k_z|} \Sigma \int dv\ \delta(\omega_k + n\omega_{ce} - k_z v_z)$$

$$\times J_n^2\left(\frac{k_\perp v_\perp}{\omega_{ce}}\right)\left(-\frac{n\omega_{ce}}{v_\perp}\frac{\partial}{\partial v_\perp} + k_z \frac{\partial}{\partial v_z}\right) f \quad . \tag{2.5}$$

The specified forms of the quasi-linear diffusion coefficients and the growth rate depend on the mode of the excited waves. The mode of interest at present is one with the cold plasma dispersion relation of

$$\omega_k = \omega_{pe} \cdot \xi \quad , \tag{2.6}$$

where $\xi = k_z/k$ are cosines of the propagating angles of the waves to the magnetic field. This mode takes frequencies from the ion plasma frequency ω_{pi} or the lower hybrid resonance frequency ω_{lh} to the elec-

tron plasma frequency ω_{pe} depending upon the propagating angle of the wave.

Now it is assumed that the electron distribution function has a long tail of the runaway electrons. In deriving the growth of the waves, only the Cerenkov and anomalous Doppler resonances are taken into account. Such circumstance is illustrated in Fig.1.

Thus we obtain the system of the quasi-linear term

$$\left(\frac{\partial f}{\partial t}\right)_{QL} = \frac{\partial}{\partial v_z}\left(D_c \frac{\partial f}{\partial v_z}\right) + \left(-\frac{\omega_{ce}}{k_z v_\perp}\frac{\partial}{\partial v_\perp} + \frac{\partial}{\partial v_z}\right) D_a \times \left(-\frac{\omega_{ce}}{k_z v_\perp}\frac{\partial}{\partial v_\perp} + \frac{\partial}{\partial v_z}\right) f \quad , \tag{2.7}$$

where

$$D_c = 8\pi^2 \frac{e^2}{m^2} \int dk \, \frac{k_z^2 \varepsilon_k}{k^2} \delta(\omega_k - k_z v_z) \quad , \tag{2.8}$$

$$D_a = 8\pi^2 \frac{e^2}{m^2} \int dk \, \frac{k_\perp^2 v_\perp^2}{4\omega_{ce}^2} \varepsilon_k \, \delta(\omega_k + \omega_{ce} - k_z v_z) \quad , \tag{2.9}$$

$$\gamma_k = \pi \frac{\omega_k}{n_e} \frac{\omega_{pe}^2}{k^2} \int dv \, \frac{\partial f}{\partial v_z} \delta(\omega_k - k_z v_z) + \pi \frac{\omega_k}{n_e} \frac{\omega_{pe}^2}{k^2} \int dv \, \frac{k_\perp^2 v_\perp^2}{4\omega_{ce}^2} \left(-\frac{\omega_{ce}}{k_z v_\perp}\frac{\partial f}{\partial v_\perp} + \frac{\partial f}{\partial v_z}\right) \delta(\omega_k + \omega_{ce} - k_z v_z) \quad , \tag{2.10}$$

where D_c is the quasi-linear diffusion coefficients due to Cerenkov resonance, and D_a is one due to anomalous Doppler resonance. In the derivation, we have employed the approximation that the electron Larmor radius r_{eL} are sufficiently small compared with the perpendicular wavelength, i.e. $k_\perp r_{eL} \ll 1$, which assures the expressions of $J_0 \simeq 1$, $J_1 \simeq k_\perp v_\perp / 2\omega_{ce}$, and $J_n = 0$ for $n \geq 2$.

By performing integrations respected with k for the diffusion coefficients and growth rates, we obtain

$$D_c(v_z,\xi,t) = 2\pi \frac{\omega_{pe}^4}{n_e m v_z^3} \int d\xi \, \xi \, \varepsilon_1 \,, \tag{2.11}$$

$$D_a(v_z,v_\perp,\xi,t) = 4\pi \frac{\omega_{pe}^4}{n_e m v_z^3} \frac{v_\perp^2}{v_z^2} \frac{\omega_{pe}^2}{\omega_{ce}^2} \int d\xi \, \frac{1-\xi^2}{4\xi^2} \, \varepsilon_2, \tag{2.12}$$

where

$$\varepsilon_1(v_z,\xi,t) = \varepsilon_0 \exp\left[2 \int \gamma\left(\frac{\omega_{pe}}{v_z},\xi,t\right) dt \right], \tag{2.13}$$

$$\varepsilon_2(v_z,\xi,t) = \varepsilon_0 \exp\left[2 \int \gamma\left(\frac{\omega_k + \omega_{ce}}{\xi v_z},\xi,t\right) dt \right]. \tag{2.14}$$

In the present, the propagating angle is from 0 to $\pi/2$ to the direction of the magnetic field. ε_0 is an initial thermal noise of the waves. ε_1 and ε_2 are corresponding to the wave number spectra in the Cerenkov resonance region and in the anomalous Doppler resonance region in velocity space, respectively.

It is noted that on application of the quasi-linear diffusion

mechanism, the associated wave spectrum must be sufficiently broad in wavenumber or in frequency.

In order to solve numerically eq.(2.1), we introduce dimensionless variables as follows:

$$\tau = \omega_{pi}\, t \qquad u = v_z / v_{Te} \qquad w = v_\perp / v_{Te} \qquad x = (u^2 + w^2)^{1/2}$$

$$\hat{D}_{c,a} = D_{c,a} / \omega_{pi}\, v_{Te}^2 \qquad F(u,w,\tau) = \frac{v_{Te}^3}{n_e}\, f(v_z, v_\perp, t) . \quad (2.15)$$

By using the above variables, we rewrite the equations (2.1),(2.8), (2.9), and (2.10);

$$\frac{\partial f}{\partial \tau} = \hat{E}\, \frac{\partial F}{\partial u} + \frac{\partial}{\partial u}\left(\hat{D}_c \frac{\partial F}{\partial u}\right) + \left(-\frac{u}{w}\frac{\partial}{\partial w} + \frac{\partial}{\partial u}\right) D_a \left(-\frac{u}{w}\frac{\partial F}{\partial w} + \frac{\partial F}{\partial u}\right) , \quad (2.16)$$

where

$$\hat{D}_c = 2\pi\eta\, \frac{1}{u^3}\, W_c , \quad (2.17.a)$$

$$\hat{D}_a = 2\pi\eta\, \frac{w^2}{u^5}\, W_a , \quad (2.17.b)$$

$$W_c = 2\pi W_0 \int d\xi\, \xi \exp\left[\int \Gamma\, d\tau\right] , \quad (2.17.c)$$

$$W_a = 2\pi W_0 \int d\xi\, \frac{1-\xi^2}{4\xi^3} \exp\left[\int \Gamma\, d\tau\right] , \quad (2.17.d)$$

$$\Gamma(u,\xi,\tau) = \gamma(u,\xi,\tau) / \omega_{pi} \quad , \tag{2.17.e}$$

Here η is the ratio of ω_{pe}/ω_{ce} , and W_0 the thermal noise normalized by n_0T_0, which is taken as 10^{-6} - 10^{-7} in the present study. When working with the function W_c and W_a , we have in mind a function of the wavenumber k and the propagating angle ξ , which are connected with conditions of $u = k_D/k$ for the Cerenkov resonance and $u = (\omega_{ce}/\omega_{pe})(k_D/k\,\xi)$ for the anomalous Doppler resonance, where $k_D = \omega_{pe}/v_e$ is the Debye wavenumber.

2.3 Numerical Method

Equation (2.16) is rewritten in the form of

$$\frac{\partial F}{\partial \tau} = A_1 \frac{\partial^2 F}{\partial u^2} + A_2 \frac{\partial^2 F}{\partial u \partial w} + A_3 \frac{\partial^2 F}{\partial w^2} + B_1 \frac{\partial F}{\partial u} + B_2 \frac{\partial F}{\partial w} \quad , \tag{2.18}$$

where

$$A_1 = \hat{D}_c + \hat{D}_a \quad , \tag{2.19.a}$$

$$A_2 = -2 \frac{u}{w} \hat{D}_a \quad , \tag{2.19.b}$$

$$A_3 = \frac{u^2}{w^2}\hat{D}_a \quad , \tag{2.19.c}$$

$$B_1 = \hat{E} + \frac{\partial}{\partial u}(\hat{D}_c + \hat{D}_a) - \frac{u}{w}\frac{\partial}{\partial w}\hat{D}_a \quad , \tag{2.19.d}$$

$$B_2 = \frac{u}{w}\frac{\partial}{\partial w}(\frac{u}{w}\hat{D}_a) - \frac{\partial}{\partial u}(\frac{u}{w}\hat{D}_a) \quad . \tag{2.19.e}$$

The integration scheme employed here is the alternating direction implicit (ADI) method.[8] The grids are 91x46 (uxw) with a space of 0.33 in both directions. The integration region is of $-10 \le u \le 20$ and $0 \le w \le 15$. In ADI scheme, a single time step is cut in half, namely, let $\tau^{n+1/2} = \tau^n + \Delta\tau/2$ and $\tau^{n+1} = \tau^{n+1/2} + \Delta\tau/2$,

$$(u_i, w_j, \tau^n) = [u_{min} + (i-1)\Delta u, (j-1)\Delta w, n\Delta\tau], \tag{2.20.a}$$

and

$$F^n_{i,j} = F(u_i, w_j, \tau^n) \quad . \tag{2.20.b}$$

Equation (2.18) is descretized implicitly in the u-direction and explicitly in the w-direction on the first half time step, the situation is reversed on the second half time step. The mixed derivative term is splitted into the explicit and implicit parts.

Now the discretized equation is in the first half time step

$$\frac{F_{ij}^{n+1/2} - F_{ij}^{n}}{\Delta\tau/2}$$

$$= \frac{A_{1,ij}^{n}}{\Delta u^2} \left(F_{i+1,j}^{n+1/2} - F_{ij}^{n+1/2} - F_{ij}^{n+1/2} + F_{i-1,j}^{n+1/2} \right)$$

$$+ \frac{A_{2,ij}^{n}}{4\Delta u\Delta w} \left(F_{i+1,j}^{n+1/2} - F_{i-1,j}^{n+1/2} - F_{i+1,j-1}^{n+1/2} + F_{i-1,j-1}^{n+1/2} \right)$$

$$+ \frac{A_{2,ij}^{n}}{4\Delta u\Delta w} \left(F_{i+1,j+1}^{n} - F_{i-1,j+1}^{n} - F_{i+1,j}^{n} + F_{i-1,j}^{n} \right)$$

$$+ \frac{A_{3,ij}^{n}}{\Delta w^2} \left(F_{i,j+1}^{n} - F_{ij}^{n} - F_{ij}^{n} + F_{i,j-1}^{n} \right)$$

$$+ \frac{B_{1,ij}^{n}}{2\Delta u} \left(F_{i+1,j}^{n+1/2} - F_{i-1,j}^{n+1/2} \right)$$

$$+ \frac{B_{2,ij}^{n}}{2\Delta w} \left(F_{i,j+1}^{n} - F_{i,j-1}^{n} \right) \quad . \qquad (2.21)$$

For the next half time step, we have

$$\frac{F_{ij}^{n+1} - F_{ij}^{n+1/2}}{\Delta\tau/2}$$

$$= \frac{A_{1,ij}^{n}}{\Delta u^2} \left(F_{i+1,j}^{n+1/2} - F_{ij}^{n+1/2} - F_{ij}^{n+1/2} + F_{i-1,j}^{n+1/2} \right)$$

$$+ \frac{A_{2,ij}^{n}}{4\Delta u\Delta w} \left(F_{i,j+1}^{n+1} - F_{i,j-1}^{n+1} - F_{i-1,j+1}^{n+1} + F_{i-1,j-1}^{n+1} \right)$$

$$+ \frac{A_{2,ij}^{n}}{4\Delta u\Delta w} \left(F_{i+1,j+1}^{n+1/2} - F_{i+1,j-1}^{n+1/2} - F_{i,j+1}^{n+1/2} + F_{i,j-1}^{n+1/2} \right)$$

$$+ \frac{A_{3,ij}^{n}}{\Delta w^2} \left(F_{i,j+1}^{n+1} - F_{ij}^{n+1} - F_{ij}^{n+1} + F_{i,j-1}^{n+1} \right)$$

$$+ \frac{B_{1,ij}^{n}}{2\Delta u} \left(F_{i+1,j}^{n+1/2} - F_{i-1,j}^{n+1/2} \right)$$

$$+ \frac{B_{2,ij}^{n}}{2\Delta w} \left(F_{i,j+1}^{n+1} - F_{i,j-1}^{n+1} \right) \quad . \qquad (2.22)$$

Then the discretized equations are transformed into the following tri-diagonal forms;

$$-\alpha_{ij}\, F^{n+1/2}_{i+1,j} + \beta_{ij}\, F^{n+1/2}_{ij} - \gamma_{ij}\, F^{n+1/2}_{i-1,j} = \psi^{n}_{ij} \quad , (2.23.a)$$

$$\psi^{n}_{ij} = \varepsilon_{ij}\, F^{n}_{i,j+1} - (\delta_{ij} - \frac{4}{\Delta\tau})\, F^{n}_{ij} + \rho_{ij}\, F^{n}_{i,j-1}$$

$$+ \mu_{ij} \left(- F^{n}_{i,j+1} + F^{n}_{i,j-1} \right)$$

$$+ \mu_{ij} \left(F^{n}_{i+1,j+1} - F^{n}_{i-1,j+1} - F^{n}_{i+1,j} + F^{n}_{i-1,j} \right)$$

$$+ \mu_{ij} \left(- F^{n+1/2}_{i+1,j-1} + F^{n+1/2}_{i-1,j-1} \right) \quad , \qquad (2.23.b)$$

$$-\varepsilon_{ij}\, F^{n+1}_{i,j+1} + \delta_{ij}\, F^{n+1}_{ij} - \rho_{ij}\, F^{n+1}_{i,j-1} = \phi^{n+1/2}_{ij} , (2.24.a)$$

$$\phi^{n+1/2}_{ij} = \alpha_{ij}\, F^{n+1/2}_{i+1,j} - (\beta_{ij} - \frac{4}{\Delta\tau})\, F^{n+1/2}_{ij} + \gamma_{ij}\, F^{n+1/2}_{i-1,j}$$

$$+ \mu_{ij} \left(- F^{n+1/2}_{i+1,j} + F^{n+1/2}_{i-1,j} \right)$$

$$+ \mu_{ij} \left(F^{n+1/2}_{i+1,j+1} - F^{n+1/2}_{i+1,j-1} - F^{n+1/2}_{i,j+1} + F^{n+1/2}_{i,j-1} \right)$$

$$+ \mu_{ij} \left(- F^{n+1}_{i-1,j+1} + F^{n+1}_{i-1,j-1} \right) \quad , (2.24.b)$$

where the coefficients are given by

$$\alpha_{ij} = \frac{1}{\Delta u}\left(\frac{A^n_{1,ij}}{\Delta u} + \frac{B^n_{1,ij}}{2}\right) + \mu_{ij} \quad , \tag{2.25.a}$$

$$\beta_{ij} = \frac{1}{\Delta u}\left(\frac{A^n_{1,ij}}{\Delta u} + \frac{A^n_{1,ij}}{\Delta u}\right) + \frac{2}{\Delta \tau} \quad , \tag{2.25.b}$$

$$\gamma_{ij} = \frac{1}{\Delta u}\left(\frac{A^n_{1,ij}}{\Delta u} - \frac{B^n_{1,ij}}{2}\right) - \mu_{ij} \quad , \tag{2.25.c}$$

$$\varepsilon_{ij} = \frac{1}{\Delta w}\left(\frac{A^n_{3,ij}}{\Delta w} + \frac{B^n_{2,ij}}{2}\right) + \mu_{ij} \quad , \tag{2.25.d}$$

$$\delta_{ij} = \frac{2\,A^n_{3,ij}}{\Delta w^2} + \frac{2}{\Delta \tau} \quad , \tag{2.25.e}$$

$$\rho_{ij} = \frac{1}{\Delta w}\left(\frac{A^n_{3,ij}}{\Delta w} - \frac{B^n_{2,ij}}{2}\right) - \mu_{ij} \quad , \tag{2.25.f}$$

$$\mu_{ij} = \frac{A^n_{2,ij}}{4\Delta u \Delta w} \quad . \tag{2.25.g}$$

These are numerically solved for the following boundary conditions;

$$F^n_{i,0} = F^n_{i,2} \qquad \text{for } j=1, \tag{2.26.a}$$

which gives the symmetry at w=0, and

$$F^n_{i,j} = 0 \qquad \text{for } i=1,\ i_{max} \text{ or } j=j_{max} \ . \tag{2.26.b}$$

The code to solve the finite difference equation and to calculate various physical quantities such as moments and wave intensities are summarized in Appendix B.

2.4 Numerical Results and Discussions

2.4.1 Numerical results

We will perform the calculations for parameters on the experiments with the NOVA II tokamak[5] : B_t = 10kG, $n_e = 5\times10^{12}\ cm^{-3}$, T_e = 100eV, and V_1 = 2V.

We start the calculations with a relevant initial distribution function of electrons as follows:[9,10]

$$F = F_0 + F_r; \tag{2.27.a}$$

$$F_0 = \pi^{-3/2}\exp[-x^2] \qquad \text{for } u<u_c, \tag{2.27.b}$$

$$F_r = A(u_c,w)\cdot\{u_0 u_c^2 \ln\frac{u^2}{u_c^2}\}^{-1} \times\exp\left\{-\frac{w^2}{u_c^2\ln\frac{u^2}{u_c^2}} - \frac{u^2}{u_0^2}\right\} \quad \text{for } u>u_c\ , \qquad (2.27.c)$$

where F_0 and F_r are the components of the bulk and runaway electrons of the distribution function, respectively. $A(u_c,w)$ is a function of the velocities to match smoothly the distribution function from the bulk electron region to the runaway region; u_c is a critical velocity, at which the electron distribution function is transformed from the bulk to the runaway in velocity space. The value of u_c is taken as 2 - 4. The velocity u_0 is a cutoff one, which is taken as 20. The above distribution function is modeled from the analytical results by Levedev, Kruskal and Bernstein.

Figure 2 shows the time evolution of contours of the electron distribution function during the process of the quasi-linear relaxation due to the anomalous Doppler resonance. It is seen from the figure that the distribution function first starts to be plateauedin the Cerenkov resonance region. Next, electrons in the anomalous Doppler resonance region are scatterred in pitch angle. The appreciable scattering gives rise to a quasi-isotropic distribution in the region, as shown in Fig.2. In the case, the effect of the pitch angle scattering becomes approximately steady in the higher velocity region by $\omega_{pi}t \simeq 200$. Figure 3 shows a

distribution function at ω_{pi} t=200. In the velocity region, $3 < u < 8$, the electrons form a plateau which is more flattened than that at the initial time. In the region, $u > 10$, the distribution function becomes isotropic due to the pitch angle scattering by the waves. The transition from the plateau to the isotropy takes place in the velocity region where the anomalous Doppler effect becomes insignificant. Figure 2 also shows a small peak near the maximum parallel velocity region. This is owing to the small quasi-linear effects in the velocity region. The peak appears in the stage when the pitch angle scattering pronouncedly takes place in the higher velocity region, and shifts gradually toward the more higher velocity region. Such phenomenon can be explained as follows: During the initial stage of the process there exists a certain velocity region near the maximum velocity, where the growth rates are negative. The resultant quasi-linear diffusion of electrons is very small because of the small noise level. On the other hand, the wave density behind the velocity region grows largely from the noise level. As a result, a 'residual' peak appears. The peak produced in this manner results in a positive slope in a certain velocity region. Therefore, the peak is unstable for excitations of waves. Figure 4 shows the time evolution of the parallel distribution function $\langle F \rangle$, which is obtained by integrating F over the perpendicular velocity space;

$$\langle F \rangle = 2\pi \int_0^{w_{max}} dw\, w\, F \quad . \tag{2.28}$$

The cases in Fig.4 are corresponding to those in Fig.2. As is seen from the figure, the plateau is pronounced in the region of $3 \lesssim u \lesssim 8$, while F drops off more rapidly above $u \sim 9$ than the initial one. At the same time, there is observed a bump near $u \simeq 8$ - 9. It is noted that the bump forms in the region where the quasi-linear effects are not significant.

In order to see the circumstance more clearly, we examine the wave spectra excited.

Figure 5 shows the contours of the wave intensity in the wavenumber space during the procces of the quasi-linear relaxation. The cases in Fig.5 are corresponding to those in Fig.3 and 4. At the very beginning of the process, the wave intensity is concentrated on the region of the very small k_z . With time, the intensity spectrum becomes dominated by the components with the wavenumbers of $k_z = 0.1\ k_D$ and $k_\perp = 0.12\ k_D$ as the quasi-linear relaxation develops, as is seen from Fig.5(a), 5(b) and 5(c). The waves with $k_z/k_\perp \simeq 0.8$ are strongly excited. This result is a good agreement with the analytical one which shows that the wave growth rate is maximum at $k_z/k_\perp = 1/\sqrt{2}$ due to anomalous Doppler resonance. In Fig.5(d), we see that the spectrun again becomes broader toward the large wavenumber; other peaks also appear in the spectrum. This is because the resonance points shift toward the lower parallel velocity as the electrons are scatterred back-

ward. This circumstance is seen more clearly in Fig.6, which shows spectra in the corresponding parallel velocity space. In each case in Fig.6, we distinguish the spectra corresponding to the Cerenkov and anomalous Doppler resonance regions. In Fig.6(a), we see that the spectra are dominated by the components corresponding to the high velocity region, $u > 15$. This is because the waves resonate with the electrons in the high parallel velocity region via the anomalous Doppler effect. We also see the sharp peak near the maximum parallel velocity. This peak is related with the small residual bump as previously described ; the peak is owing to the positive slope around the bump. As the quasi-linear ralaxation develops sufficiently, the spectrum becomes rather broad in the profile. The sharp peak near u_{max} disappears in Fig.6(b). Some other peaks appear in the lower parallel velocity region. We have the peaks at $u \simeq 7$ and 9 in the case of Fig.6(b). Their locations are corresponding to the plateau region. In the region, the derivative $\partial F/\partial u$ is negligibly small, while F itself increases as the electrons are scattered into the region. The waves grow in the plateau region since the growth rate due to the anomalous Doppler resonance is proportional to F itself.

2.4.2 Discussion

One important result investigated in the published works is a formation of a bump in the tail of the integrated distri-

bution function at the sufficiently developed stage of the quasi-linear process. Such a bump can cause another quasi-linear relaxation with resultant excitation of waves near lower-hybrid and/or ion plasma frequencies. This may bring about intense ion heating as observed in the TM-3 experiments. When a special propagating angle ,for example, $k_z/k = 1/\sqrt{3}$ is chosen for the waves, there can exist a gap region in velocity space. The electrons in the region are offresonance. The existence of such gap region is essential to the formation of the bump. The physical picture is as follows: When the electrons are scattered in pitch angle due to the anomalous Doppler resonance, they move toward the lower parallel velocity region and arrive in the region without any quasi-linear effect. If there is no other effect except for the quasi-linear effects, the electrons sequentially scattered from the higher velocity region pile up in the velocity region. Consequently, a bump forms in the gap region.

However, the circumstance can be changed when the waves are excited dependently upon the propagating angle.[11] In the present case, the spectra of the excited waves are sufficiently broad in wavenumber space, resulting in an intersection of both the resonance regions, as is shown in Fig.7. As a result, the scattered electrons cannot remain in the region unlike the case above-mentioned. Sequentially the electrons diffuse toward the more lower velocity region due to the Cerenkov resonance, until they establish a plateau with more negligible $\partial F/\partial u$. Only after

that, a bump can appear at the edge of the plateau. At the same time, the waves become again unstable in the corresponding plateau region, and becomes more broader in the spectrum. Of course, the last picture related with the plateau may be modified when taking into account the influence such as the Coulomb collisions since the effects may tend to destroy the plateau. In our present study, emphasis is mainly devoted to the quasi-linear effect on the electron distribution function, especially, with the broad wave spectra. We will examine a system with the collision effects in the next chapter.

2.5 Conclusion

Thus we have numerically studied the dynamics of the runaway electrons in velocity space under the influence of the quasi linear effect due to the waves. The results are as follows :

1) The distribution function starts to change in the lower velocity region where the Cerenkov resonance are predominant. Then as the plateau grows in this region, the quasi-isotropic distribution function establishes in the higher velocity region where the anomalous Doppler resonance is essential to the quasi-linear effects.
2) When the spectra for the excited waves are enough broad to intersect each other for both resonances due to the Cerenkov

and anomalous Doppler effects, a plateau in the tail becomes more pronounced than that in the initial distribution function.

3) The excited wave energy density increases exponentially until the appreciable development of the distribution function terminates. The wave spectrum of the excited waves is dominated by the components with the wavenumbers of $k_z = 0.1\ k_D$ and $k_\perp = 0.12\ k_D$ after $t = 200\ / \omega_{pi}$. Sequentially, the spectrum again becomes broader toward the large k since the resonance points shift toward the lower parallel velocity.

References

1) G.A.Bobrovskii, et al.: MATT-TRANS 92 (1969)

2) EQUIPE TFR: Nucl.Fusion 16(1976) 473

3) V.S.Vlasenkov, V.M.Leonov, V.G.Merezkhin and V.S.Mukhovatov: Nucl.Fusion 13(1973) 509

4) V.V.Alikaev, K.A.Razumova and Y.A.Solokov: Sov.J.Plasma Phys. 1(1975) 303; Sov.-Phys.-Tech.Phys. 20(1975)

5) T.Michishita et al.: J.Phys.Soc.Jpn. 47(1979) 1035; ibid 50 (1981) 2720

6) V.V.Parail and O.P.Pogutse: Nucl.Fusion 18(1978) 303; Sov.J.Plasma Phys. 2(1976) 228

7) J.Killeen and K.D.Marx, 'Methods in Computational Physics', ed. B.Alder, S.Fernbach, and M.Rotenberg, vol.9 (1970)

8) R.C.Davidson, 'Methods in Nonlinear Plasma Theory', Academic Press. New York-London

9) A.N.Levedev: Sov.Phys.-JETP 21 (1965) 931

10) M.Kruskal and Ira.B.Bernstein: Princeton Plasma Physics Laboratory Report MATT-Q-20(1962)

11) C.F.Kennel and F.Engelmann; Phys. Fluids 9 (1966) 2377

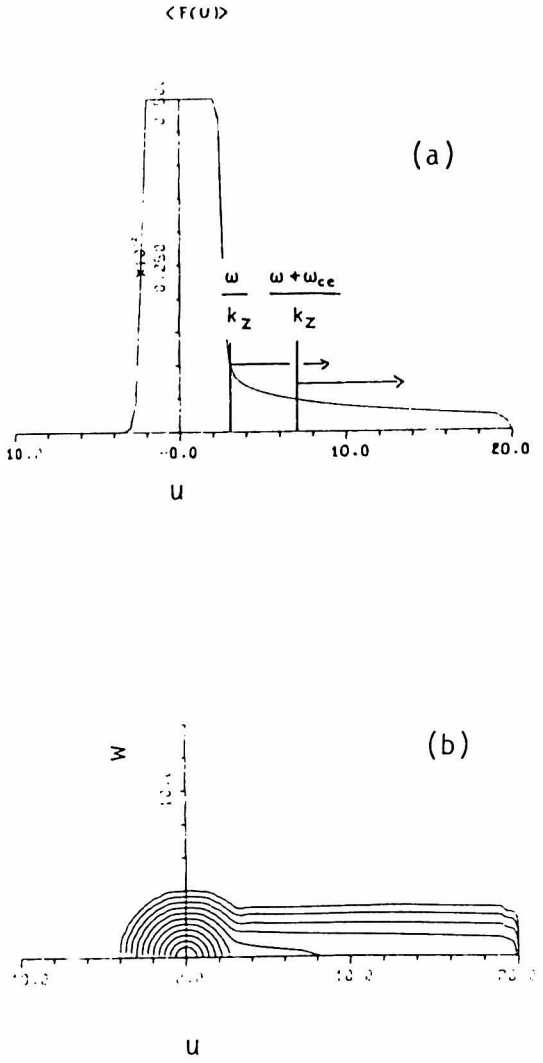

Fig.1. Anisotropic distribution function of electrons and corresponding regions in velocity space of Cerenkov and anomalous Doppler resonances. The distribution function is corresponding to the initial distribution function employed in the present study. (a) ; the parallel distribution function. (b) ; the contours map.

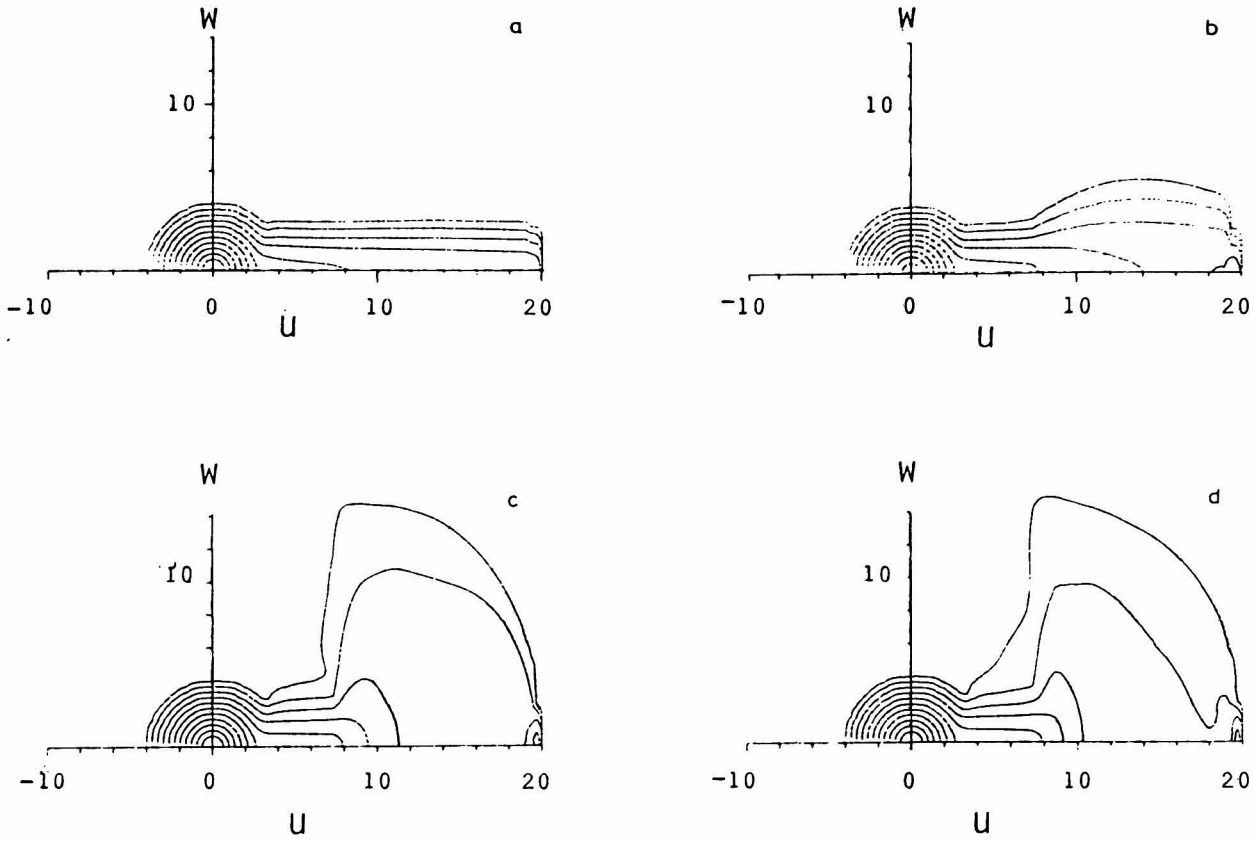

Fig.2. Time development of contours of the electron distribution function of due to excitation of the high frequency waves via anomalous Doppler resonance. The magnitude for each curve is corresponding to $f_j=\pi^{-3/2}\exp[-(j\cdot\Delta x)^2]$, where $\Delta x=1/3$. From (a) to (e), the distribution function are those at $t=200/\omega_{pi}$ (a), $250/\omega_{pi}$(b), $300/\omega_{pi}$(c), and $330/\omega_{pi}$(d).

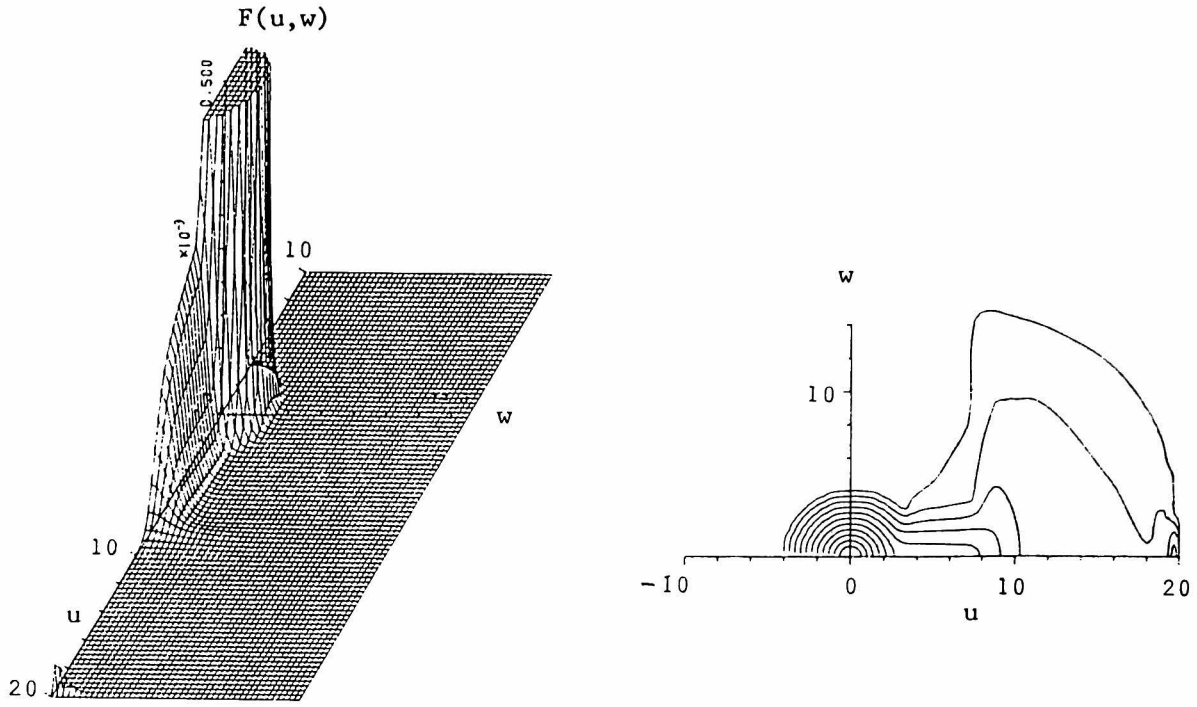

Fig.3. The distribution functions and contours at $t=330/\omega_{pi}$.

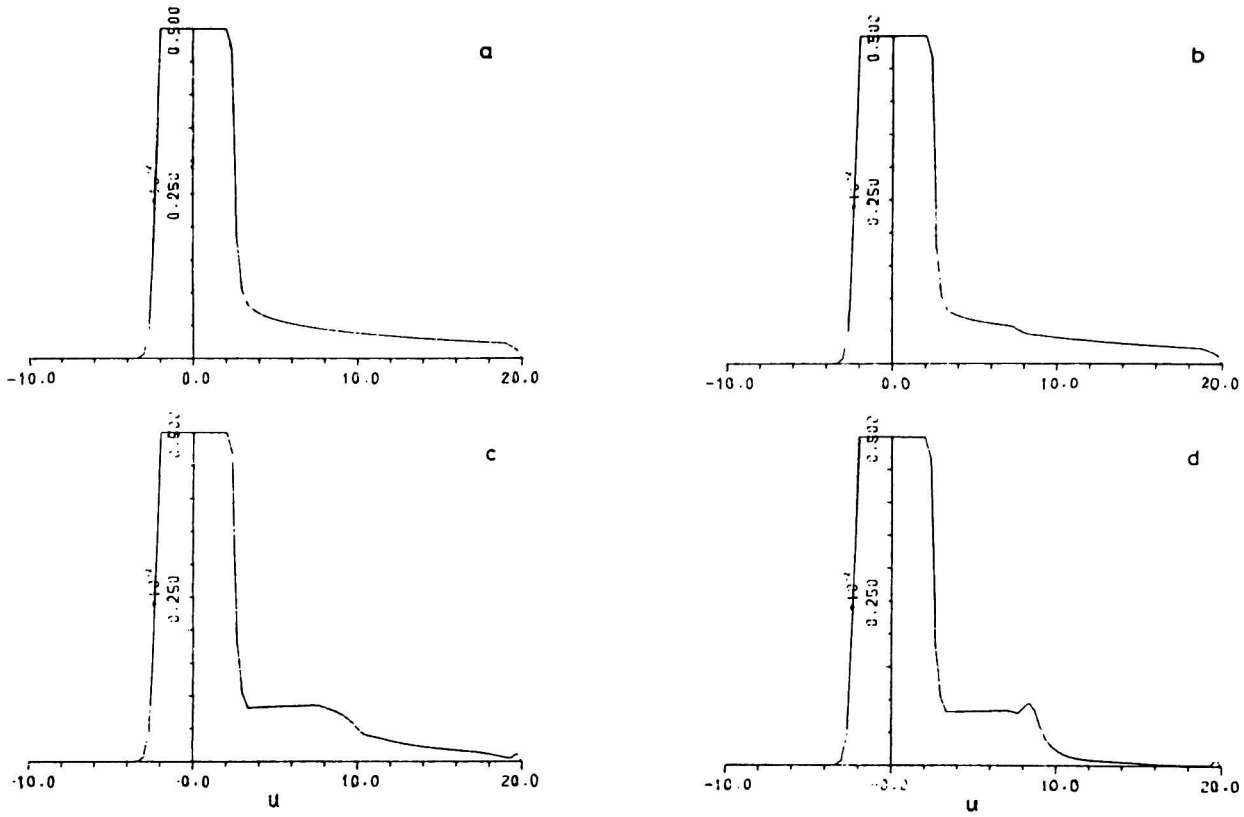

Fig.4. Time development of the parallel distribution function. Each case is corresponding to that shown in Fig.2.

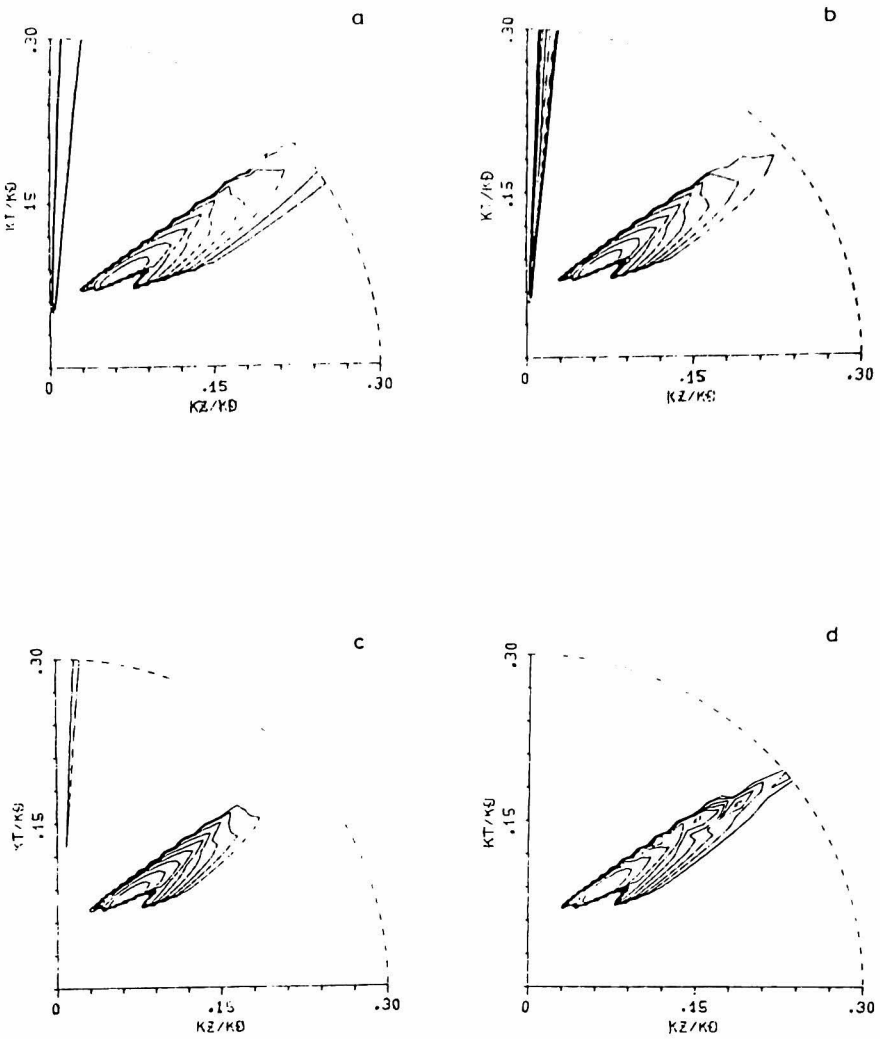

Fig.5. Time development of equi-level lines of the spectrum intensity in wavenumber space during time corresponding to that in Fig.2. The magnitude for each level is corresponding to $W_k = W_{max} \cdot \exp(-k \cdot \Delta W)$, where $\Delta W = 0.5$. Note that at each time, the level values are different from the previous time.

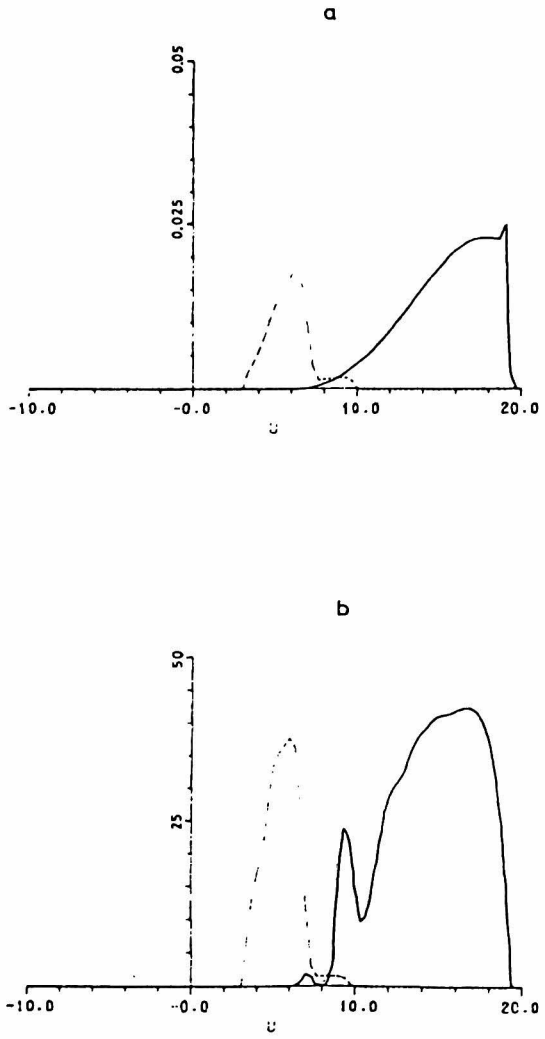

Fig.6. The wave intensities in the corresponding velocity regions of the Cerenkov and anomalous Doppler resonances. Both the effects intersect with each other in the region of $7 < u < 10$.

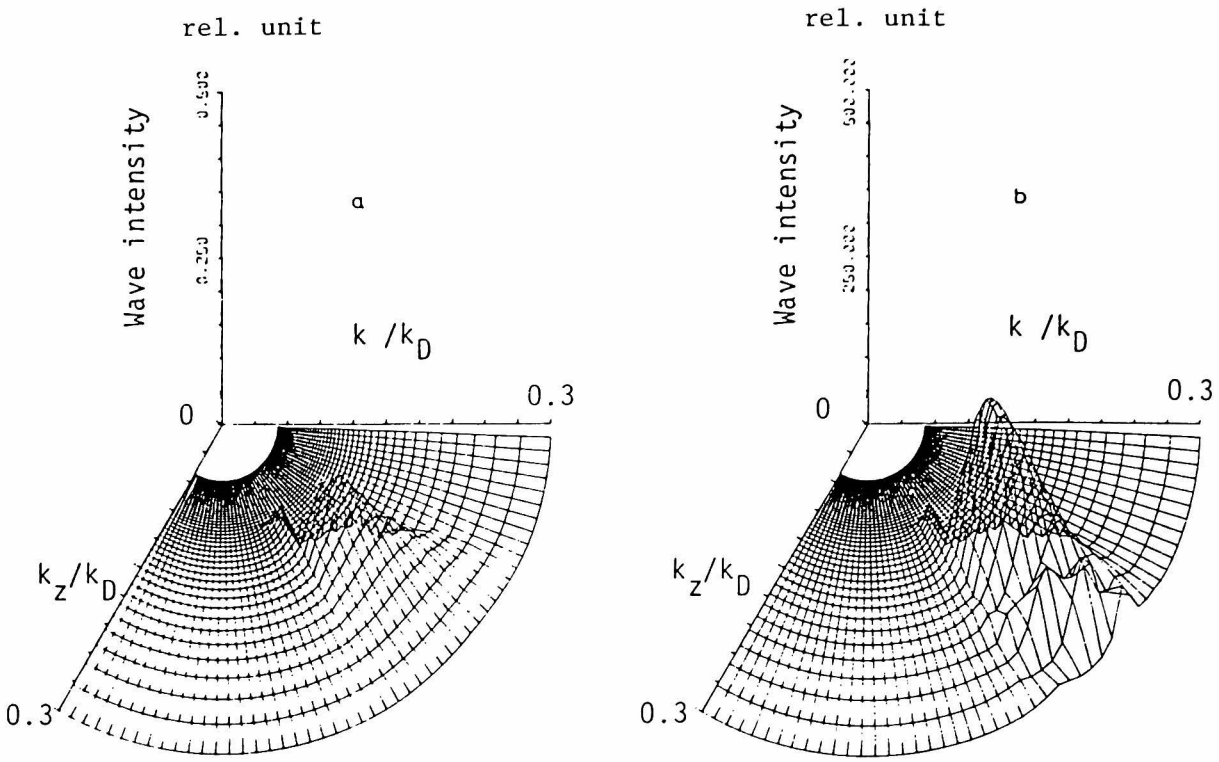

Fig.7. The wave spectral profiles in wavenumber space, which are corresponding to those in Fig.6.

Chapter 3 Relaxation in Energy of Runaway Electrons due to Excitation of High Frequency Waves

3.1 Introduction

In this chapter, we study relaxation of runaway electron energies due to excitation of high frequency waves by numerically simulating the time development of the electron distribution function. Recently the relaxation of runaway electron energies due to the plasma waves have been studied based on the quasi-linear theory.[1-7] Such relaxation phenomena are frequently observed in the low density discharges of the tokamak operations[8-11] and in the current drive experiments by applying the lower-hybrid-wave.[12,13]

Parail and Pogutse showed analytically that the relaxation is due to the interaction of the runaway electrons with the plasma waves, and reproduced the time development of the runaway electron energies by using the moment equations.[3] Choi and Horton examined in detail such time development of the macroscopic energies also by using the moment equations.[7] The moment method, however, provides no result of the detailed structure of the distribution function.

Papadopoulos et al. showed numerically a formation of a bump in the tail due to the anomalous Doppler resonance by using the one dimensional Fokker-Planck equation combined with a quasi-linear

term.[5] Furthermore Hui and Wisnor developed the investigation by using the two-dimensional Fokker-Planck equations.[6] Nevertheless, no detailed numerical results are avaiable about the relaxation in energy as well as the structure of the distribution function.

For studying the relaxation of the runaway electron energies, we use the quasi-linear equations combined with a Fokker-Planck collision term. In the present calculations, we choose the plasma parameters of the NOVA-II tokamak; B_t=10 kG, n_e=5x10^{12} cm^{-3}, and T_e=100 eV.[11] Under these conditions, the Coulomb collision time scale $t_{Coul.}$ is of the order of 10^{-6} sec, while the wave growth time scale is of the order of 10^{-8} sec. Simulation is performed until the system reaches a steady state after a period several times as long as the time scale $t_{Coul.}$ It may be worthy to notice that in the presence of a static electric field the collisions no longer establish a steady Maxwellian distribution because of the runaway phenomenon of the electrons ; thus we obtain a quasi-steady distribution.

The theoretical model for the computer simulation is described in the following section. The numerical method and results are given in Section 3. The final section is devoted to conclusions.

3.2 Theoretical Model

In the present study, we make the non-relativistic approximation for runaway electrons in a uniform plasma. It is also assumed that the velocity distributions of electrons and ions of the background species

are Maxwellians with equal and constant temperature, i.e. $T_0=T_e=T_i$. Although these assumptions are not self-consistent themselves, they lead us to the numerical expediency. The latter linearizes the Fokker-Planck collision term. This provides a model of a Maxwellian heat-bath of the temperature T_0, which may bring about a cooling effect.

The electric field acts tolet some electrons run away. This brings about less accuracy in determining the Fokker-Planck term when the calculations are continued until the characteristic collision time, $t_{Coul.}$. In order to compensate the runaway loss in the system, we introduce a source term, $S_0 \cdot \delta(v)$, to the kinetic equation. The source term will be determined self-consistently to balance the electron loss in the lower velocity region. Then the quasi-linear equation governing the electron distribution function is given by

$$\frac{\partial f}{\partial t} = \frac{e}{m} E_0 \frac{\partial f}{\partial v_z} + \left(\frac{\partial f}{\partial t}\right)_{QL} + \left(\frac{\partial f}{\partial t}\right)_{FP} + S_0 \delta(v) \qquad (3.1)$$

Here the first term on r.h.s represents the force term due to the toroidal electric field E_0, the second the quasi-linear diffusion term, the third the Fokker-Planck collision term, and the last the source term.

For the interaction of the runaway electrons with the plasma waves of $\omega_k = \omega_{pe} k_z/k$, only the Cerenkov and anomalous Doppler resonances are taken into account, since it is assumed that the ruaway electrons form a long tail in the distribution function. Then the

quasi-linear term becomes

$$\left(\frac{\partial f}{\partial t}\right)_{QL} = \frac{\partial}{\partial v_z}\left(D_c \frac{\partial f}{\partial v_z}\right) + \left(-\frac{\omega_{ce}}{k_z v_\perp}\frac{\partial}{\partial v_\perp} + \frac{\partial}{\partial v_z}\right) D_a \times \left(-\frac{\omega_{ce}}{k_z v_\perp}\frac{\partial}{\partial v_\perp} + \frac{\partial}{\partial v_z}\right) f \quad , \tag{3.2}$$

where

$$D_c = 8\pi^2 \frac{e^2}{m^2} \int dk \frac{k_z^2 \varepsilon_k}{k^2} \delta(\omega_k - k_z v_z) \quad , \tag{3.3}$$

$$D_a = 8\pi^2 \frac{e^2}{m^2} \int dk \frac{k_\perp^2 v_\perp^2}{4\omega_{ce}^2} \varepsilon_k \delta(\omega_k + \omega_{ce} - k_z v_z) \quad , \tag{3.4}$$

$$\varepsilon_k = \frac{|E_k|^2}{4\pi} \tag{3.5}$$

and

$$\gamma_k^{LN} = \pi \frac{\omega_k}{n_e}\frac{\omega_{pe}^2}{k^2} \int dv \frac{\partial f}{\partial v_z} \delta(\omega_k - k_z v_z) + \pi \frac{\omega_k}{n_e}\frac{\omega_{pe}^2}{k^2} \int dv \frac{k_\perp^2 v_\perp^2}{4\omega_{ce}^2} \times \left(-\frac{\omega_{ce}}{k_z v_\perp}\frac{\partial f}{\partial v_\perp} + \frac{\partial f}{\partial v_z}\right) \delta(\omega_k + \omega_{ce} - k_z v_z) \quad . \tag{3.6}$$

In the above expression, ε_k is the energy intensity of the wave with the wavenumber k, γ_k^{LN} the linear growth rate, D_c the quasi-linear diffusion coefficient due to the Cerenkov resonance, and D_a that due to the anomalous Doppler resonance. In the derivation, we have

employed such approximation that the electron Larmor radius r_{eL} is sufficiently smaller than the perpendicular wavelength, i.e. $k_\perp r_{eL} \ll 1$, which assures the expressions of $J_0 \simeq 1$, $J_1 \simeq k_\perp v_\perp / 2\omega_{ce}$, and $J_n \simeq 0$ for $n \geq 2$.

As is well known, the quasi-linear approximation is applicable only to the early stage in which the wave energy densidy is less than the particle energy density. As the wave energy density increases with the linear growth rate, non-linear effects will become appreciable between the waves. Such non-linear mechanisms have been investigated in connection with mode-mode coupling interactions.[21,22] At present, however, we have as yet no rigorous quantitative theory for the non-linear mechanism. Here we use a phenomenological approach for the non-linear effect. This is done by adding a non-linear damping term to the wave equation. Then we have the following wave equation;

$$\frac{\partial \varepsilon_k}{\partial t} = 2\gamma_k^{LN} \varepsilon_k + \gamma_k^{NL}(\varepsilon_k)\cdot\varepsilon_k - \gamma_{Coll.} \tag{3.7}$$

where

$$\gamma_k^{NL} = -\beta\omega_k \varepsilon_k \tag{3.8}$$

and

$$\gamma_{Coll.} = \nu_{ei} \tag{3.9}$$

The first term represents the linear growth, the second the non-linear growth, and the last the damping due to the electron-ion collisions.

As regards the non-linear effect, it is assumed that the parameter depends upon the asymptotic wave energy density. In the limit of low wave energy density, the second and the last terms can be neglected in eq.(7), which is the quasi-linear approximation. For higher wave intensity, the intensity saturates at the level, $\varepsilon_k^{sat} = 2\gamma_k^{LN} / \beta\omega_k$, provided that the collisional damping is not significant.

It should be noted that although we have been forced to adopt a phenomenological approach to the non-linear effect, the approach is not less suitable than other approaches which do treat the non-linear effect 'exactly' and are computationally more time-consuming. The reason is that the development of the distribution function depends basically upon the width in k-space of the spectra and rather insensitive to the other spectral detail. Furthermore, considering the alternative approach which, for example, treats the non-linear effect exactly based upon the three wave decay interaction, we are demanded on the other several important limitations; the dispersion relation must be such that the laws of conservation of momentum and energy can be satisfied simultaneously at discrete surfaces in momentum space, the interaction between the waves must provide an additional dissipation in momentum space, and so forth. In practice, however, some of the limitations are often infringed for the strong non-linear interactions between the waves.[16,17] Thus in the absence of the rigorous theory, such 'exact' treatment of the non-linear term may not yield more accurate calculated results.

The linearized Fokker-Planck collision term is written in the

cylindrical coordinates (u,w) as follows:[18]

$$\left(\frac{\partial f}{\partial t}\right)_{FP} = \sum_b \frac{\Gamma_{eb}}{v^2}\left\{\mathcal{L}_d\left[A_{eb} + \frac{v_b^2}{2v} B_{eb}\mathcal{L}_d\right] + \mathcal{L}_p\left[\frac{v^2}{v} C_{eb}\mathcal{L}_p\right]\right\} f, \quad (3.10)$$

where $\Gamma_{eb} = 4\pi e^4 Z_b n_b \ln\Lambda/m$, (the symbol b denotes the species of the background plasma particles.) ,

$$\mathcal{L}_d = \frac{v_z \partial}{v\ \partial v_z} + \frac{v_\perp \partial}{v\ \partial v_\perp} \quad , \quad (3.11.a)$$

and

$$\mathcal{L}_p = -\frac{v_z \partial}{v_\perp \partial v_\perp} + \frac{\partial}{\partial v_z} \quad . \quad (3.11.b)$$

The coefficients of A_{eb}, B_{eb}, and C_{eb} are

$$A_{eb} = \frac{m}{m_b}\left\{-\frac{v}{v_b}\frac{2}{\sqrt{\pi}}\exp\left[-\frac{v^2}{v_b^2}\right] + \Phi\left(\frac{v}{v_b}\right)\right\}, \quad (3.12)$$

$$B_{eb} = \frac{m_b}{m} A_{eb}, \quad (3.13)$$

$$C_{eb} = \frac{1}{2}\left\{\left(1 - \frac{v_b^2}{2v^2}\right)\Phi\left(\frac{v}{v_b}\right) + \frac{1}{2v}\frac{d\Phi}{dv}\right\}, \quad (3.14)$$

respectively, where

$$\Phi(x) = \frac{2}{\sqrt{\pi}}\int_0^x dy \exp[-y^2] \quad . \quad (3.15)$$

In calculating the coefficients, we assume, as is mentioned earlier, the heat-bath of temperature T_0 to linearlize the collision term.

3.3 Numerical Method and Results

3.3.1 Method

For the adopted plasma parameters, the characteristic collision time is at least two orders in magnitude greater than the wave growth time. In performing the numerical calculations, we divide the whole process into the following two stages: One is the initial stage, and the other is the asymptotic stage.

In the initial stage where the wave grows up exponentially, we introduce the dimensionless variables,

$$\tau_1=\omega_{pi}t, \quad u=v_z/v_e, \quad w=v_\perp/v_e, \quad x=(u^2+w^2)^{1/2},$$
$$\hat{\nu}_{c,a}=D_{c,a}/\omega_{pi}v_e^2, \quad F=f\cdot v_e^3/n_e. \tag{3.17.a}$$

and simulate the time development of the wave. Then we assume that at the stage the wave energy builds up and becomes saturated; it starts to decay due to the collisions. After the period, we continue to calculate by using the following variables;

$$\tau_2=\nu_s t,\ u=v_z/v_e,\ w=v_\perp/v_e,\ x=(u^2+w^2)^{1/2},$$
$$\hat{D}_{c,a}=D_{c,a}/\nu_s v_e^2,\ F=f\, v_e^3/n_e\ . \qquad (3.17.b)$$

The kinetic equation is transformed into a set of finite difference equations and solved by using the ADI method. The number of grids ia 91×46 (u×w) with a space of 0.33 in both directions. The time steps are typically $\Delta\tau_1=0.05$ and $\Delta\tau_2=0.006$.

Once the distribution function is determined, we determine the perpendicular and parallel energies of the runaway electrons, $\hat{E}_\perp$ and $\hat{E}_{//}$, respectively, from the following eqations;

$$\hat{E}_\perp = \frac{\pi}{\hat{n}_r}\int_{u_c}^{u_{max}}\int_0^{w_{max}} dudw\ w^3 F\ , \qquad (3.18.a)$$

$$\hat{E}_{//} = \frac{\pi}{\hat{n}_r}\int_{u_c}^{u_{max}}\int_0^{w_{max}} dudw\ w\,u^2 F\ , \qquad (3.18.b)$$

where

$$\hat{n}_r = 2\pi\int_{u_c}^{u_{max}}\int_0^{w_{max}} dudw\ w\ F\ . \qquad (3.18.c)$$

Here u_c is the critical velocity of the runaway electrons. We distinguish the total electron energy $\hat{T}_e$, and its perpendicular and parallel components, $\hat{T}_{e\perp}$ and $\hat{T}_{e//}$, which are defined by

$$\hat{T}_e = \frac{1}{\hat{n}_e}\int d^3x\ \frac{1}{2}x^2 F\ , \qquad (3.19.a)$$

$$\hat{T}_{e\perp} = \frac{1}{\hat{n}_e} \int d^3x \ \frac{1}{2} w^2 F \quad , \tag{3.19.b}$$

$$\hat{T}_{e//} = \frac{1}{\hat{n}_e} \int d^3x \ \frac{1}{2} u^2 F \quad , \tag{3.19.c}$$

where

$$\hat{n}_e = \int d^3x \ F \quad . \tag{3.19.d}$$

The wave energy density is normalized by the electron energy density of n_0T_0 as follows;

$$W = \frac{1}{n_0T_0} \int d^3k \ \varepsilon_k \quad . \tag{3.20}$$

The source term in eq.(1) evaluated at intervals of 20 - 50 time steps.

3.3.2. Results

We start the calculations with the following distribution function;[19,20)]

$$F = F_0 + F_r; \tag{3.21.a}$$

$$F_0 = \pi^{-3/2} \exp[-x^2] \qquad \text{for } u < u_c \ , \tag{3.21.b}$$

$$F_r = A(u_c,w)\ [u_0 u_c^2 \ln(\frac{u^2}{u_c^2})]^{-1}$$

$$\text{xexp}\ [-\frac{w^2}{u_c^2 \ln(\frac{u^2}{u_c^2})} - \frac{u^2}{u_0^2}]\quad \text{for } u > u_c. \qquad (3.21.c)$$

Here F_0 and F_r are the distribution functions of the bulk and the runaway electrons, respectively; $A(u_c,w)$ is the coefficients to provide smooth transition at u_c from F_0 to F_r. The cutoff velocity u_0 and the critical velocity u_c are chosen to be 20 and from 2 to 4, respectively.

First we describe the results concerned with a typical case of the maximum wave energy density $W_m = 1.49 \times 10^{-2}$. In Figs. 1 and 2, we show the distribution functions at the initial state and those at $t = 1.4 \cdot \nu_s^{-1}$, respectively. Figure 1 shows a long tail of the runaway electrons in the parallel direction. In Fig.2(a), this tail is much flattened and stretched towards the perpendicular direction for $u>3$. The distribution is isotropic for higher velocities $u>10$; the electrons in this region are predominantly scatttered by the wave in pitch angle through the anomalous Doppler resonance. The parallel distribution shown in Fig.2(b), which is obtained by integrating the distribution function in Fig.2(a) with respect to the perpendicular velocity, presents evidently a plateau in the intermediate velocity region $3<u<8$. In this region, the runaway electrons diffuse towards the parallel direction through the Cerenkov resonance and are also scattered in pitch angle by the Coulomb collisions.

In Fig.3, we show log F as a function of the perpendicular energy $w^2/2$ for u=-3, 0, 3, 6, 9, and 12; the time is 0.004 for the case of Fig.3(a) and 1.4 for that of Fig.3(b). In the early stage, the distribution shows a steep down-slope for velocities up to 12, as is shown in Fig.3(a). In the asymptotic stage the distribution becomes flattened for u=12, while in the intermediate region the distribution apparently consists of two components; one is the bulk component with the steep slope and the other is the scattered runaway electron component with the flat slope. It may be worth to notice that the appearance of this flat component is due to the wave excited, and that the wave has no effect below u=3.

In Fig.4, we show log<F> against the parallel energy $u^2/2$. It can be seen from the figure that the parallel energy of the electrons, $\hat{T}_{e//}$, is higher for u>0 ($\hat{T}_{e//}$=1.15) than for u<0 ($\hat{T}_{e//}$=0.83).

In Fig.5, we show the time developments of the runaway electron energies, $\hat{E}_\perp$ and $\hat{E}_{//}$, in the initial stage, together with the accumulation of the wave energy density W_m. The wave energy density increases exponentially in the very biginning and gradually draws towards the asymptotic level, which is $W_m = 1.49\times10^{-2}$ in the case of Fig.5. The wave energy spectrum concentrates around the wave numbers of k_z/k_D=0.10 and $k_\perp/k_D$=0.12 at the times (a) and (b), while the nonlinear wave damping makes the spectrum broader at the time (c). Figure 6 also shows the time development of the energy components up to $t=3\cdot\nu_s^{-1}$. The fast rise time of $\hat{E}_\perp$, t=0.2 μsec, is due to the pitch angle scattering of the runaway electrons through the anomalous

Doppler resonance. The relatively slow decay of $\hat{E}_{//}$ is due to the small derivative $\partial F/\partial u$. Such relaxation leads to the isotropic in the energies, as is shown in Fig.7; the anisotropy is reduced with time.

Both the runaway electron energy and the total electron energy draw towards their respective asymptotic values after a sufficiently long lapse of time. These asymptotic values of the electron energies depend upon the asymptotic wave energy density W_m , as is shown in Figs.8, 9, and 10. The rise time of $E_\perp$ and the decay time of $\hat{E}_{//}$ also depend upon the asymptotic wave energy density. In Fig.8, we see that $\hat{E}_\perp$ takes on its maximum around $W_m = 10^{-1}$, where $\hat{T}_e$ presents transition to the significant low level. The rise time of $\hat{E}_\perp$ decreases rapidly with increase in W_m .

3.4 Conclusion

The present computer simulation has been performed on the relaxation of the runaway electron energies due to the electrons with the plasma waves. It has been found that the electron distriburion function reaches an asymptotic distribution by the time $t_{Coul.}$. In the initial stage the energy spectrum of the waves excited concentrates around the wave numbers of $k_z/k_D = 0.10$ and $k_\perp/k_D = 0.12$, which is due to the anomalous Doppler resonance. The spectrum is then broadened by the nonlinear effect.

In the asymptotic stage, the electron distributiuon function a-

bove u=3 becomes isotropic with a perpendicular energy 50 times as large as the background energy T_0. The relaxation process of the electron energy strongly depends upon the maximum wave energy density attained, W_m . For W_m less than 10^{-1}, the perpendicular energy $E_\perp$ increases with increase in the wave energy density W_m . For W_m exceeding 10^{-1}, the parallel energy $\hat{E}_{//}$ decreases with increase W_m , which is due to the slowing-down of the electrons. Typically, for $W_m \simeq 0.1$ the asymptotic value of the total electron energy $\hat{T}_e$ is 0.71 together with the parallel runaway electron energy $\hat{E}_{//}$ of 0.57.

Similar relaxation process have been observed in tokamak experiments with current drive by applying the lower-hybrid waves. The present method can be also applicable to these process by putting the electron-wave interaction into the Cerenkov term of eq.(2).

References

1) B.B.Kadomtsev and O.P.Pogutse: Sov.Phys.JETP 26(1968) 1146

2) V.D.Shapiro and V.I.Shevchenko ; Sov. Physics JETP 27 (1968) 635

3) V.V.Parail and O.P.Pogutse: Nucl.Fusion 18(1978) 303; Sov.J.Plasma Phys. 2(1976) 228

4) C.S.Liu and Y.C.Mok: Phys.Rev.Lett. 38(1978) 162

5) K.Papadopoulos, B.Hui and N.Winsor: Nucl.Fusion 17(1977)

6) B.H.Hui and N.Wisnor ; Phys.Fluids 21 (1978) 940

7) Duk-In Choi and W.Horton.Jr.; Plasma Physics 20 (1978) 903

8) EQUIPE TFR: Nucl.Fusion 16(1976) 473

9) V.V.Alikaev, K.A.Razumova and Y.A.Solokov: Sov.J.Plasma Phys. 1(1975) 303; Sov.-Phys.-Tech.Phys. 20(1975)

10) P.Brossier: Nucl.Fusion 18(1978) 1069

11) T.Michishita et al.: J.Phys.Soc.Jpn. 47(1979) 1035; ibid 50 (1981) 2720

12) T.Maekawa et al.; Physics Lett.85A (1981) 339

13) K.Ohkubo et al.; Nucl.Fusion 22 (1982) 203

14) J.Killeen and K.D.Marx, 'Methods in Computational Physics', ed. B.Alder, S.Fernbach, and M.Rotenberg, vol.9 (1970)

15) R.H.Fowler, J.D.Callen, J.A.Rome, and J.Smith; ORNL/TM-5487,1976

16) B.B.Kadomtsev, 'Plasma Turbulence', Academic Press. New York (1965)

17) V.N.Tsytovich, 'Non-Linear Effects in Plasma', Plenum Press. New York (1970)

18) M.N.Rosenbulth, W.M.MacDonald, and D.J.Judd; Phys.Rev. 107(1957) 1

19) M.Kruskal and Ira.B.Bernstein: Princeton Plasma Physics Laboratory Report MATT-Q-20(1962)

20) A.V.Gurevich; Sov.Phys.JETP 12 (1961) 904

21) I.H.Hutchison, K.Molvig and S.Y.Yuen: Phys.Rev.Lett.40(1978) 1091

22) I.Fidone, G.Ramponi and P.Brossier: Phys.Fluids 21(1978) 237

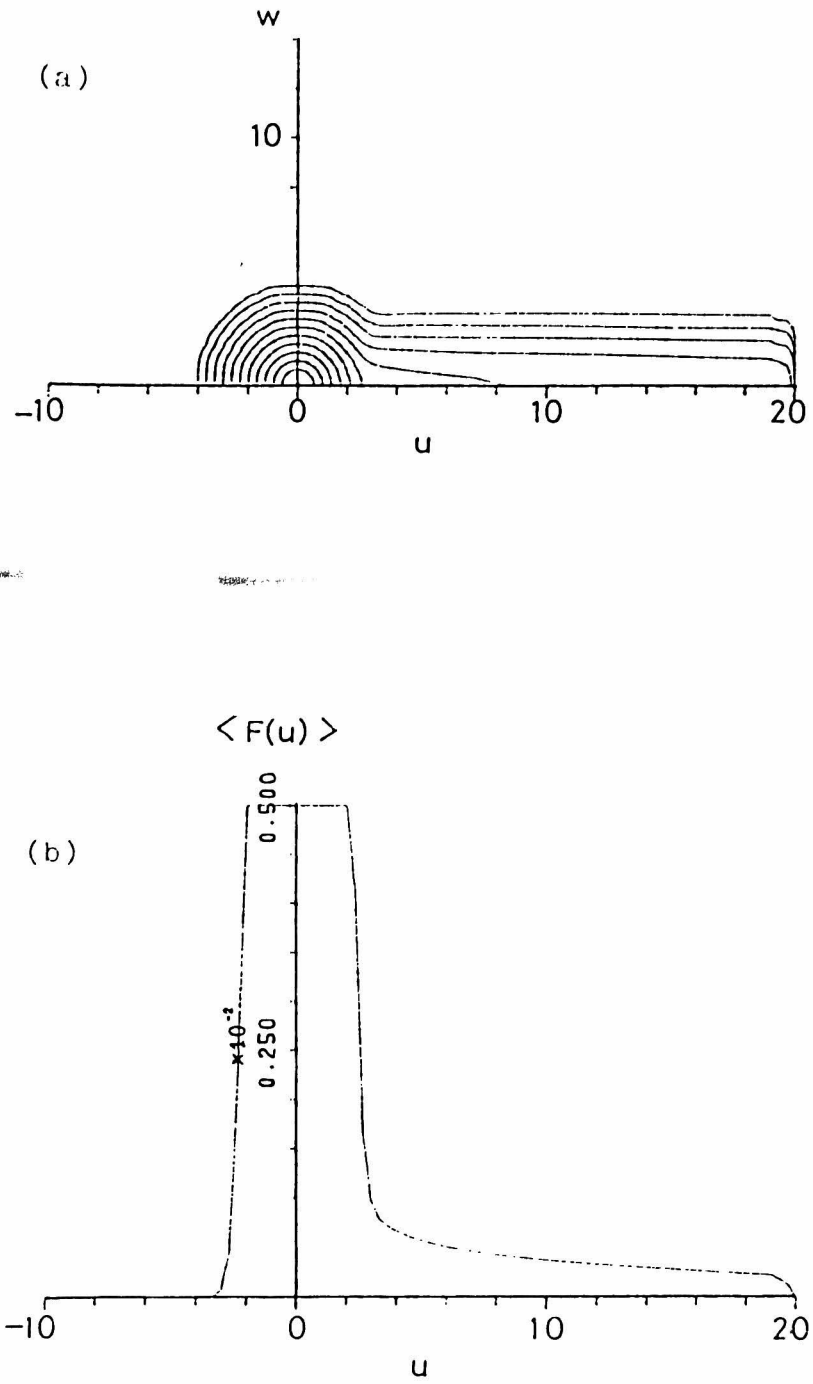

Fig.1. Initial distribution function of electrons; (a) - contour map. (b) parallel distribution function.

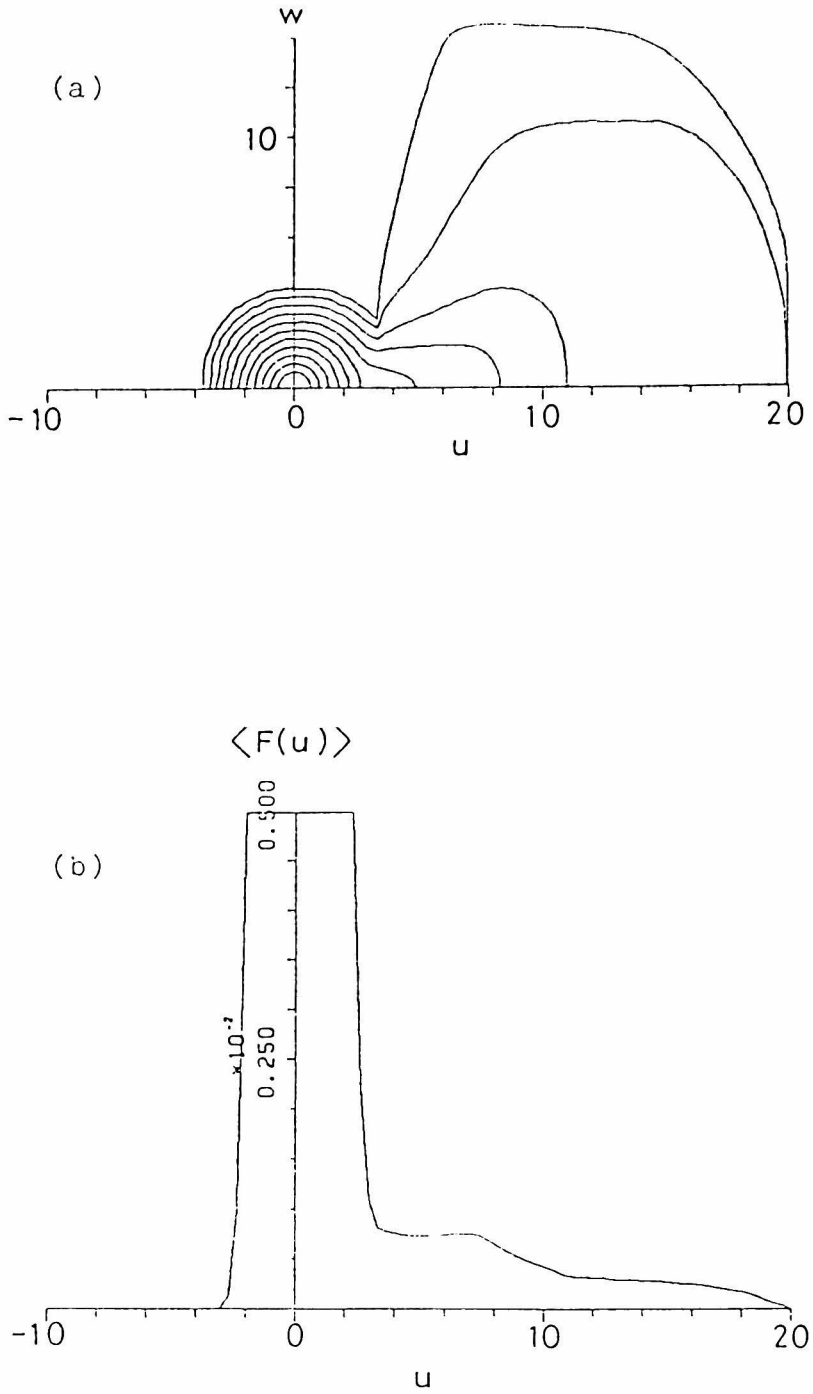

Fig.2. A distribution function of electrons at $\nu_s t=1.4$ as a result of the wave -particle interactions via Cerenkov and anomalous Doppler resonances.

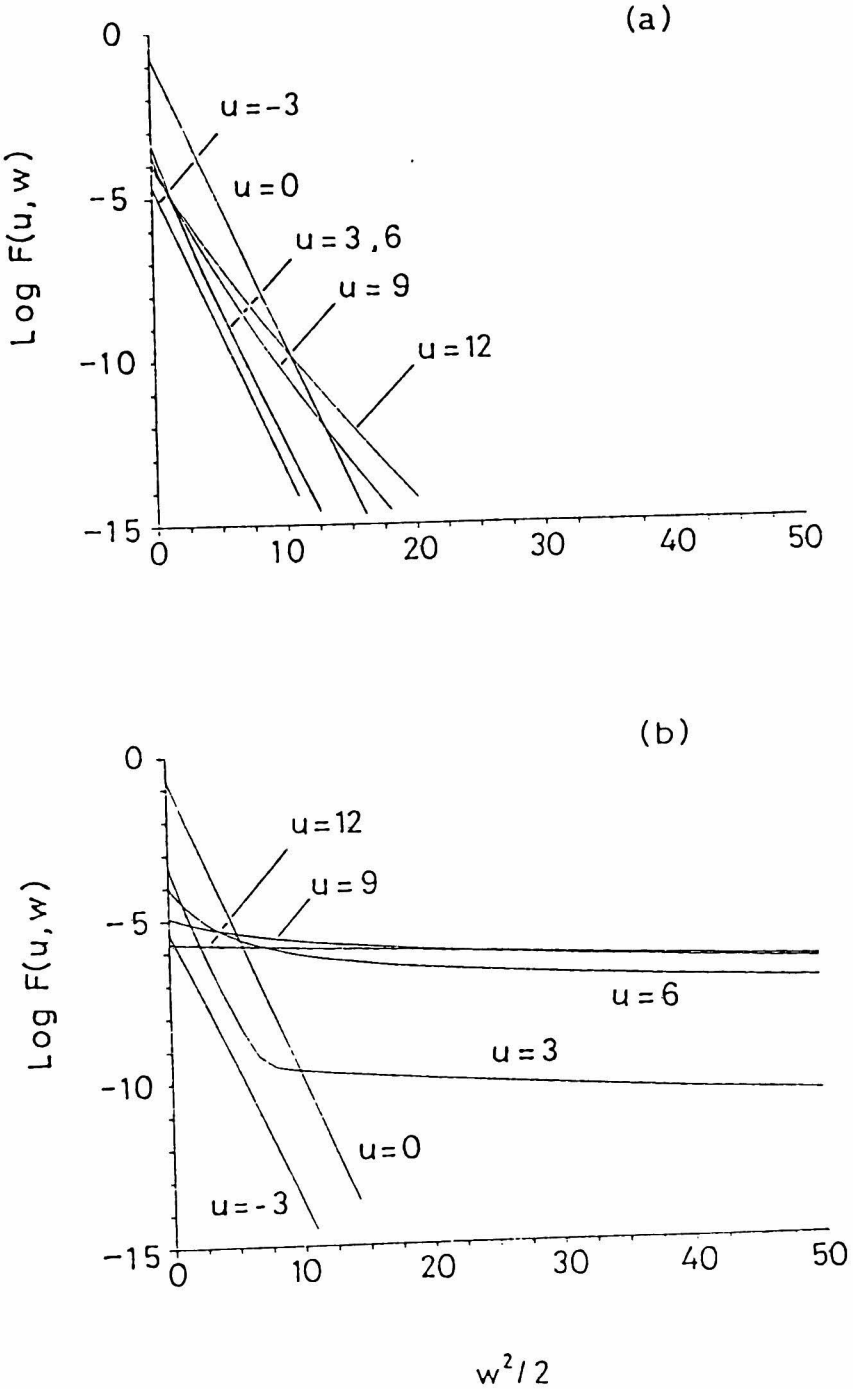

Fig.3. LogF(u,w) versus $w^2/2$ for values of u=-3,0,3,6, 9, and 12; (a) is for the case at $\nu_s t=0.004$ and (b) for the case at $\nu_s t=1.4$.

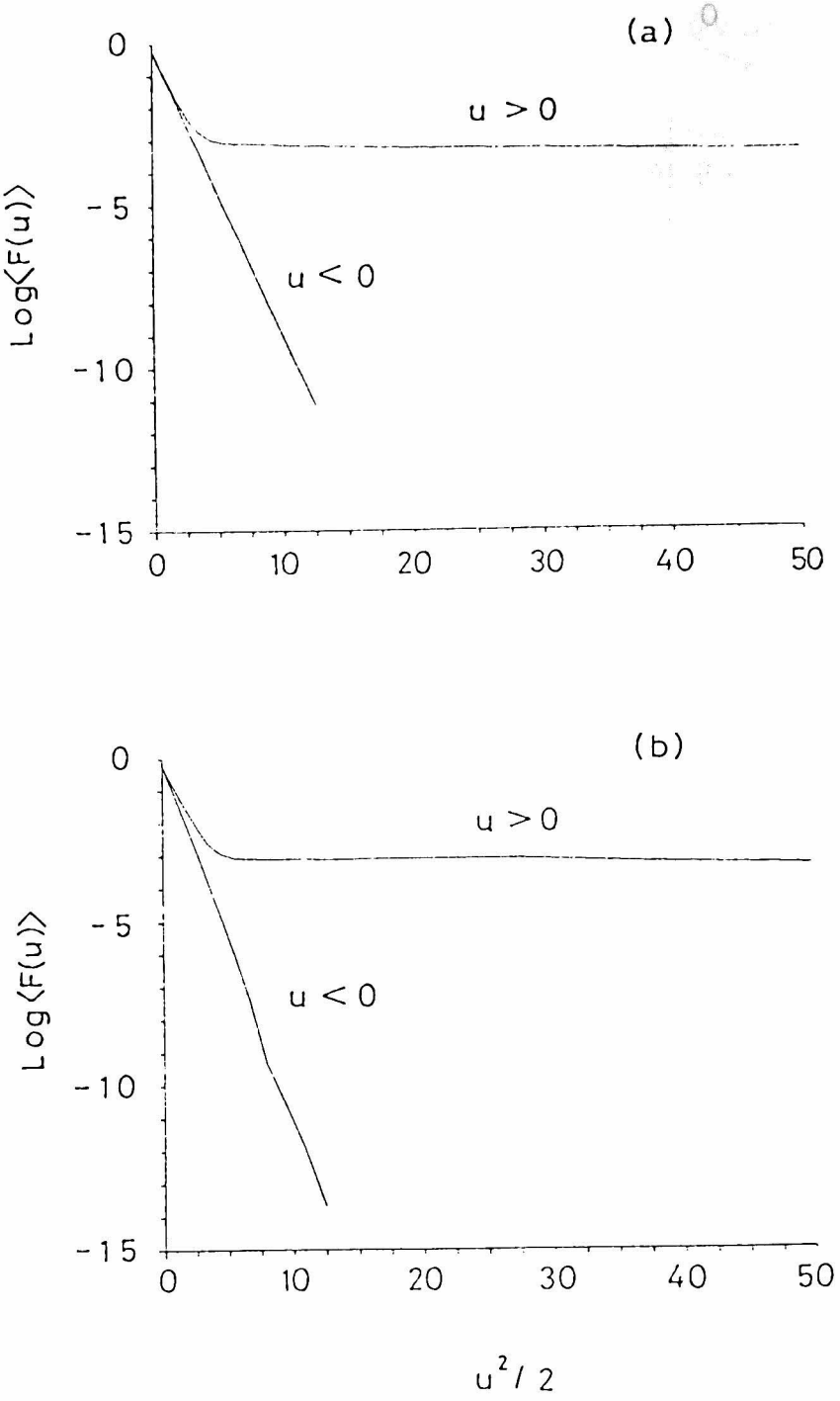

Fig.4. Log F(u) versus $u^2/2$; (a) and (b) are corresponding to those of Fig.2.(a) and 2.(b), respectively.

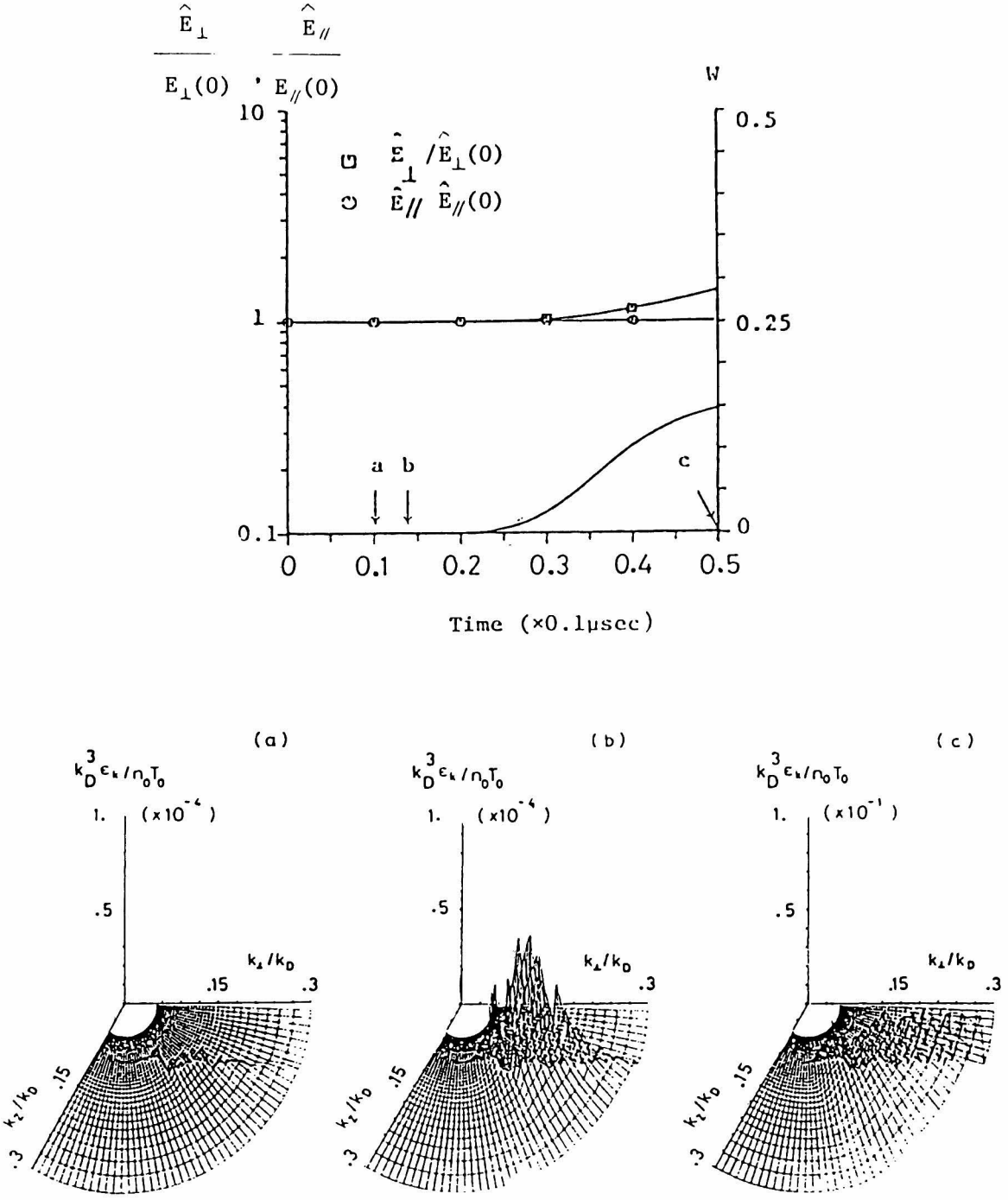

Fig.5. Typical time developments of $\hat{E}_\perp$, $\hat{E}_{//}$, and W in the initial stage. The lower shows the energy intensity spectra at the times (a), (b), and (c) in the upper. Note that each energy of the electrons is nornalized by its initial value.

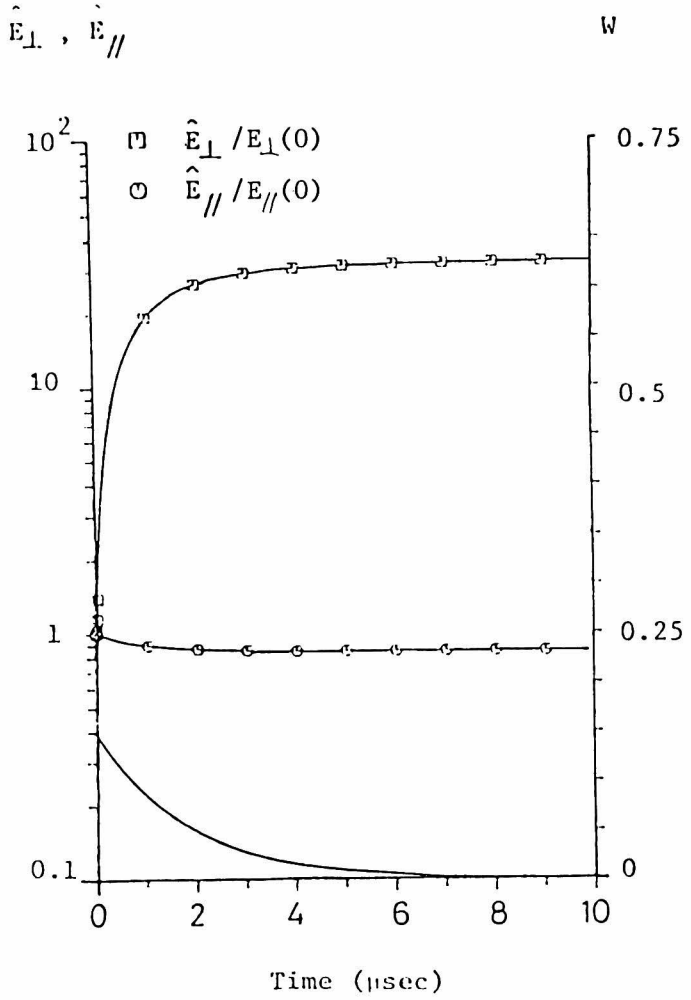

Fig.6. Typical time developments of $\hat{E}_\perp$, $\hat{E}_{//}$, and W until $\nu_s t = 2.8$.

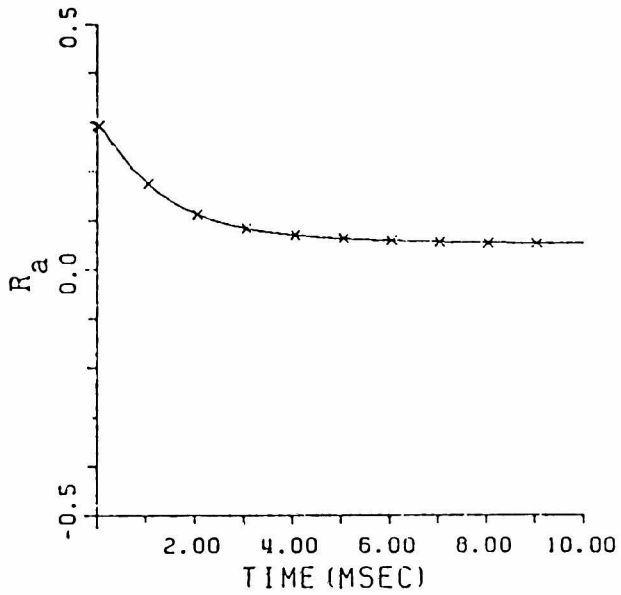

Fig.7. A time development of the anisotropy in energy ; $R_a = 1 - \hat{T}_{e\perp}/\hat{T}_{e//}$.

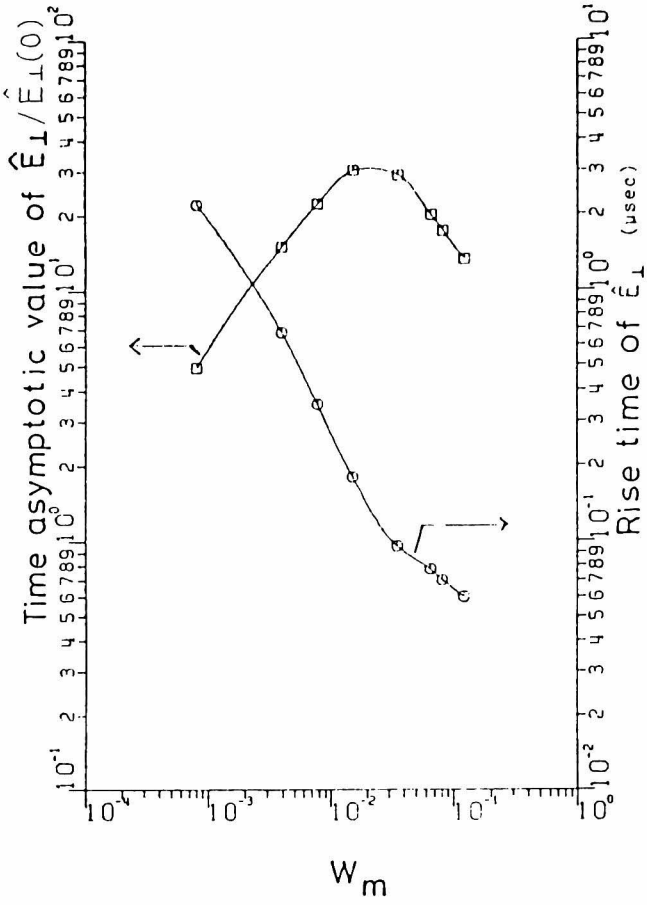

Fig.8. Wave energy dependence of the time-asymptotic value of $\hat{E}_\perp$, and that of its rise time t_r.

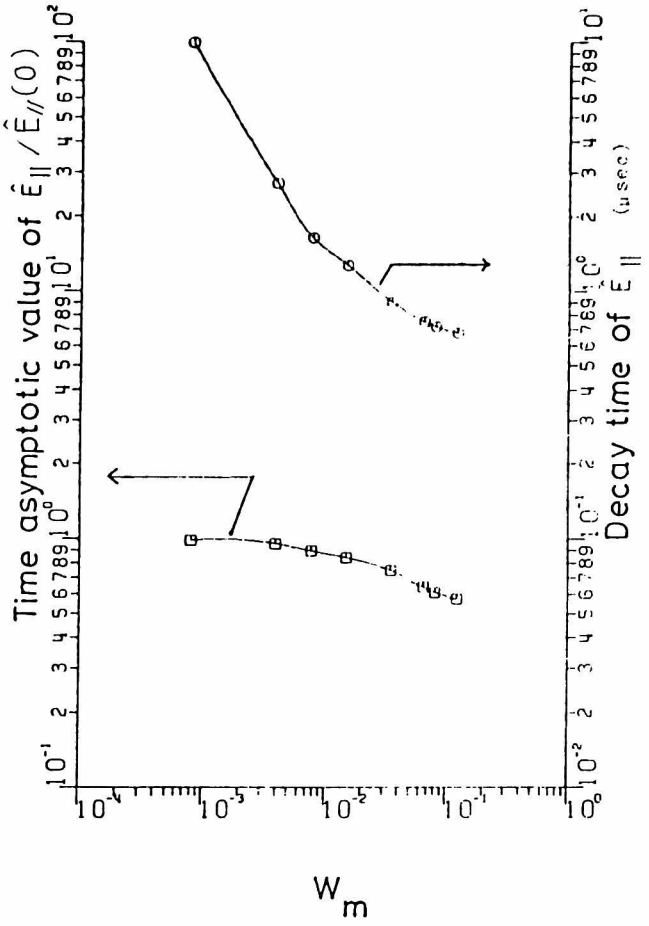

Fig.9. Wave energy dependence of the time-asymptotic value of $\hat{E}_{//}$, and that of its decay time t_d.

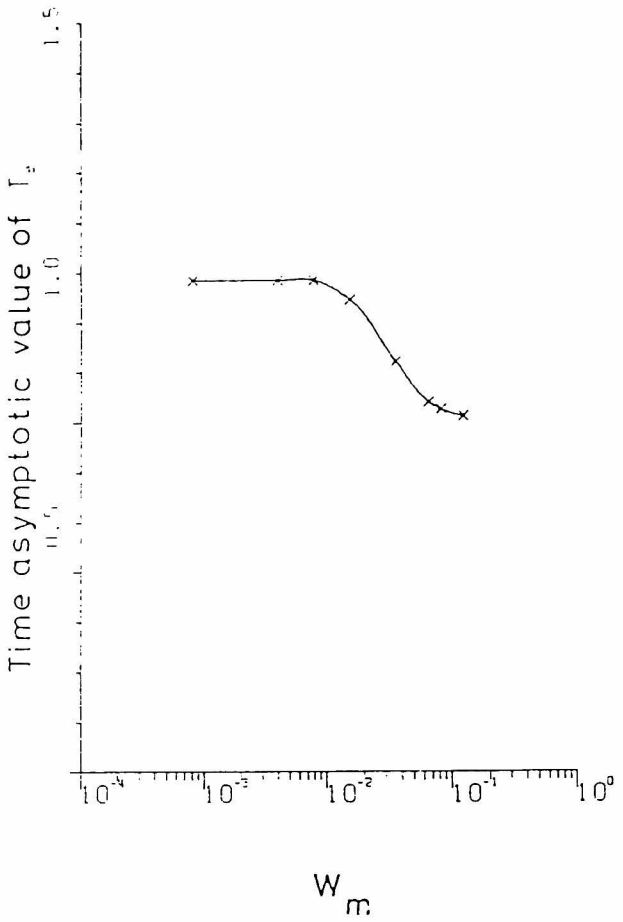

Fig.10. Wave energy dependence of the electron temperature $\hat{T}_e$.

Chapter 4 Instability Driven by Runaway Electrons in a Tokamak Plasma

4.1 Introduction

Instability driven by runaway electrons in tokamak plasmas, which is called 'runaway electron instability', has been studied by many authors not only for the fundamental plasma physics associated with the non-linear problem but also for the practical purpose such as the diagnostics, the further heating, and the maintenance of the devices. This instability frequently brings about a sawtooth oscillation in the one turn loop voltage when a tokamak is operated with low densities below 1×10^{13} cm^{-3}.[1-6] Recent experiments show that at the onset of the instability there occur a rapid increase in synchrotron radiation intensity[3-5] and a production of intense energetic ions.[2] The serious damage of the liners observed in T.F.R. is also regarded as a result of the bombardment of the runaway electrons repelled from the main plasma owing to the instability. Furthermore, the intense non-thermal radiation observed in a high density regime of the tokamak operations may be connected with the instability.[4,6,10,11]

Several models associated with the above-mentioned phenomena

have been considered. There is, however, a fundamental difference among the models on the 'initial' distribution of the runaway electrons; one has the positive slope tail or the bump, the other the monotonously decreased tail with velocity or the flat one.[7-12] In spite of the difference, each of them is in a reasonable agreement with the existent experiments. From such agreement, one expects that the models associated with the phenomena have evolved separately. Recent theories have shown that these phenomena can occur succesively during the whole stage of the instability;[9] there occurs an alternation of the monotonously decreased tail with the bump in the distribution function of the runaway electrons. As a result there occurs a relaxation in energy of the runaway electrons as well as a pitch angle scattering. In most of the experiments, emphasis is put on the pitch angle scattering. A significant feature of the above mentioned phenomena, however, is the relaxation in energy. The phenomena such as the production of the energetic ions, and the rapid escape of the runaway electrons from the main plasmas are expected to be a result of such relaxation. Also the repetition of the instability would not occur without the relaxation. In fact the experiments in TM-3 showed that the runaway electrons lost their energies by participating in the instability.[2] In the experiments the macroscopic quantities such as the diamagnetism and the displacement of the current channel were measured. Nevertheless it was hard to distinguish strictly the effect re-

sponsible for the runaway electrons from that for the bulk plasmas.

The principal purpose of the present work is to investigate the energy relaxation of the runaway electrons during the instability. For this purpose, the hard X-ray radiation measurement is done by using dual scintillation detectors with a fast time resolution. High frequency fluctuations are also detected in order to study the impelling motive of the relaxation observed. The next section describes the experimental setup and the results on the instability. In Section 3, discussions are given. The final section is devoted to summary on the results.

4.2 Experimental Setup

The experiments were performed with a small tokamak NOVA-II.[11] The major radius is R = 30 cm and the minor (limiter bore) a = 6 cm. It was operated with the toroidal magnetic field intensity B_t = 5-10 kG and with hydrogen or helium gas filled as a working gas with pressure $P_f < 2\times10^{-4}$ Torr. The gas was injected with a fast acting valve. Discharges were monitored with macroscopic quantities such as the loop voltage V_l, the plasma current I_p, the horizontal and vertical displacements of the current channel, $I_p \cdot \Delta_R$ and $I_p \cdot \Delta_Z$, respectively, and the diamagnetic signal $\Phi_{dia.}$. The torus and the arrangement of the diagnostics are shown in Fig. 1.

The line average electron density was measured along a vertical chord with a 6-mm interferometer.

Microwave radiations were detected at 10- and 50-GHz bands through a quartz window in the side wall of the vacuum chamber. The radiations detected were extraordinary modes.

Hard X-ray radiation due to the bombardment of the runaway electrons onto the molybdenum limiter and/or the stainless steel chamber wall was measured with dual plastic scintillation detectors. The scintillators have a short decay time, 4 nsec, and a large figure of merit, ~20. This is useful for studying phenomena with fast rise times, compared with detectors with NaI(Tl)-scintillators. In order to determine average energies of the runaway electrons, the dual scintillators were located along a ray path, and lead absorber of Pb was inserted between them, as shown in Fig. 1.

A Langmuir electrical probe was used as an antenna to detect high frequency fluctuations in the frequency range of 400- to 1000-MHz. The probe tip was made of tungsten wire of 1 mm in length and 0.5 mm in diameter. It was located in the shadow region behind the limiter.

4.3 Experimental Results

4.3.1 Rapid increase in perpendicular energy of runaway electrons

Figure 2(a) shows an example of discharges with low de-

nsities in the NOVA-II. Non-thermal microwave radiations were observed over the whole stage of the discharges. The radiations were emitted from the runaway electrons via a synchrotron mechanism, and was stronger than the thermal by more than a few tens of dB. When density reached at its peak, a sawtooth oscillation appeared in the loop voltage. In the phase of the discharges, plasma parameters were as follows; V_l =2-5 V, I_p= 8 kA, $\bar{n}_e$=(4-8)x10^{12} cm^{-3}, and T_e= 50 eV assuming Z_e =1 for the hydrogen plasmas. The diamagnetic temperature became approximately of the order of 1 keV. This implies that the diamagnetism was governed by the runaway electrons with large perpendicular energies. Figure 2(b) shows time variations of the loop voltage V_l, the diamagnetic signal $\Phi_{dia.}$, the horizontal displacement signal of the current channel, $I_p\Delta_R$, and the plasma current I_p during the unstable phase. As seen from the figure, the diamagnetic signal rapidly increased accompained by the positive spike of the loop voltage, while the current remained almost unchanged. Further, as shown in Fig. 2(c), the synchrotron radiation intensities observed at 10- and 50-GHz bands increased together with the spike of the loop voltage. Both the diamagnetism and the synchrotron radiation intensity originated from the perpendicular energies of the runaway electrons. It is concluded that there occurred the rapid increase in the perpendicular energy of the runaway electrons due to the instability resulting in the positive spike of the loop voltage.

We can estimate increment of the perpendicular energies from the diamagnetism measurement. The increment $\delta\varepsilon_{\perp}$ is obtained by the relation,

$$\delta\varepsilon_{\perp}=\frac{\delta\beta_{p\perp}}{n_b}\cdot\frac{B_p^2}{2\pi} \tag{4.1}$$

where n_b, $\delta\beta_{p\perp}$, and B_p are the average runaway electron density, the increment of the poloidal β-value perpendicular to the toroidal magnetic field, and the poloidal magnetic field at the periphery of the plasma column, respectively. Assuming that the density of the runaway electrons remained unchanged, and that the current was carried by only the runaway electrons, n_b is determined from the equation $n_b=I_p/v_0 e\pi a^2$ for the experimental parameters of I_p=8 kA and v_0/c=0.9 for ~500-keV electrons, we obtain $n_b\simeq 10^{10}$ cm^{-3}, where v_0 is the average velocity of the runaway electrons, and c the light velocity. Hence we obtain $\delta\varepsilon_{\perp}\simeq 10$ keV for a typical value $\delta\beta_{p\perp}$~0.1 in the present experiments.

On the other hand, an inward displacement of the current channel also took place with the increase in the diamagnetic signal. This is, as reported by Alikaev,[2] owing to a decrease in energy of the runaway electrons in the direction of the toroidal field. In the next subsection, such slowing down of the runaway electrons is described from the hard X-ray radiation measurements.

4.3.2 Slowing down of runaway electrons

The hard X-ray radiation signal was also enhanced at the onset of the instability as shown in the insertion of Fig. 3. This was resulted from a destruction of stable drift surfaces of the runaway electrons in the minor cross section, which was caused by the instabiliy. As is well-known in the framework of the single particle model,[14] a drift surface of electrons with given energy is determined by the ratio of the parallel energy to the perpendicular in a tokamaks. Therefore, the enhanced X-ray signal observed was closely related with changes in such energy ratio. Figure 3 gives an example of relative signal ratio of the hard X-ray radiation signals measured by the dual scintillation detectors during the instability. Open and filled circles are corresponding to the ratio before and after the enhancements of the hard X-ray radiation signals, respectively. The data were obtained by shot-to-shot measurements at t=3.5 msec of the discharges. In order to determine average energies of the runaway electrons, the hard X-ray signals are analyzed below by asuming that the runaway electrons are 'mono-energetic'. Then the energy flux of the X-ray radiations into the scintillators is the following function of the thickness of the lead absorber, d, and the kinetic energy of the electrons ;[15]

$$I_X(d,\varepsilon_0)= \int_0^{\varepsilon_0} d\varepsilon_X \; I_X(\varepsilon_0,\varepsilon_X)\cdot\exp[-\mu(\varepsilon_X)\cdot d], \qquad (4.2)$$

where ε_X and μ are the energy of the X-ray and the absorption

coefficient of the absorber Pb, respectively; $I_X(\varepsilon_0, \varepsilon_X)=j_0(Ax(\varepsilon_0, \varepsilon_X) + B)$ is the spectral density of the energy flux due to Bremsstrahlung of the electron striking the limiter, where the coefficients of A and B are taken from ref. 15. Values of ε_0 are determined by fitting the theoretical curves of $I_X(d,\varepsilon_0)/I_X(0,\varepsilon_0)$ to the experimental data. It is assumed that there is no absorption of the hard X-ray by the chamber wall and the housing of the detectors, since the energy of interest was more than a few tens of keV. The solid curves in Fig. 3. are the best fitted; the energy ε_0 is 640 keV before the enhancement, while ε_0=400 keV at the peak. It is found that there occurred a decrease in energy of the runaway electrons during the instability; the decrement in energy was 240 keV in the case of this figure. Figure 4 shows a time variation of the energy . The results are corresponding to three cases of t=2.5 (±0.2), 3.5 (±0.2), and 4.5 (±0.2) msec, respectively. From the results, it is found that the runaway electrons were prevented by such relaxation from being freely accelerated. Each decrement in energy was approximately 200 to 300 keV, which was an order of magnitude larger than the increment in perpendicular energy, typically 10 keV. As a result such slowing down of the runaway electrons brought about the inward displacement of the current channel because of dependence of $\Delta_R \propto \beta_{p\perp}+\beta_{p//}$, in spite of the increase in perpendicular energy. The positive spike in the loop voltage also originated from the suddenly enhanced resistance due to such

slowing down.

4.3.3 High frequency fluctuations

Figure 5(a) shows a correlation between a high frequency fluctuation signal and synchrotron radiation intensity at 10-GHz band during the unstable phase. The high frequency fluctuation signal appeared suddenly just when the enhancement in intensity of the synchrotron radiation terminated, and lasted only for a few tens of μsec. This suggests that the high frequency fluctuations were excited following the instability which resulted in the increase in perpendicular energies of the runaway electrons.

Figure 5(b) shows spectra measured when the densities $\bar{n}_e = 4,\ 6,\ 8\times10^{12}$ cm^{-3}, respectively, at $t \simeq 3.5$ msec by shot to shot measurements. For the hydrogen plasmas, the observed spectra were dominated by frequency components near the ion plasma frequencies, which were determined from the equation $\omega_{pi} = (4\pi e^2 \bar{n}_e / M_i)^{1/2}$; $\bar{n}_e$ is the line average electron density, and M_i the ion mass. For the helium plasma, no predominant frequency component was observed when the ion plasma frequencies for He^+ were set beyond the detectable frequency range; those for He^{2+} did not play a dominant role in forming the spectra because of the low temperature.

One may expect that the beam oscillations with the frequency of $\omega_{pb} = (4\pi e^2 n_b / m_e)^{1/2}$ were responsible for the observed spectra. In the present experiments this possibility would be excluded as

follows: Figure 6 shows an example of density dependence of the hard X-ray radiation signal and the displacement signal of the current channel. As seen from the figure, the hard X-ray radiation flux became lower with increased the plasma electron density; the displacement of the current channel also became smaller. These give such an evidence that the runaway electron population decreased with increase in the plasma electron density. Hence one expects that ω_{pb} decreased with increase in the plasma electron density. On the contrary, the predominant frequencies observed in the experiments increased with increase in the plasma electron density.

Local electron plasma oscillations near the probe tip were not appreciable in the spectra, since the electron densities near the tip was of the order of 10^{10}-10^{11} cm^{-3}, which is corresponding to $\omega_{pe}/2\pi \gtrsim 1$ GHz; the density was measured by the usual probe characteristic method with the same probe.

4.3.4 Rapid escaping of the energetic electrons

Another interesting phenomenon on the instability is rapid escape of the runaway electrons into the scrape-off layer. Figure 7 shows the correlation of the three probe current signals with the hard X-ray radiation signals. The probes were placed at the same radius of r =7 cm from the center of the minor cross section with the different poloidal angles of $+90^{\circ}$, 0°, and -90°, as shown in Fig .7(a). The results exhibit that there observed an

appreciable correlation between the hard X-ray bursts and the probe signal at -90°(Fig.7(d)); for the other probe signals both at 0° and $+90^{\circ}$, such correlation became to be less appreciable, as is seen in Fig.7(b) and(c). This fact suggests that the major fraction of the runaway electrons escaping from the main plasma into,the scrape-off layer drifted vertically down at the instability. From the experiments, we have a typical time scale of 10^{-5} sec for such electrons to escape from the main plasma into the scrape-off layer. The time gives us a typical drift velocity of $V_D = a/t_D = 5 \times 10^5$ cm/sec.

It is well-known, on the other hand, that the dynamics of the guiding center of the electrons in a magnetic field are described by the following equations;

$$V_D = v_z \hat{b} + \frac{c(\hat{b} \times \nabla\phi)}{B} + \frac{v_z^2 + v_\perp^2/2}{\omega_{ce} R} \cdot (\hat{b} \times \nabla B) \tag{4.3}$$

$$\hat{b} = \frac{B}{B} \tag{4.4}$$

$$B = \frac{B_0}{1 + (r/R_0)\cos\theta} \tag{4.5}$$

Here, V_D is the drift velocity, v_z and $v_\perp$ are the parallel and perpendicular components, respectively, of the electron velocities, and ϕ is an electric potential. For the simplicity, we neglected the second term in the right hand side of eq.(4-3), which is the ExB term.

When the energetic electrons have velocities such as $v_\perp/v_z \lesssim 1$, they drift mainly parallel to the magnetic field with

the outward displacements relative to the magnetic surfaces. The displacements increase with increase in energy of the electrons. In the experiments, the energies of the runaway electrons, however, decreased at the onsets of the instability as has been described. Such electrons, therefore, result neither in the burst of the hard X-ray radiation, nor in the escaping in to the scrape-off layer. On the other hand, if the electrons with the sufficiently large perpendicular velocities, e.g. $v_\perp/v_z > (B/\delta B)^{1/2}$ were generated as a result of the instability, the electrons should be trapped in the various magnetic mirrors in the tokamak, as is studied in Ref.6. Once trapped, the electrons will drift vertically down with the drift velocity $V_D \simeq v_\perp^2/2\,R\omega_{ce}$. When the energies exceed $E_{cr}=(\omega_{ce}/\omega_{pe})^2(E_D/E)\cdot T_e$, the electrons can penetrate vertically down into the scrape-off layer without suffering detrapping due to the Coulomb collisions. For the present experimental parameters of $B_t=8.5$ kG, $\bar{n}_e=5\times10^{12}$ cm^{-3}, and $T_e=50$ eV, we have $E_{cr}=2$ keV with $E_D/E=30$; the expected drift velocity for the electrons with the energy is $V_D=8\times10^5$ cm/sec, and a typical drift time is $t_D=a/V_D \simeq 10^{-5}$ sec. Thus the agreement between the observed and estimated values for the characteristic time scale provides a strong evidence that the electrons trapped in the local mirrors escaped into the scrape-off layer at the instability.

Now we estimate the power directly delivered by the energetic electrons. From the probe signals, we have the increments

of the current, $I_{pr} \simeq 1$ mA at the instability. If we take $A_e = \pi mm^2$ as a value of the effective collecting area of the probe, we have the current density $j_e = I_{pr} / A_e \simeq 3 \times 10^2$ Amp/m^2. We choose 5 keV for the energy typical of the escaping electrons. Supposing that the electrons with such energy were delivered over the whole surface of the scrape-off layer, we obtain an over-estimated value for the power; $E_{escape} = m_e n_{escape} V_D^2/2 = m_e^2/2e \cdot j_{escape} V_D S = 1 \times 10^{-4}$ Joule at the instability, so that $P_{escape} = E_{escape}/t_D \sim 10$ W.

4.4 Discussion

The experimental results have shown that the runaway electrons increased their perpendicular energies as they were slowed down in the toroidal direction. The phenomena took place rapidly ($\lesssim 10$ μsec) and repeated with the periods of 200 microsec.

As has been shown in Fig. 4, the runaway electrons, which participating in the phenomena, had the energies approximately from 300 to 700 keV. The runaway electrons with such energies are essentially free from the classic dynamic friction resulted from the Coulomb scattering by the plasma ions and/or electrons. The dynamic friction force for a test particle in a plasma with Maxwell distributions is given by

$$F_{dyn.} = \frac{4\pi e^4 n_e (1+Z_e) \ln\Lambda}{m v_0^2} \qquad (4.6)$$

where $\ln\Lambda$ is the Coulomb logarithm, n_e the plasma electron density, and Z_e the effective Z-number of the plasma. For simplicity the relativistic effect is neglected in the formula since observed energies were not very high, i.e. of the order of 500 keV. With this formula, the equation $F_{dyn.}=m_e v_0 \nu_e$ gives the relaxation time $\tau = \nu_e^{-1}$, where v_0 is the velocity of the test particle, and ν_e the collision frequency. In the experiments we choose the energy $\varepsilon_0 \simeq$ 500 keV, $n_e = 5\times10^{12}$ cm^{-3}, and T_e =50 eV, so that we obtain the time $\tau \simeq$ 0.1 sec. This expected relaxation time was far from the observed, $\geq$200 microsec. Thus the present experiments exclude the possibility that the classic dynamic friction plays a dominant role in the observed relaxation.

As has been described in the previous section, the relaxation was always accompanied by the excitation of the high frequency fluctuations. This fact gives such an evidence that the relaxation arose from the interactions between the runaway electrons and the plasma waves. Simultaneously the experiment shows that the interactions must excite low frequency oscillations near ω_{pi}. In the experiments, the plasma temperature was low, T_e ~50 eV, while the runaway electron energies were high, $\varepsilon_0 \sim$ 500 keV. One of possible mechanisms is that the runaway electrons interact with the cold plasma mode via the anomalous Doppler effect ($\omega_k + \omega_{ce} = k_z v_z$) and/or the Cerenkov effect ($\omega_k = k_z v_z$). The linear growth rate for the mode due to such effects is given by

$$\gamma_k = \frac{1}{n_e}\pi \frac{\omega_k^3}{k_z^2}\left\{\int d^3v\, k_z \frac{\partial f}{\partial v_z}\,\delta(\omega_k - k_z v_z) + \int d^3v \left(\frac{k_\perp v_\perp}{2\omega_{ce}}\right)^2 \right.$$

$$\left. \left(-\frac{\omega_{ce}}{v_\perp}\frac{\partial f}{\partial v_\perp} + k_z \frac{\partial f}{\partial v_z}\right)\delta(\omega_k + \omega_{ce} - k_z v_z)\right\} \qquad (4.7)$$

where n_e is the plasma electron density, ω_k the angular wave frequency, ω_{ce} the angular cyclotron frequency, k_z the parallel wavenumber, $k_\perp$ the perpendicular wavenumber, and f the distribution function of the plasma and runaway electrons. The first term in the parentheses represents the Cerenkov effect, and the second the anomalous Doppler effect. The growth rate is strongly dependent on the velocity distribution of the electrons. As the dynamic friction force does not prevent the runaway electrons from being accelerated by the toroidal electric field, they cannot accumulate around a velocity in a quasi-steady state. A reasonable distribution for the tail is one monotonously decreasing with velocity. Figure 8(a) shows calculated results of the growth rates given by eq.(4.7) for the cold plasma mode with the dispersion relation, $\omega_k = \omega_{lh}\cdot(1+(M_i/m_e)^2(k_z^2/k^2))^{1/2}$, where ω_{lh} is the lower hybrid frequency, when the tail is monotonously decreased with velocity, which is given in Appendix C. As seen from the figure, the instability can develop under the assumed conditions which are reasonably determined from the experiments. The instability is predominantly owing to the anomalous Doppler effect, which can lead to the pitch angle scattering of the run-

away electrons. The observed increase in perpendicular energy of the runaway electrons may be as a result of the pitch angle scattering of the runaway electrons. Nevertheless the observed relaxation in energy cannot solely attributed to the pitch angle scattering, since the decrement in energy was larger than the increment in perpendicular energy. It should be noticed that the d.c. electric field acts to accelerate the electrons even during the stage of the pitch angle scattering. Consequently a positive slope may appear in the tail. On the assumption, for simplicity's sake, that the distribution has a bump in the tail (see Appendix C), the growth rates calculated are shown in Fig. 8(b). The results show that the lower branch of the mode near ω_{lh} and ω_{pi} is unstable owing to the Cerenkov effect, and that the higher branch $\omega_k \simeq \omega_{pe} \cdot k_z/k > 10\omega_{pi}$ is unstable owing to the anomalous Doppler effect. With decreased the average velocity of the beam, the whole of the mode can become unstable mainly owing to the Cerenkov effect. Such results mainly result from the large spread in velocity of the bump. In contrast with the case of the monotonously decreasing tail, the Cerenkov effect can scatter the runaway electrons with relaxation in energy, and result in abroad spectrum. The relaxation in energy and the spectra observed in the experiments are consistent with the appearances which were caused by the instability responsible for the Cerenkov effect. The intability can repeat again due to the acceleration of the electrons by the electric field. It should be mentioned that the

observed periods of the relaxation oscillation, ~ 200 microsec, are enough time for the runaway electrons with energies above 100 keV to gain ~100 keV in energy from the electric field of V_l =2-5 V.

4.5 Summary

The experimental results on the instability driven by the runaway electrons are summarized as follows: The instability resulted in the rapid increase in the perpendicular energies of the runaway electrons as indicated by the increase in the diamagnetism as well as that in the synchrotron radiation intensity; the increment was estimated to be of the order of 10 keV from the diamagnetism. It is also found from the analysis of the hard X-ray radiation measurements that there occurred the slowing down of the runaway electrons; the decrement in energy was a few hundred of keV, which was larger than the increment in the perpendicular energy. Such relaxation in energies of the runaway electrons led to the inward displacement of the current channel as well as the positive spike in the one turn voltage.

Further the relaxation was always accompanied by the excitation of the high frequency fluctuations. Their frequency spectra show that there was the unstable mode near the ion plasma frequencies.

The results are consistent with the appearances of the

instability due to the interactions between the runaway electrons and the cold plasma mode, of which the critical condition was exceeded.

References

1) V.S.Vlasenkov, V.M.Leonov, V.G.Merezkhin and V.S.Mukhovatov: Nucl.Fusion 13(1973) 509

2) V.V.Alikaev, K.A.Razumova and Y.A.Solokov: Sov.J.Plasma Phys. 1(1975) 303; Sov.-Phys.-Tech.Phys. 20(1975)

3) D.A.Boyd, F.J.Stauffer and A.W.Trivelpiece: Phys.Rev.Lett. 37(1976) 98

4) P.Brossier: Nucl.Fusion 18(1978) 1069

5) T.Michishita et al.: J.Phys.Soc.Jpn. 47(1979) 1035

6) EQUIPE TFR: Nucl.Fusion 16(1976) 473

7) B.B.Kadomtsev and O.P.Pogutse: Sov.Phys.JETP 26(1968) 1146

8) C.S.Liu and Y.C.Mok: Phys.Rev.Lett. 38(1978) 162

9) V.V.Parail and O.P.Pogutse: Nucl.Fusion 18(1978) 303; Sov.J.Plasma Phys. 2(1976) 228

10) I.H.Hutchison, K.Molvig and S.Y.Yuen: Phys.Rev.Lett.40(1978) 1091

11) I.Fidone, G.Ramponi and P.Brossier: Phys.Fluids 21(1978) 237

12) K.Papadopoulos, B.Hui and N.Winsor: Nucl.Fusion 17(1977)

13) M.Fukao et al.: The Memoir of Faculty of Engineering, Kyoto Univ. 39(1977) 431

14) H.E.Knoepfel and S.J.Zweben: Phys.Rev.Lett. 35(1975) 1340

15) 'Plasma Diagnostic Techniques', ed. R.H.Huddlestoneand S.L.Lenard

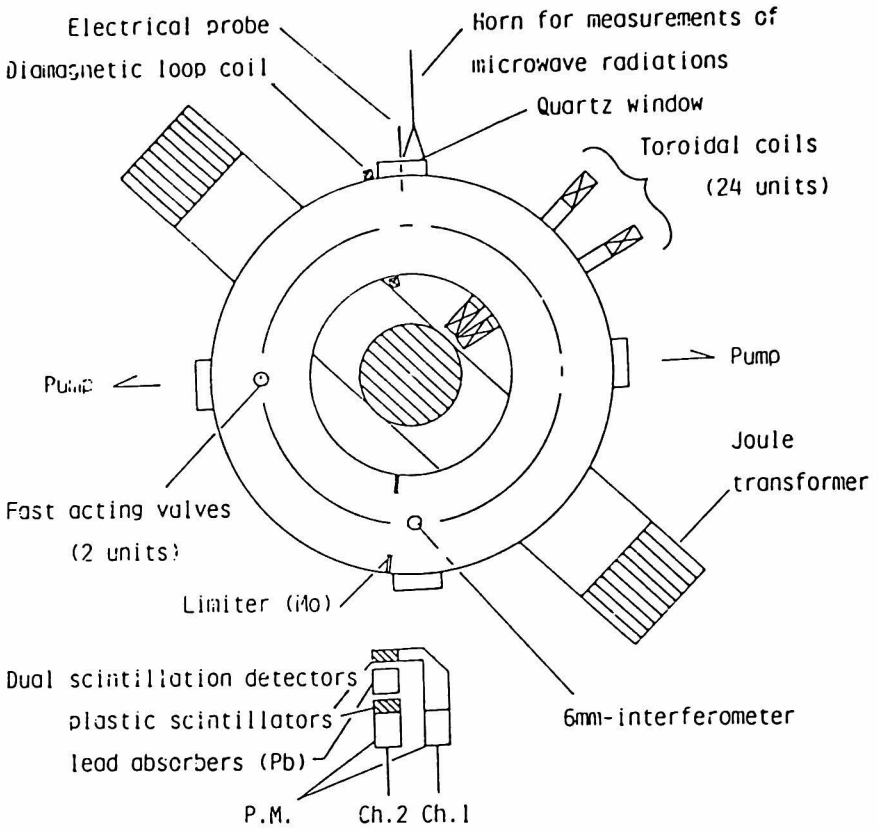

The NOVA II TOKAMAK

Fig.1. The torus of the NOVA-II and the arrangement of the diagnostics.

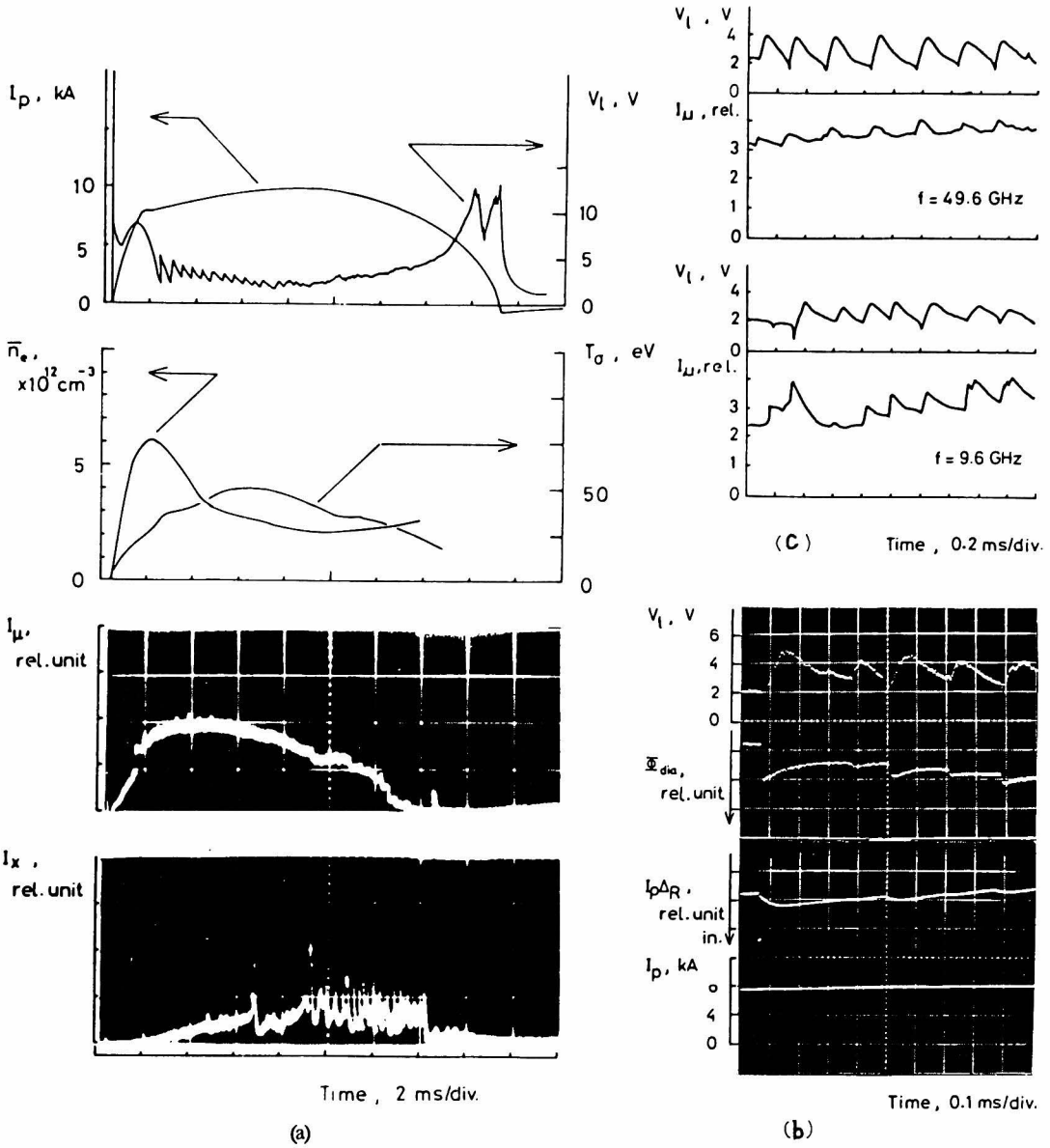

Fig. 2. (a): Typical examples of the low density discharges; from the top to the bottom, the plasma current I_p, the loop voltage V_{loop}, the line average density $\bar{n}_e$, the conductivity temperature T_σ, the microwave radiation intensity at 50-GHz band, and the hard X-ray signal. (2 ms/div.) $B_t = 10$ kG. (c): Time variations of microwave radiation intensities at 10- and 50-GHz bands and the loop voltage; each oscillogram shows the loop voltage (upper) and the radiation intensity (lower). (0.2 ms/div.). (b): Time variations of the loop votage, the diamagnetic signal Φ_{dia}., the horizontal displacement of the current channel, $I_p \cdot \Delta_R$, and the plasma current during the unstable phase of the discharge. (0.1 ms/div.)

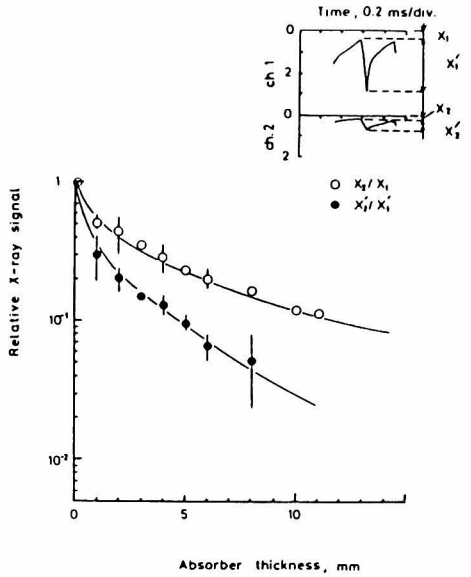

Fig. 3. Relative hard X-ray signal vs thickness of the lead absorber during the runaway electron instability. Open and filled circles are corresponding to the ratios shown in the insertion. Solid lines are the theoretical ones determined from eq. (2) with the fitting parameters ε_0; $\varepsilon_0=640$ keV for the line (a) and $\varepsilon_0=400$ keV for the line (b).

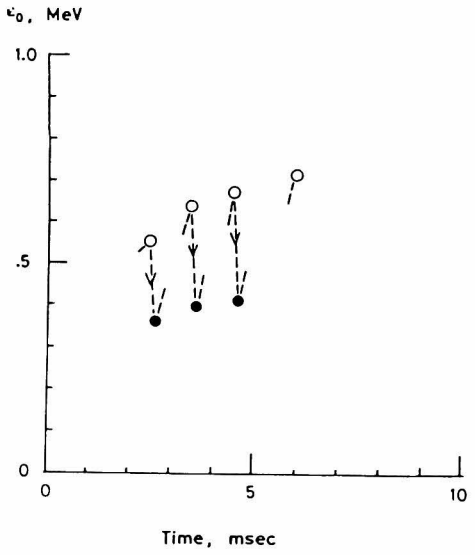

Fig. 4. Relaxation oscillation of the energy of the runaway electrons. The energy ε_0 were obtained from the analysis of the hard X-ray signals by shot-to-shot measurements.

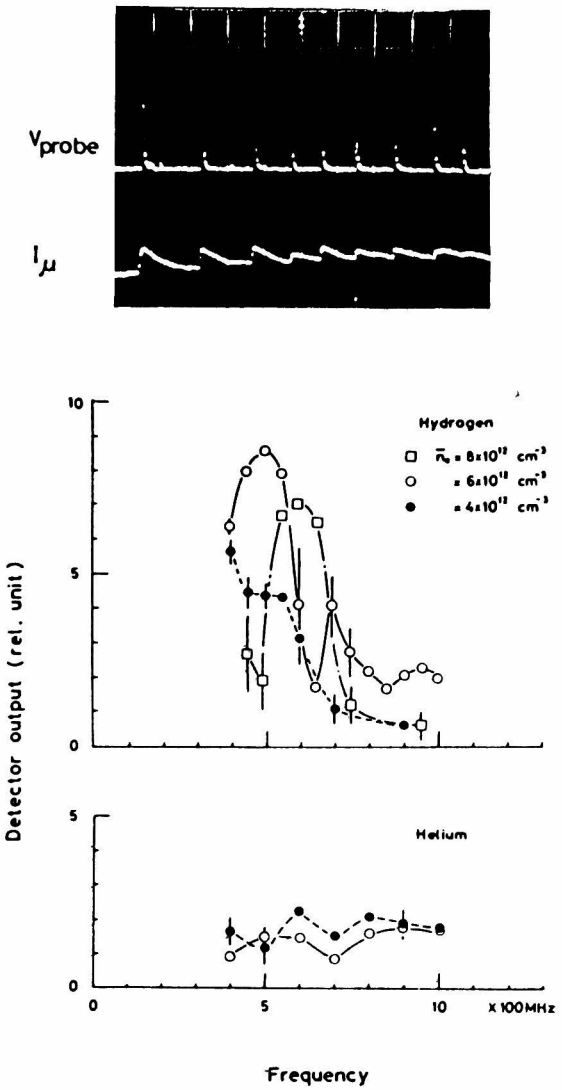

Fig. 5. High frequency fluctuation signals and their spectra observed for different cases of the densities; oscillogram shows the high frequency fluctuation signal with the probe and the synchrotron radiation signal of 10 GHz band (2 msec/div.). The spectra were observed for the hydrogen and helium plasmas by shot-to-shot measurements taken with the discharge parameters of $B_t = 10$ kG, and $I_p \simeq 8$ kA.

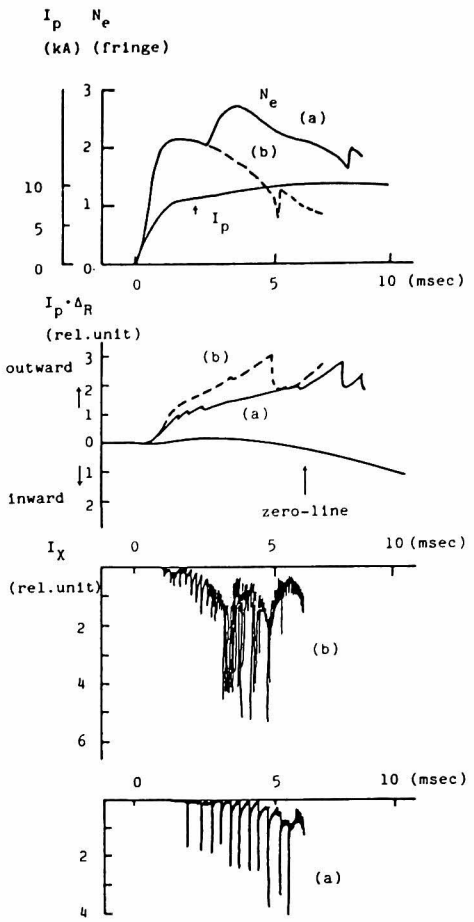

Fig. 6. Density dependence of the hard X-ray radiation flux and the displacement of the current channel. From the top to the bottom, the plasma current I_p, the line density N_e ($1.8 \times 10\,\mathrm{cm}^{-2}$/div.), the displacement signal of the current channel, $I_p \cdot \Delta_R$, and the hard X-ray radiation signal; (a) is corresponding to the case of the higher density discharge, and (b) to that of the lower density discharge.

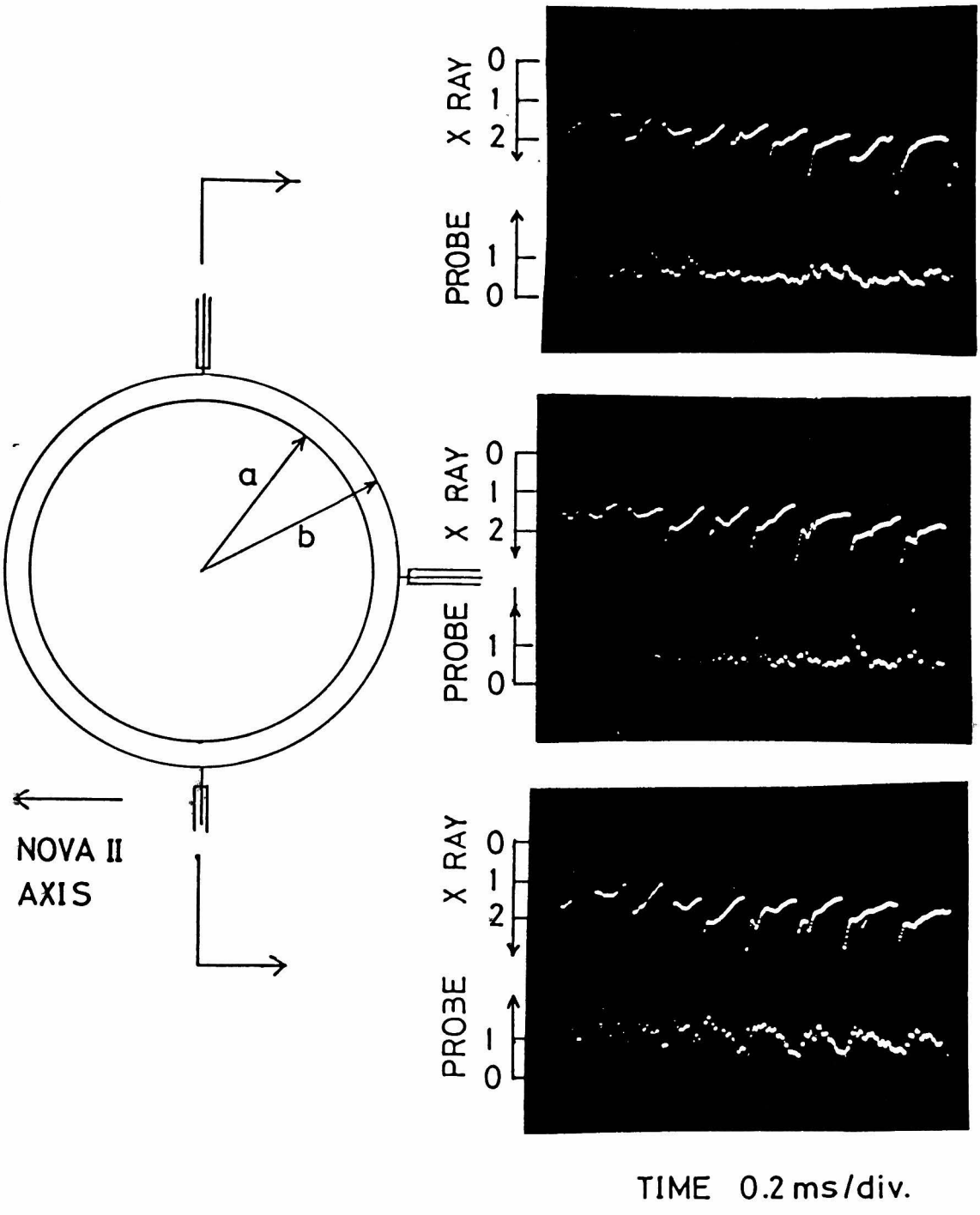

Fig.7. Time correlation of the probe signals at the different poloidal angles of -90°, 0°, and 90° with the hard X-ray radiation signals. Conditions are B_t=10kG, V_l=2-4V, I_p=8.5kA, and n_e=8x10^{12}cm^{-3}.

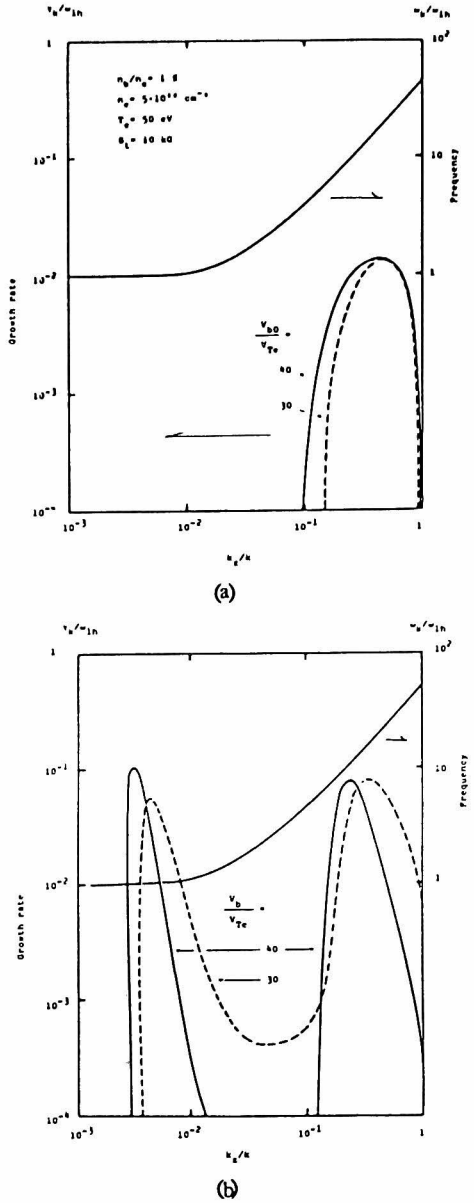

Fig.8. Calculated growth rates of the cold plasma mode. The dispersion relation is given by the equation of $\omega_k=(1+(M_i/m_e)(k_z^2/k^2))^{1/2}$. The growth rates is calculated from eq. (4) with the distribution function given by eqs. (A·1) and (A·3). (a) parameters; $n_b/n_e=1\%$, $n_e=5\times10^{12}\,\mathrm{cm}^{-3}$, $T_e=50\,\mathrm{eV}$, $B_t=10\,\mathrm{kG}$, $v_{Tb0}/v_{Te}=5$, $v_{b0}/v_{Te}=30$, and 40, and $k=50\,\mathrm{cm}^{-1}$. (b) parameters; $v_{Tb}=12$, $v_b=30$ and 40, and the others are the same as those in (a).

Chapter 5 Nonthermal Microwave Radiation Generated by Runaway Electrons

5.1 Introduction

When microwave radiations are emitted from plasmas via cyclotron mechanism, radiation intensity measurements near each harmonic of the cyclotron frequency are utilized for the diagnostic of the local electron temperature with the time evolution.[1-5] In a typical discharge of tokamak operations, the electron cyclotron radiation at the few harmonics is that the plasma radiates like a black body at the local plasma electron temperature.

On the other hand, microwave radiations are very sensitive to the presence of energetic electrons such as runaway electrons in the plasma.[6-10] In order to study dynamics of the runaway electrons, the measurement of microwave radiations was performed with three receivers which detect the radiations at frequencies of 1) $f > 2f_{ce}$, 2) $f_{pe} \geq f$, and 3) $f_{pe} >> f \sim f_{pi} \sim f_{lh}$; f, f_{ce}, f_{pe}, f_{pi}, and f_{lh} are detected radiation, electron cyclotron, electron plasma, ion plasma, and lower hybrid frequencies, respectively. The experimental results concerned with the radiation at the third frequency region have been described in Chapter 4. Here, the author describes the results concerned with those at the first two frequencies.

Section 2 is devoted to the basic considerations of the properties of the microwave radiations emitted from the energetic runaway electrons. We concentrate the radiations from the high energetic electrons during the discharges with the relaxation of the runaway electron energies, which has been described previously. The radiation at the frequency region $f \leq f_{pe}$ also exhibited an anomalous feature both in time behavior and in spectral profile. The results are described in Section 3.

In Section 4, the anomalous radiation observed in the experiment is discussed, and the experimental results are summarized.

5.2 Basic Considerations

When the plasma includes energetic electrons, intense non-thermal radiation is emitted from the electrons via synchrotron mechanism.[11-13] The radiation even near the lower harmonic number of the cyclotron frequency no longer has any excellent correlation between the radial location of the emitting layer and the radiated frequencies due to the large Doppler broadening.

Now we examine the properties of the synchrotron radiations emitted from the runaway electrons, from which the dynamics of the electrons of interest can be deduced for the working conditions of the NOVA-II tokamak.

According to the Trubnikov formula,[11] we may write the emissivity for the wave propagating perpendicularly to the magnetic

field;

$$j_\omega = \int dp[\ \eta_\omega^{O} + \eta_\omega^{X}\ ]\cdot f(p) \tag{5.1}$$

$$\eta_\omega^{O} = \frac{e^2\omega^2}{2\pi c}\ \Sigma\ \beta_{//}^{2} J_n^{2}(n\beta\ )\delta(n\omega_c-\omega), \tag{5.2}$$

$$\eta_\omega^{X} = \frac{e^2\omega^2}{2\pi c}\ \Sigma\ \beta_{\perp}^{2} J_n'^{2}(n\beta\ )\delta(n\omega_c-\omega), \tag{5.3}$$

where j_ω is the emissivity, η_ω the n-th components; 'O' and 'X' denote the ordinary and extraordinary modes, respectively.

Let us assume that the energy distribution function of the run-away electrons is

$$f_r = A(E_0)\cdot \exp(\ -E/E_0\ ), \tag{5.4.a}$$

$$A(E_0) = \int dE\ f_r\ /\ \int\ dE\ \exp[-E/\ E_0] \ . \tag{5.4.b}$$

Then the emissivity perpendicularly to the magnetic field is found to be (see Apendix D)

$$j_\omega = \Sigma\ (\ j_{\omega,n}^{O} + j_{\omega,n}^{X}\ ), \tag{5.5}$$

where

$$j_{\omega,n}^{X} = B_\omega\cdot\alpha nX\cdot\exp\ [-\ \alpha(nX\ -\ 1\ )]\cdot(1\ -n^{-2}X^{-2}\ )\ \sin^2\theta$$

$$\times J_n'^2 [\, n\sin\theta \cdot (1 - n^{-2}X^{-2})^{1/2} \,], \qquad (5.6)$$

$$j^{O}_{\omega,n} = B_\omega \cdot \alpha n X \exp[- \alpha(nX - 1)] \cos^2\theta$$

$$\times J_n^2 [\, n\sin\theta \cdot (1 - n^{-2}X^{-2})^{1/2} \,], \qquad (5.7)$$

where $B_\omega = (e^2\omega / 2\pi c) A(E_0)$, $\alpha = mc^2/E_0$, $X = \omega_{ce}/\omega$, and θ is the pitch angle of the runaway electrons.

We make a weakly relativistic approximation for the electrons. Expanding the Bessel functions to the first order in eqs.(5.6) and (5.7), we obtain

$$j_\omega \simeq B_\omega \Sigma n X \exp [- \alpha(nX - 1)] (1 - n^{-2}X^{-2}) \sin^{2n}\theta$$

$$\times \frac{n^{2n-1}}{2^n(n-1)!^2} \cdot [\, 1+(1-n^{-2}X^{-2}) \cos^2\theta \,]. \qquad (5.8)$$

Figure 1 shows the spectra calculated in the range of n=1-5 for the various values of α and θ. In Fig.1, we see that the spectrum is strongly depended upon the energy of the runaway electrons, E_0, equivalently α ; its profile is rather insensitive to the pitch angle θ.

Optical depth $\tau_{o.d.}$ is given by

$$\tau_{o.d.} \simeq D_n \mu^{1-n} R^2 \frac{n_e}{n_{e0}} , \qquad (5.9)$$

breakdown to the time of the first onset of the voltage spikes. In the following stage of the discharges, the radiation intensities exhibited the relaxation oscillation together with the voltage spikes; the intensities themselves no longer increased significantly as seen from the figure.

We now concentrate our attention on the dynamics of the runaway electrons in such stage of the discharges that the relaxation exhibited a repetition. At first, we note that the increment in intensity due to the relaxation was the largest at the first occurrence; the moderate increments followed it. Intensity profiles of the microwave radiation at 49.6GHz were measured by changing the values of the toroidal magnetic field for the similar conditions. The results are shown in Fig.6; the profiles are corresponding to those at t= 1, 1.5, 2, 4, and 6 msec. As is seen from the figure, the intensities enhanced rapidly at the first onset of the instability, which appeared at time t= 1.5 msec in the present experiments. Such enhancement took place over the whole range of the normalized frequencies f/f_{ce0} where f_{ce0} is the cyclotron frequency at the center of the minor cross section. The profiles themselves remained almost unchanged during the stage, t = 4 - 6 msec, when the intensities were maximum. In the stage, the radiations were very stronger more than 20 - 30 dB compared with those in the normal discharges of the NOVA-II tokamak.

On the other hand, the measured diamagnetism exhibited similar time evolution like the microwave radiations. Figure 7 shows the time evolutions of the diamagnetic temperature $T_{dia.}$ and the poloidal

β -value perpendicular to the magnetic field, which were determined from the diamagnetic signals and the line average electron densities. It is seen from the figure that the increment of the β -value the increment at the first enhancement was $\delta\beta_{p\perp} \sim 1$, while the increments at the following ones were no more than $\delta\beta_{p\perp} \sim 0.2$. The same estimation as has been done in Chapter 4 shows that at the first enhancement the increment in the perpendicular energy of the runaway electrons was of the order of 100 keV with the density $n_b \sim 10^{10}$ cm^{-3} ; the following increments remained of the order of 10 keV.

On the basis that both the synchrotron radiation and the diamagnetism are solely attributed to the runaway electrons in the present experiments, these results lead us to the following picture on the dynamics of the runaway electrons: When the runaway electrons develop sufficiently in energy and population, the instability is driven by them, and results in the pronouncedly large increase in their perpendicular energies. The major fraction of the electrons with the resultant large perpendicular energy of $\sim$ 100keV remains well-confined in the plasma. These electrons continue to emit the intense microwave radiation via synchrotron mechanism and to produce the large diamagnetism. This gives a suggestion that the runaway electrons establish an isotropic-like distribution function at the first onset of the instability. As a result, the following instability brings about only the small changes both in the synchrotron radiation and in the diamagnetism. It is noted that the distribution function of the runaway electrons should be somewhat isotropic rather than directionary,

at least, under the present circumstance.

We turn now to anomalous radiation at 9.6 GHz generated by the runaway electrons. Figure 8 shows two kinds of the relaxation oscillations of the microwave radiation intensities. The operation condition differed the values of the vertical magnetic field. Comparing the time evolution in Fig.8(a) with that in Fig.8(b), it is apparent that there is a significant difference in the feature of the relaxation. The radiation intensity in Fig.8($_b$) increased before the onset of the voltage spike, and then decayed with that. The characteristic period in Fig.8(^{b}) was also larger than that in Fig.8(a). Figure 9 shows the spectra measured as a function of B_t ; the cases in Fig.9 are corresponding to those in Fig.8, respectively. The open and filled circles are of the peak and the bottom intensities, respectively. The solid lines in Fig.9 are best fitted curves by adjusting α with eq.(5.8). The best fitting is obtained by α = 1.0 (E_0 = 510 keV) for the curves (a) and (b), and by α = 0.8 (E_0 = 640 keV) for the curve (c) The energies obtained from the spectra are well agreement with those determined from the measurement of the hard X-ray radiation, ~ 500 keV. The enhancement from (a) to (b) was caused by a resultant increase of the pitch angle of the runaway electrons due to the instability. The time behavior of the radiation, therefore, can be explained as that of the synchrotron radiation emitted from runaway electrons.

On the contrary, the peak intensities in Fig.9(b) exhibited the different dependence on B_t . In Fig.9(b), we see that during the

instability, the radiation decreased about more than 10 dB in intensity. Such phenomenon is not expected from the time behavior of the synchrotron radiation, which was described previously. Figure 10 shows time correlations of the intensity of the radiation in Fig.9(b), the loop voltage, the diamagnetic signal, and the hard X-ray radiation. Clearly, the radiation intensity decreased in spite of the enhancement in the diamagnetic signal. At the onset of the instability, the runaway electrons slowed down in the parallel direction to the toroidal magnetic field as well as increased their perpendicular energies. Taking into account the fact, the parallel motion of the runaway electrons should be essential to the generation of the anomalous radiation, contrary to the synchrotron radiation. The vertical magnetic field can bring about various influences on the initial phase of the discharges. In the experiments, an appreciable effect observed was a change in the line average density. The anomalous radiation was observed when the density increased by varing the values of the vertical magnetic field; in the present experiments, this was done by weakening the field. It was therefore natural to study whether the microwave radiation of interest can be brought about by changing the densities. In order to study the density dependence of the radiation the injection of the working gas were performed with a fast acting valve. Figure 11 shows the results by the injection during the discharges. The results are corresponding to the cases of different amounts of the injected gas; the injection times are the same, i.e. t=1.0 msec after the joule power was applied. As increased in the

amount of the injected gas, the line average density increased. The densities attained were restricted within relatively low limits, $\bar{n}_e < 1.2\times10^{13}$ cm^{-3}, because of the low temperature ($T_e \lesssim 50$ eV) in the runaway discharges. Futher, the plasma became more turbulent with the increase of the injected gas. Under such circumstance, as far as the density were far less than $\bar{n}_e = 1\times10^{13}$cm^{-3}, the relaxation of the radiation intensities did not change its feature except for the characteristic period. The radiation gradually changed the feature of the relaxation with further increase in the density; the intensity increased following the onset of the voltage spike, and the amplitude of the relaxation oscillation became larger when the density became to be $\bar{n}_e = 1\times10^{13}$ cm^{-3}. Figure 12 shows the detailed time evolutions of the radiation intensity, the loop voltage, and the hard X-ray signal. Clearly, the enhancements of the radiation intensity preceded the burst of the hard X-ray radiation as well as the onset of the voltage spike. These features of the radiation intensity were akin to those of the radiation brought about by varying the vertical magnetic field intensity.

5.4 Discussion and Summary

The present experiments show that in the runaway discharges the non-thermal microwave radiations were emitted from the runaway electrons with large perpendicular energies of the order of 100 keV. Such electrons were formed at the first onset of the instability, and were

well confined during the discharges. The time evolutions of the non-thermal radiation during the instability were consistent with the expectation from the pitch angle scattering of the runaway electrons.

As has been shown in the experiments involving the effects of magnetic field and the injection of the working gas, the radiation at 9.6 GHz changed the relaxation feature dependently upon the bulk electron density. The population of the runaway electrons should decrease as the density increases, since the production rates of the runaway electrons is $S_R \propto \exp(- n_e / T_e)$. At the same time, a plasma turbulence may become greater with the increased in the density. Taking into account the spatial inhomogenity of the density, the anomalous radiation at 9.6 GHz might be related with the electron plasma oscillations. In this case, the radiation should be emitted from the layer near the periphery of the plasma column. Radiations near electron plasma frequencies can arize from various mechanisms, as has been studied by a numerous number of the authors. In the present experiments, the plasma densities and the temperatures were relatively low, i.e., $n_e < 1 \times 10^{13}$ cm^{-3} and $T_e \leq 50$ eV. Further, the plasma involved the energetic runaway electrons. The generation of the anomalous radiation was not accompanied by the relaxation in energy of the runaway electrons. This fact excludes a possibility that the quasi-linear relaxation, which has been studied, results in the generation of the radiation. We note that the generation of the radiation was observed with the enhancement in the plasma turbulence. It is reasonably supposed that in a system including the energetic electrons ion acous-

tic turbulence enhances. In such a circumstance, one of possible mechanisms responsible for the anomalous radiation near the electron plasma frequency is the three wave decay interaction proposed by Hutchison et al.[14] According to the theory, an ordinal electromagnetic wave can decay into a long-wavelength electron plasma wave with frequency $\omega_k = \omega_{pe} k_z/k$ and an ion acoustic wave with $\omega_s = k_z C_s$. Consequently, this mechanism can enhance the radiation near ω_{pe}, as was observed in the present experiment.

In summary, the present experiments show that

1) The runaway electrons emitted strong synchrotron radiations during the whole phase of the discharges. Such electrons were formed even at the first onset of the instability, and well-confined with the large perpendicular energy of the order of 100 keV.

2) Another non-thermal microwave radiation was generated by the runaway electrons near the electron plasma frequency. The radiations were depended both upon the bulk electron density and upon the parallel energy. The radiations may also related with the plasma turbulence.

References

1) A.E.Costley, R.J.Hastie, J.W.M.Paul, and J.Chamberlain: Phys.Lev.Lett.33 (1974) 758

2) D.A.Boyd et al.; in Plasma Physics and Controlled Nuclear Fusion Research (Proc. 6th Int. Conf. Berchtesgaden 1976) 1, IAEA, Vienna (1977) 399

3) P.Brossier et al.; ibid 409

4) R.Cano et al.; Nucl.Fusion 9 (1979) 1415

5) D.A.Boyd, F.J.Stauffer and A.W.Trivelpiece: Phys.Rev.Lett. 37(1976) 98

6) P.C.Efithimion, V.Arunasalam, and J.C.Hosea; Phy.Rev.Lett.44 (1980) 396

7) EQUIPE TFR: Nucl.Fusion 16(1976) 473

8) V.V.Alikaev, K.A.Razumova and Y.A.Solokov: Sov.J.Plasma Phys. 1(1975) 303; Sov.-Phys.-Tech.Phys. 20(1975)

9) P.Brossier: Nucl.Fusion 18(1978) 1069

10) T.Michishita et al.: J.Phys.Soc.Jpn. 47(1979) 1035; ibid 50 (1981) 2720

11) B.A.Trubnikov; Ph.D Thesis(1958)

12) G.Bekefi, 'Radiation Processes in Plasma' (Wiley, New York, 1966)

13) C.M.Celata and D.A.Boyd; Nucl.Fusion 17 (1977) 735

14) I.H.Hutchison, K.Molvig and S.Y.Yuen: Phys.Rev.Lett.40(1978) 1091

15) I.Fidone, G.Ramponi and P.Brossier: Phys.Fluids 21(1978) 237

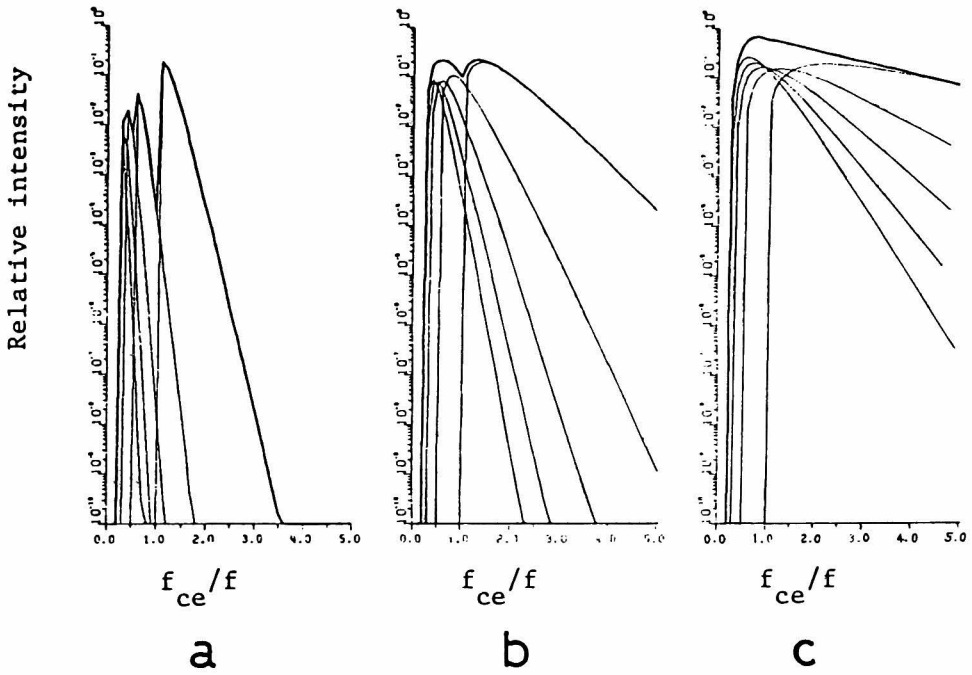

Fig.1 Synchrotron radiation spectra emitted from runaway electrons. The parameters are $\alpha = 5$ for the case of (a), $\alpha = 2$ for (b), and $\alpha = 1$ for (c). Pitch angle $\theta=45°$.

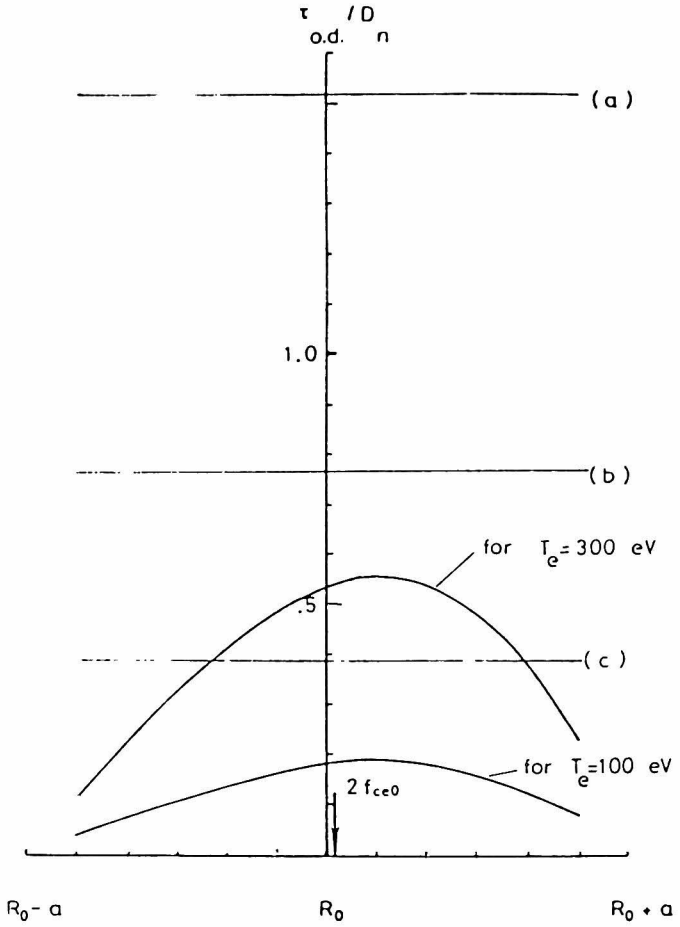

Fig.2. Calculated optical depth for cases of the density $n_{e0}=1x10^{12}cm^{-3}$ (a), $5x10^{12}cm^{-3}$ (b), and $1x10^{13}cm^{-3}$ (c); B_t=10 kG.

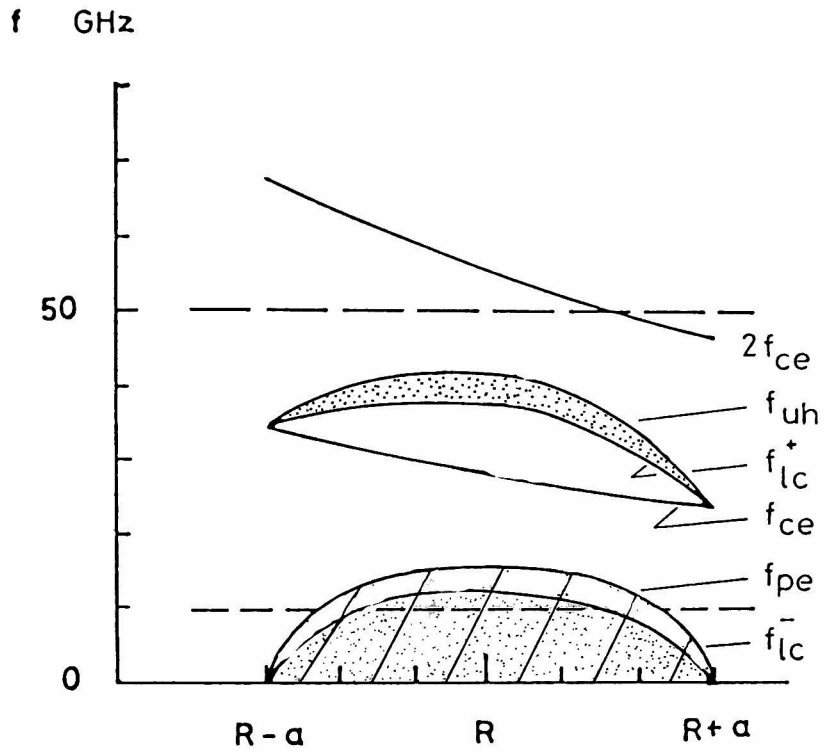

Fig.3 Spatial profiles for the characteristic frequencies f_{ce}, f_{pe}, $2f_{ce}$, f_{uh}, and f_{lc}. The hatched region denotes the non-propagating region for the O-mode, and the dotted that for the X-mode.

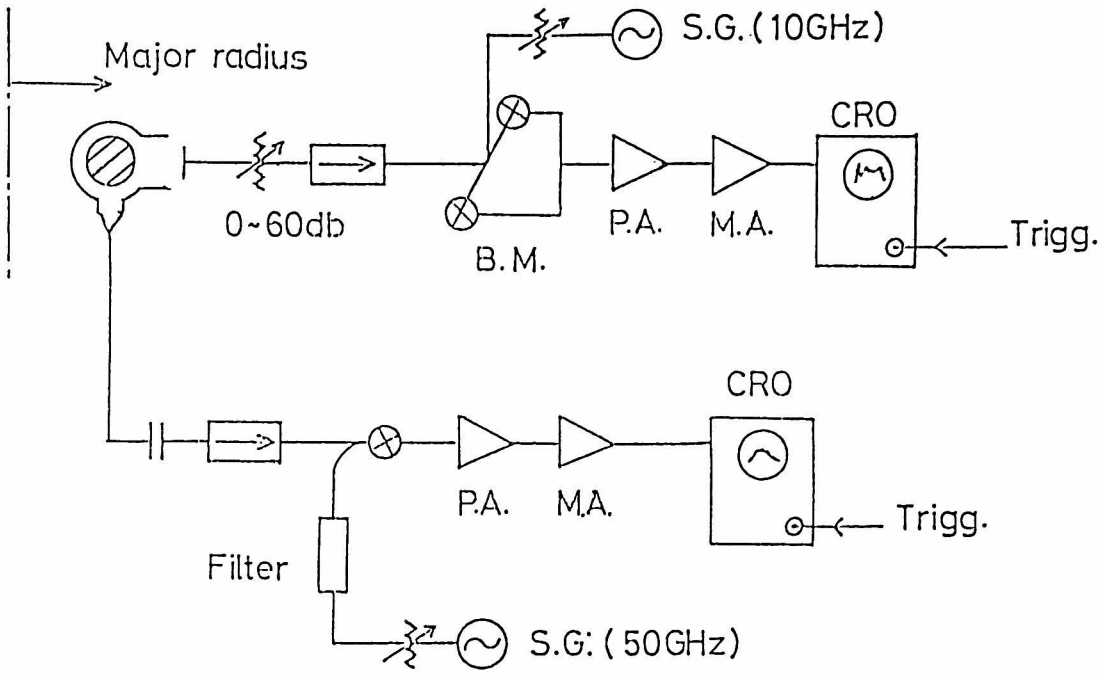

Fig.4 Arrangement of the microwave radiation measurements.

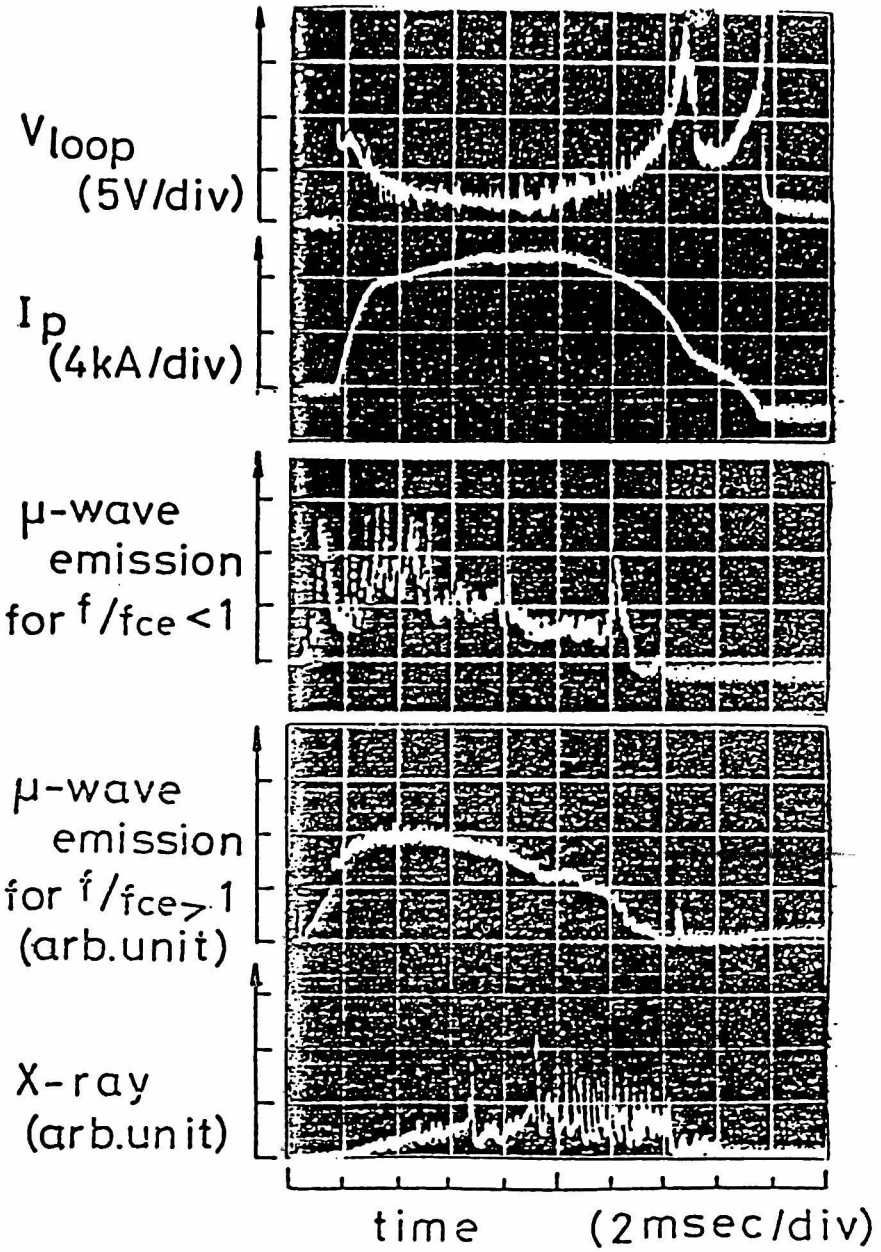

Fig.5. Typical time developments of the microwave radiations at 9.6 and 49.6 GHz; those of the loop voltage V_l, the plasma current I_p, and the hard X-ray radiation I_X are also shown.

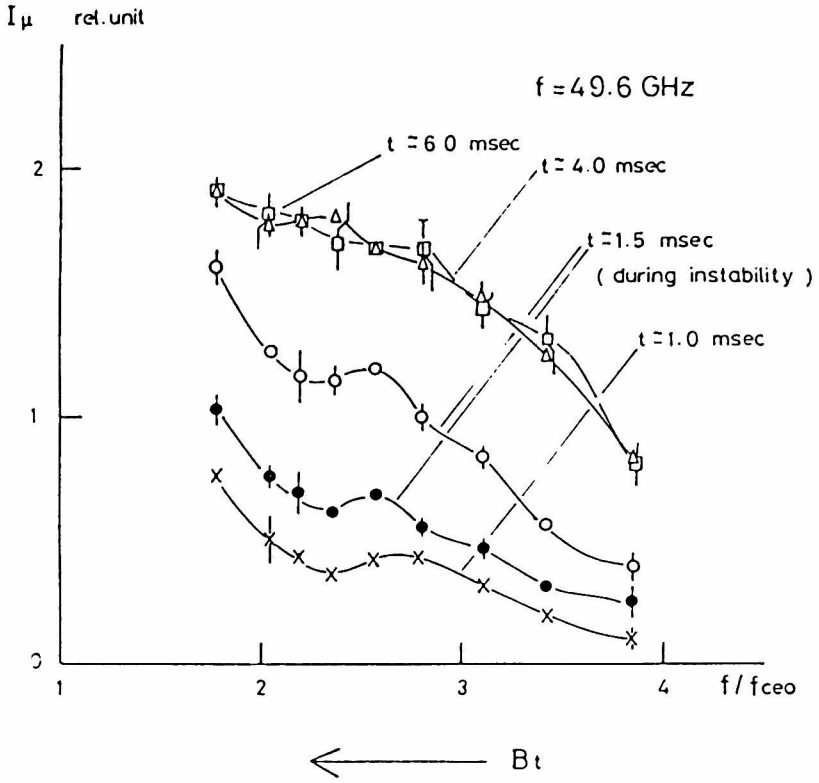

Fig.6.Time development of spectra measured during the discharges as a function of the toroidal magnetic field. The detected frequency was 49.6-GHz.

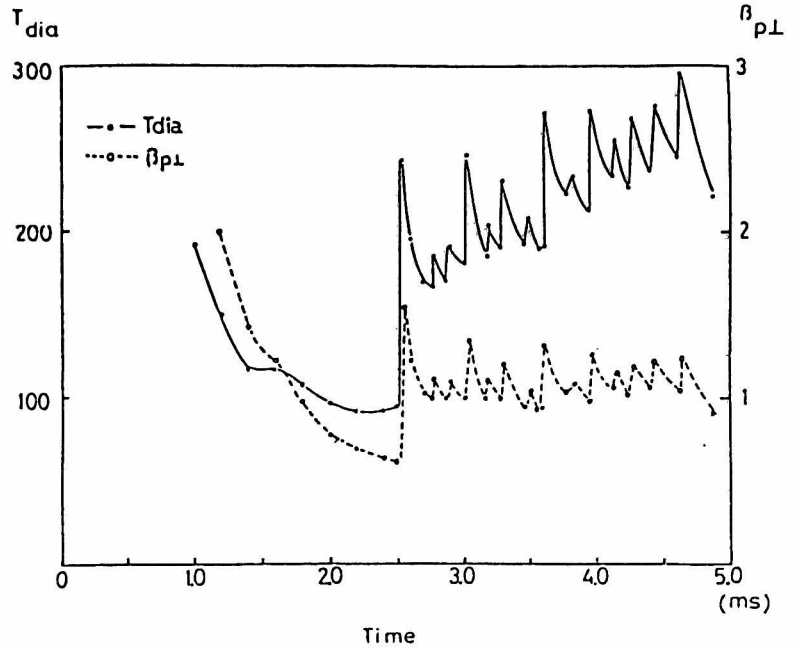

Fig. 7 Time development of the diamagnetic temperature $T_{dia.}$ and the poloidal β-value during the discharge.

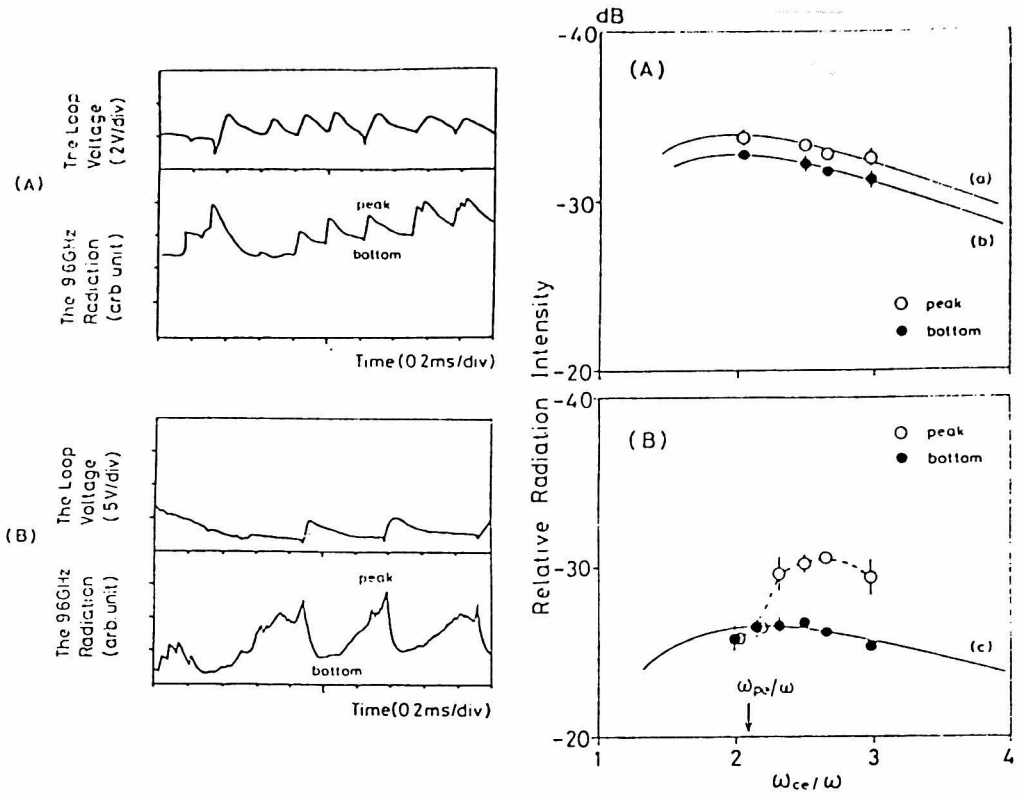

Fig. 8. Two distinct relaxation behaviors of the microwave radiations at 9.6 GHz. Each oscillogram shows the loop voltage (upper trace) and the radiation intensity (lower trace); (A) is of the optimum of the vertical magnetic field and (B) is of the weaker. The plasma current I_p was kept same.

Fig. 9. Spectra as a function of the toroidal magnetic field. The open and filled circles correspond to the peak and the bottom intensities shown in Fig. 8, respectively. Solid lines are theoretical ones.

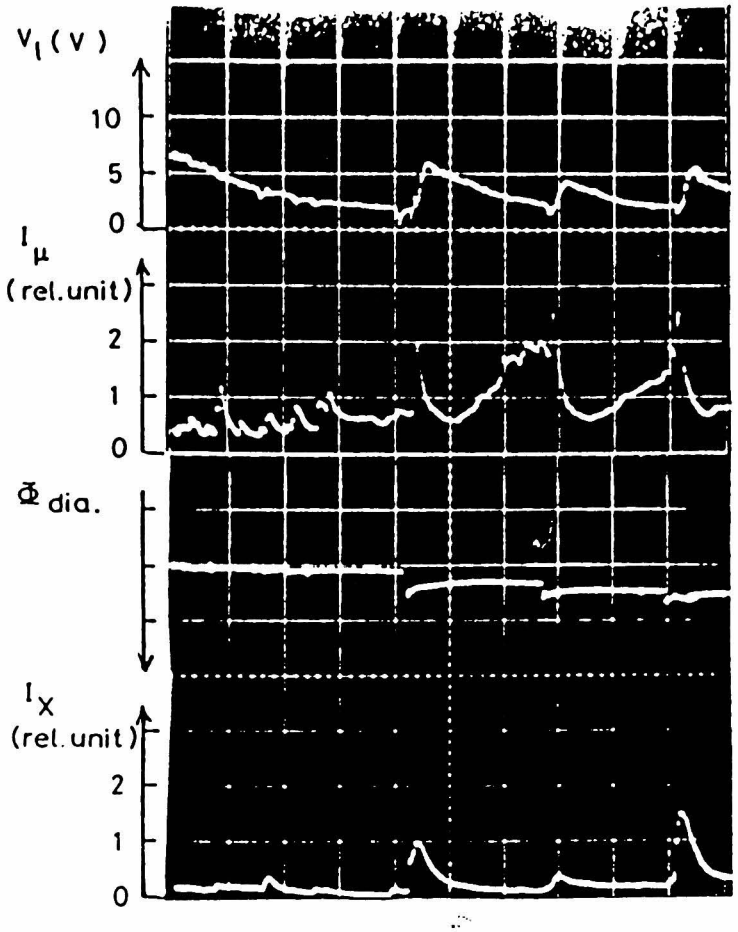

Fig.10. Detail of time correlation of the loop voltage V_l, the microwave radiation I_μ, the diamagnetic signal $\Phi_{dia.}$, and the hard X-ray radiation I_X.

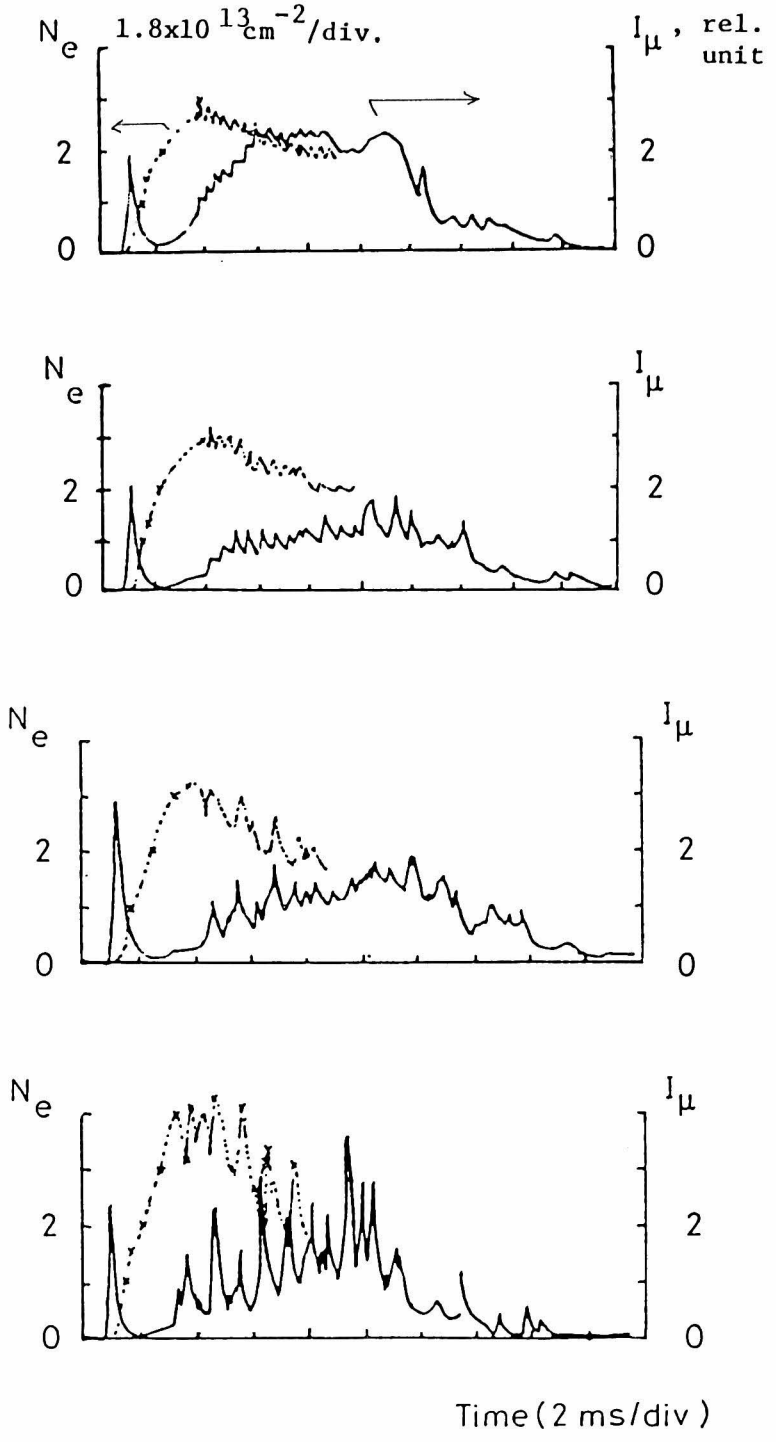

Fig.11. Time evolutions of N_e and I_μ for various amounts of the injected gas H_2.

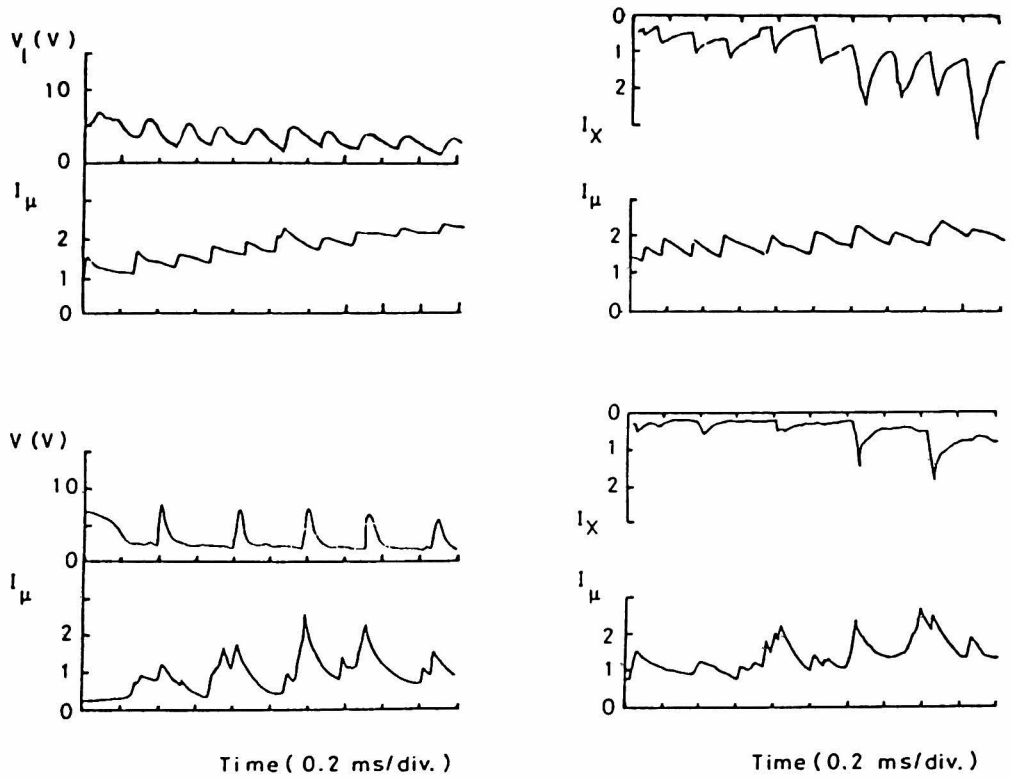

Fig.12. Density dependence of the microwave radiation I_μ, the loop voltage V_l, and the hard X-ray radiation I_X.

Chapter 6 Summary and Conclusions

The principal purpose of the present work is to make it clear how energy relaxation of runaway electrons takes place in a tokamak. When runaway electrons interact with background plasma only through the classical dynamic frictrion, they will continue to be accelerated by the d.c. toroidal electric field until their energy reaches a critical value, typically several of MeV, at which they escape from the main plasma region into the scrape-off layer and the limiter through the orbit-loss in the tokamak. In actual tokamak discharges, runaway electrons experience energy relaxation before the orbit-loss through interaction with high frequency waves.

The physical picture of this energy relaxation mechanism is described in brief as follows:

A) A small fraction of background plasma electrons are accelerated over a critical velocity v_{cr} by the toroidal electric field. The critical velocity is the velocity at which the dynamic friction force balances with the electric force. The electrons which pass over the critical velocity are called 'runaway electrons'.

B) When the strong anisotropy in the tail develops suffiently, it is unstable against kinetic instability due to an interaction with cold plasma waves via anomalous Doppler resonance($\omega_k + \omega_{ce} = k_z v_z$).

C) The resonant interaction causes pich-angle scattering of the runaway electrons and results in increse in their perpendicular energy together with decrease in their parallel energy.

D) The runaway electrons with the resultant increased perpendicular energy enhance sychrotron radiation intensity.

E) The pitch angle scattering leads to isotropic distribution function in the high energy tail. Consequently the electrons form a bump in the distribution function with respect to the parallel velocity.

F) This bump in the tail sequently becomes unstable against instability which excites waves in the frequency range including the ion plasma and lower hybrid frequencies.

G) An inverse Landau damping flattens the bump and the electrons lose their parallel energy until the waves excited decay.

H) Then the whole process returns to the step A after the runaway electrons again form the high energy tail in the distribution function due to the acceleration by the toroidal electric field. Consequently the relaxation repeatedly takes place in the discharge.

The above-described picture is supported by the conclusions and facts in each chapter as follows:

In Chapter 2, the numerical calculations based on the quasi-linear model have shown as follows:

1) The electrons almost free from the Coulomb collisions are scattered in pitch angle by the plasma waves via the anomalous Doppler resonance.

2) As a result, the electrons produce an isotropic distribution in the corresponding velocity region of the anomalous Doppler reso-

nance, and a quasi-plateau in the corresponding velocity region of the Cerenkov one.

3) The associated wave spectrum bocomes concentrated on the components with $k_z/k_D \simeq 0.1$ and $k_\perp/k_D \simeq 0.12$ as the quasi-linear relaxation develops in the high velocity region. Further, the wave again becomes unstable for the components with the large wavenumbers, resulting in the more broader wave spectrum.

In Chapter 3, the author has numerically examined the relaxation in energies of the electrons due to the excitation of the high frequency waves under the influence of the Coulomb collisions. As a result, it is found as follows:

1) The electrons reach a quasi-steady state by $\nu_s t \sim 1$. At this stage, the distribution function is more flattened in the tail as well as is isotropizated in the higher velocity region.

2) By $\nu_s t \sim 3$, the electron-associated energies become steady in time. The perpendicular energy of the runaway electrons increases up to more than an order of magnitude larger than the initial as the wave energy density increases. The rise time of the perpendicular energy is approximately inversely proportional to the wave energy density. For the relatively large wave energy density, $W_m/n_0 T_0 \sim 10^{-1}$, the rise time is less than 10^{-6}sec.

3) The parallel energy becomes half of the initial one with the relatively large decay time, about more than 10^{-2}sec, for the wave energy density, $W_m/n_0 T_0 \sim 10^{-1}$. Incidently, the relaxation in

the total electron energy noticeably takes place because of the slowing down of the runaway electrons in spite of the acceleration by the toroidal electric field.

In Chapter 4, the following results have been experimentally found concerned with the instability driven by the runaway electrons:

1) The instability characterized by the voltage spikes was accompanied by the rapid (~10 μsec) increase in the perpendicular energy of the runaway electrons. The increase resulted in the enhancements of the synchrotron radiation intensity and the diamagnetism. The increment typical of the perpendicular energy was of the order of 10 keV.
2) The measurement of the hard X-ray radiations showed that the runaway electrons lost their energy in the parallel direction; the decrement was of the order of 100 keV.
3) Such relaxation in energy was always accompanied by the excitation of the high frequency fluctuations of which the spectrum was dominated by the components near the ion plasma frequency.
4) A small fraction of the energetic electrons participating the instability rapidly escaped vertically down from the main plasma region to the scrape-off layer. The amount of the power delivered directly by the electrons was less than about 10 W.

In Chapter 5, the following experimental results have been found mainly from the measurement of the microwave radiations:

1) The runaway electrons emitted strong synchrotron radiations during the whole phase of the discharges. Such electrons were formed even at the first onset of the instability, and well-confined with the large perpendicular energies of the order of 100 keV.

2) Another non-thermal microwave radiation was generated by the run-away electrons near the electron plasma frequency. The radiations were depended both upon the bulk electron density and upon the parallel energies. The radiations may also related with the plasma turbulence.

Now the author notices that the following problems are left:

1) The computer simulation concerned with the dynamics of the run-away electrons has been performed in the framework of the non-relativistic approximation. The relativistic effects become increasingly important for very fast electrons; for example, the diffusion paths in the velocity space are distored for them when they interact superluminous waves ($\omega_k/k_z > c$), which may resulting in somewhat changes in the asymptotic energies themselves. These effects are not yet examined.

2) For more practical situation, it will be necessary to examine the effects of inhomogenity of the plasma on the relaxation and those of the convective transport of the wave energy.

3) It is important for experiments to analyze quantitatively the

electron distribution function, for example, from the hard X-ray energy spectrum with the pulse hight analysis method.

4) In tokamak experiments, the runaway electrons are also influenced by the MHD activities. Then, it is necessary to examine the dynamics of the runaway electrons against the MHD activities.

Finally the author would like to emphasize that the results obtained are useful for examining the dynamics of the fast electrons under influence of waves in fusion plasmas: the current sustain utilizing the fast electrons in tokamaks and the hot electrons to improve the stability in mirrors.

Appendix A

We will derive the quasi-linear diffusion term of eq.(2.2). In the case of the electrostatic instability, the quasi-linear term can be written from the Vlasov equation as follows;

$$\frac{\partial f^0}{\partial t} = \left\langle \frac{e}{m} \sum_k ik\phi_k \frac{\partial f_k^1}{\partial v} \right\rangle \tag{A-1}$$

Here ϕ_k is the amplitude of the electrostatic potential of the excited wave. The perturbed distribution function associated with ϕ_k is given from the linearized Vlasov equation as

$$f_k^1 = \frac{e}{m}\phi_k \sum\sum J_n\left(\frac{k_\perp v_\perp}{\omega_{ce}}\right) J_m\left(\frac{k_\perp v_\perp}{\omega_{ce}}\right) e^{i(m-n)\theta} \times \frac{-\frac{n\omega_{ce}}{v_\perp}\frac{\partial f^0}{\partial v_\perp} + k_z \frac{\partial f^0}{\partial v_z}}{\omega_k + n\omega_{ce} - k_z v_z} \tag{A-2}$$

where θ is the phase angle in v_x-v_y plane. After substituting eq.(A-2) into (A-1) and averaging over the phase angle θ, we have

$$\frac{\partial f^0}{\partial t} = 2\pi \frac{e^2}{m^2} \sum |\phi_k|^2 \sum \left(-\frac{n\omega_{ce}}{v_\perp}\frac{\partial}{\partial v_\perp} + k_z \frac{\partial}{\partial v_z}\right) \left\{ J_n^2\left(\frac{k_\perp v_\perp}{\omega_{ce}}\right) \left(-\frac{n\omega_{ce}}{v_\perp}\frac{\partial f^0}{\partial v_\perp} + k_z \frac{\partial f^0}{\partial v_z}\right) \delta(\omega_k + n\omega_{ce} - k_z v_z) \right\} \tag{A-3}$$

Replacing $k^2|\phi_k|^2/4\pi$ by ε_k, we obtain the quasi-linear diffusion term of eq.(2.2).

Appendix B

All subroutines used in the program (Runaway Eectron Instability Code) are as follows:

GRDREI	initialization of the (u,w) grid
WAVE	calculation of the wave parameters
WAVEGZ	calculation of the propagating angles; fixed or free ones
FPO	calculation of the variables associated with Fokker-Planck term
FPI	calculation of the Fokker-Planck term; called from ADPUSH
QLO	initialization of the variables associated with the quasi-linear term
QLA	calculation of the quasi-linear terms; called from ADPUSH
QLS	calculation of the saturated quasi-linear terms; called from ADPUSH
ADPUSH	calculation of the solution of the finite deference equation
MOMENT	calculation of the density momentum, energy moments and the wave density
TSTFNC	calculation of the initial electron distribution function

FVALUE	calculation of the values associated with the distribution function and the wave density
SIMP	modified Simpson integration
INTEG1	calculation of the integrals of the form $2\pi \int P(u)xF(u,w)\, w\, dudw$
INTEG3	calculation of integrals of the form $2\pi \int P(u)xF(u,w)\, w^{3}\, dudw$
OUTIT	for output with LP, debugging, etc.
OUTXY	for plotter output
XYCNTR	plotting out of contours; called from OUTXY
XYFINT	plotting out of the parallel distribution function; called from OUTXY
XYWAVE	plotting out the wave spectrum in velocity space; called from OUTXY
XYTHST	plotting out time history of the various energies; called from OUTXY

All subroutines are written in FORTRAN IV and are in single precision.

Appendix C

The growth rates shown in Fig.6(a) are calculated for the following distribution function in a quasi- steady state; the plasma electrons have a Maxwellian distribution, and the runaway a 'beam' distribution, i.e.,

$$f = n_e \pi^{-3/2} v_{Te} \exp[- v^2/v_{Te}^2]$$

$$+ n_b \pi^{-3/2} v_{b0}^{-1} v_{Tb0}^{-2} \exp[-v_\perp^2/v_{Tb0}^2 - v_z^2/v_{Tb0}^2], \qquad (C.1)$$

$$v_{Te} = (2T_e/m_e)^{1/2}, \quad v_{Tb0} = (2T_{b0}/m_e)^{1/2}, \qquad (C.2)$$

where n_e and v_e are the plasma electron density and the thermal velocity, respectively; n_b and v_{Tb0} are the runaway electron density and the average parallel velocity. On the other hand, the results shown in Fig.6(b) are obtained for the distribution given by

$$f = n_e \pi^{-3/2} v_{Te}^{-3} \exp[- v^2/v_{Te}^2]$$

$$+ n_b \pi^{-3/2} v_{Tb}^{-3} \exp[- v_\perp^2/v_{Tb}^2 - (v_z - v_b)^2/v_{Tb}^2], \qquad (C.3)$$

where

$$v_{Tb} = (2T_b/m_e)^{1/2} \qquad (C.4)$$

where v_{Tb} is the velocity spread of the electrons, and v_b the beam velocity.

The values of parameters are reasonably determined from the present experiments: The wavenumber must satisfy the following inequalities; $v_{Te} << (\omega_k + \omega_{ce})/k_z \sim \omega_{pe}/k < c$ for the anomalous Doppler resonance, while $v_{Te} << \omega_k/k_z \sim \omega_{pe}/k < c$ for the Cerenkov. These are required for the instability to develop against the Landau damping by the plasma electrons. For the experimental conditions of $\bar{n}_e \sim 5 \times 10^{12}$ cm^{-3}, $T_e \sim 50$ eV, and $B_t = 10$ kG, the inequalities are reduced to $10 < k_z << 500$ cm^{-1} for the anomalous Doppler and $10 < k_z << 100$ cm^{-1} for the Cerenkov. The average velocity v_{b0} is determined from the hard X-ray measurements, typically $\varepsilon_0 \sim 500$ keV, and it is assumed that $v_b \sim v_{b0}$. The velocity spread v_{Tb0} is determined from the diamagnetism in the quasi-steady state, typically $T_{b0} \sim 1$ keV. v_{Tb} is determined from the increment in the diamagnetism to yield $T_b \sim 10$ keV. The assumed values of such parameters are given in Fig.7.

Appendix D

The equation in Chapter 5 is given as follows: The optical depth $\tau_{o.d.}$ for the n-th harmonics is determined from

$$\tau_{o.d} = \int \alpha_n(\omega,R)dR, \tag{D.1}$$

where $\alpha_n(\omega, R)$ is the absorption coefficient, and R is the position along the direction of the ray. It is assumed that the radiation is absorved only by the thermal electrons. For the narrowness of the resonance region at any given frequency, the electron temperature T_e can be regarded as a constant in the calculation of the absorption Analogously to the calculation of the emissivity j_ω, in eq.(5.8), we can calculate the emissivity $j_{\omega,th}$ for the thermal electrons with a Maxwellian;

$$j_{\omega,th} = \frac{\omega_{pe}^2}{\omega_{ce}} \frac{\omega^2 T_e}{8\pi^3 c^2} \sum (2\pi)^{1/2} n^2 X^4 (1-n^{-2}X^{-2})^{n+1/2} \frac{n^{2n+1}}{(2n+1)!}$$

$$\times \mu^{5/2} \exp[-\mu(nX-1)]$$

$$\times \begin{cases} 1 & \text{for X-mode} \\ \dfrac{1-n^{-2}X^{-2}}{2n+3} & \text{for O-mode} \end{cases} \tag{D.2}$$

For each harmonic peak, we can determine the position, X_p , from the equation

$$\frac{dj_{\omega,n}(X)}{dX} = 0. \tag{D.3}$$

This gives

$$X_p^{-1} = n\cdot\left(1 - \frac{n+1/2}{\mu}\right) \tag{D.4}$$

The resonance length, ΔR is defined as that for which $j_{\omega,n}$ falls to half of its peak value at X_p . This yields from eq.(D.2)

$$\Delta R_n \simeq 2.4\cdot(n+1/2)^{1/2}\, R\mu^{-1} \tag{D.5}$$

According to the Kirchoff's law, i.e.

$$j_{\omega,n} = \frac{\omega^2 T_e}{8\pi^3 c^2}\,\alpha_n(\omega,R), \tag{D.6}$$

we can evaluate the maximum α_n ;

$$\alpha_{n,max} = \alpha_n(\omega, X=X_p)$$

$$= \frac{8\pi^3 c^2}{\omega^2 T_e}\, j_{\omega,n}(X=X_p)\ . \tag{D.7}$$

Let's express the optical depth $\tau_{o.d}$ as $\alpha_{n,max}$ times the effec-

tive resonance length, ΔR_n, namely

$$\tau_{o.d.} = \alpha_{n,max} \Delta R_n \tag{D.8}$$

Thus the optical depth $\tau_{o.d.}$ in eq.(5.9) is determined from eqs.(D.5) and (D.7).